Evolution of Carbon Structures in the Pyrolysis of Petroleum Pitches

by

Firuze Okyay

Submitted to the Graduate School of Sabancı University
in partial fulfillment of the requirements for the degree of
Master of Science

Sabancı University

July, 2009

To my beloved family

Evolution of Carbon Structures in the Pyrolysis of Petroleum Pitches

Firuze Okyay

MAT, Master's Thesis, 2009

Thesis Supervisor: Prof.Dr.Yuda Yürüm

Keywords: Pyrolysis, petroleum pitches, hydrographene, turbostratic structure, non-isothermal kinetics.

Abstract

The present study focuses on the carbon structure analysis of hydrographene like materials produced during the pyrolysis of petroleum pitches under various experiment conditions and non-isothermal kinetics of pyrolysis of petroleum pitches. Non-isothermal kinetic studies of pyrolysis of the pitches based on the TGA measurements at different heating rates resulted that the average activation energy of the pyrolysis of pitch B (213.2 kJ/mol) was higher than that of the average activation energy of pitch A (185.7 kJ/mol) whereas the reaction orders of pitches A and B were 1.3 and 0.91, respectively. Experiments were carried out under an argon atmosphere at the temperature range of 500-1000°C for 30, 60 and 120 minutes in a tube furnace. FTIR, ^{1}H-NMR, and ^{13}C-NMR results showed that the aromatic structure of the hydrographenes were increasing with respect to increasing temperature as well as increasing time. Raman spectra results demonstrated the increase in orderness with increasing I_D/I_G ratio from 0.65 to 0.92 when the temperature of pitch A pyrolysis was increased from 500°C to 900°C. XRD patterns of the hydrographenes showed the crystallinity increased with increasing time and temperature. The calculated average numbers of graphene layers were 5 to 10 with respect to XRD patterns. The SEM images visualized the amorphous structure of hydrographenes that was highly rich in turbostratic structures. All the results of characterizations

were consistent indicating the formation of highly amorphous hydrocarbon materials that contain turbostratic structures and higher heat treatments formations of aromatic structure with an increasing crystallinity and orderness. Highly amorphous hydrocarbon materials containing turbostratic structures were produced by two different types of pitches. Temperature seemed to be the dominating parameter of the pyrolysis reactions. As the pyrolysis temperature was increased aromatic structure formation was favored with an increasing crystallinity and orderness in the hydrographene materials.

Petrol Ziftlerinin Pirolizinde Oluşan Karbon Yapilarin Gelişimi

Firuze Okyay

MAT, Master Tezi, 2009

Tez Danışmanı: Prof.Dr.Yuda Yürüm

Anahtar Kelimeler: Piroliz, petrol zifti, hidrografen, turbostratik yapı, izotermal olmayan kinetik

Özet

Bu çalışma, farklı koşullar altında yürütülen petrol ziftinin pirolizi deneylerinde oluşan hidrografen benzeri malzemelerin karbon yapılarının analizine ve petrol zifti pirolizinin izotermal olmayan kinetiğine odaklanmaktadır. Zift pirolizinin farklı ısıtma oranlarında yapılan TGA ölçümlerine dayanan izotermal olmayan kinetik çalışmalarının sonucunda zift B'nin ortalama aktivasyon enerjisi (213.2 kJ/mol) zift A'nın ortalama aktivasyon enerjisinden (185.7 kJ/mol) daha yüksek çıkmıştır. Bunun yanında, A ve B ziftlerinin reaksiyon dereceleri, sırasıyla 1.3 ve 0.91 olmaktadır. Piroliz deneyleri tüp fırında argon atmosferi altında, 500-1000°C sıcaklıkları arasında 30, 60, ve 120 dakikalık süreler boyunca gerçekleştirilmiştir. FTIR, ^{1}H-NMR, ve ^{13}C-NMR sonuçlarına göre sıcaklık ve zaman arttıkça hidrografenlerdeki aromatik yapılarda artış görülmüştür. Raman spektrası, zift A'nın piroliz sıcaklığı 500°C'den 900°C'e yükseldikçe, I_D/I_G oranınındaki 0.65'den 0.92'ye olan artışa bağlı olarak yapıların daha düzenli hale geldiğini ortaya koymuştur. XRD paternleri, artan sıcaklık ve zamanla beraber hidrografenlerin yapısındaki kristal oranının arttığını göstermiştir. XRD paternlerindeki verilere göre hesaplanan ortalama grafen katman sayıları 5 ile 10 arasında değişmektedir. SEM görüntüleri, bol miktarda turbostratik yapıları olan hidrografenlerin sentezlendiğini ortaya çıkarmıştır. Bütün karakterizasyon sonuçları tutarlı bir şekilde çok amorf, turbostratik yapıların oluşumuna ve yüksek sıcaklıkların artan kristal ve düzenli yapıyla aromatik yapıların

oluşumunu desteklediğine işaret etmektedir. Turbostratik yapılı çok amorf hidrokarbon malzemeler iki farklı ziften üretilmiştir. Piroliz reaksiyonları sırasında sıcaklığın daha baskın parametre olduğu görülmüştür. Piroliz reaksiyon sıcaklığının yükselmesi, kristallik ve düzenlilikle beraber aromatik yapı oluşumunu desteklemiştir.

Acknowledgements

Contents

List of Figures

xvi

List of Tables

Chapter I

1   Introduction

Carbonaceous materials such as graphite, graphene, hydrographene, coke, pitch, and coal have characteristic structures which vary from high amorphous to perfect graphitic structure. Thermal treatment of the carbonaceous materials and types of the precursors are the main factors that orderness of their structure depends on [1]. Coal, biomass, and pitches are the main feedstocks of pyrolysis process in order to generate useful materials such as chemicals and substitutes of petroleum [2]. As a result, it is very essential to study the pyrolysis mechanism of at least one of these materials. Among these materials, petroleum pitches were chosen due to their less toxic and carcinogenic properties with respect to coal-tar pitches, and due their less complex structure. Two different types of petroleum pitches were pyrolyzed under different temperatures and times, in order to investigate the effect of temperature, time, and precursor on the formation of carbonaceous structures. The evolutions of molecular, crystalline, and morphological structures of the products were the main interest of this work. Therefore, variation of carbon structure during petroleum pitch pyrolysis done in different temperatures and times were investigated by using thermogravimetric analysis (TGA), scanning electron microscopy (SEM), nuclear magnetic resonance spectroscopy (NMR), Fourier Transform Infrared Spec-

troscopy (FTIR), Laser Raman Spectroscopy (RAMAN), and powder X-ray diffraction.

Chapter II

2 Literature Review

2.1 Pyrolysis and Carbonization

Pyrolysis, a special case of thermolysis that is mostly processed for organic materials, is the thermal decomposition of large molecules such as coal, heavy petroleum, biomass, oil shale etc. into mixture of smaller molecules of gases, liquids and solids. Pyrolysis reactions can occur spontaneously at temperatures higher than 300°C depending on the feedstock. Although it does not require oxygen or any other reagents in reaction atmosphere, it can occur in their presence because in real world experiments it is almost impossible provide a completely oxygen-free atmosphere. So, it is possible that a very small amount of oxidation can occur during pyrolysis processes [3]. Also some pyrolysis experiments can be done under oxygen atmosphere specially [4].

Carbonization is the extreme case of pyrolysis in which the composition of residue increases in carbon content during the process, tending to approach graphite with high stability. Carbonization process occurs at higher temperatures than pyrolysis and has condensation, isomerization, dehydrogenation and hydrogen transfer reactions in its mechanism. Also, the rate of carbonization reaction is faster, which makes it different than processes like coalification [5]. The degree of carbonization is strongly dependent on

the final pyrolysis temperature. For example, the final pyrolysis temperature around 1200 K results about 90 wt. % of carbon content in residue whereas with a final pyrolysis temperature around 1600 K results above 99 wt. % of carbon content [6]. Characteristic carbonization temperatures and stages of coal can be summarized in Figure 2.1 [7].
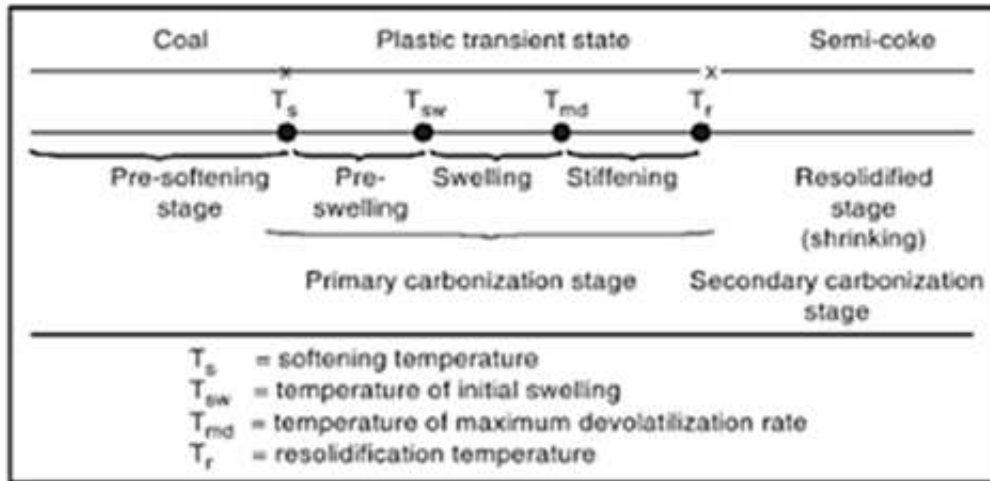
Figure 2.1: Temperatures and stages of carbonization

The properties of feedstock strongly affect yields and composition of the products. From chemical point of view, pyrolysis can be noted as depolymerization in parallel with functional groups' thermal decomposition where there is a competition of primary reaction products for hydrogen donation in order to achieve stabilization [2, 8]. During pyrolysis reactions, there is loss of weight of the raw material. The material that is lost during thermal decomposition process is called volatile matter, which consists of decomposition products of gases and liquids. Liquids and tars can be obtained due to the condensation of these matters [2]. In chemical industry, pyrolysis is a mainly used process in order to produce methanol, activated carbon, charcoal from wood, coke from coal, vinyl chloride from ethylene, synthesis gas from biomass, liquid hydrocarbons with lighter weights such as gasoline from heavy oil, and also it can be used for obtaining environment friendly disposable materials from wastes. Also, pyrolysis is the first rapid step in

combustion and gasification processes in order to obtain char that later reacts with steam, hydrogen, oxygen or carbon dioxide. Although pyrolysis can be processed for obtaining valuable products, it is analytically very important because it can provide information about the parent hydrocarbon structure [2].

Besides the chemical usage of pyrolysis, it is also an everyday use process in some of the cooking procedures. Baking, grilling, frying, and caramelization are known methods of pyrolysis in cooking. In frying procedure, the used fats have much higher boiling temperatures than water under atmospheric pressure. During frying the surface of the foods can be carbonized during caramelization of sugars. Caramelization is mainly used for cooking sugar in order to obtain nutlike aromas and brown color which occurs as a result of oxidation of sugar. During cooking or pyrolysis of sugar the relief of volatile chemicals results in caramel taste. The complex mechanism of caramelization process results in hundreds of chemical products caused by different types of reactions. Inversion of fructose and glucose from sucrose, isomerization of ketoses from aldoses, unsaturated polymer formation, intramolecular bonding, fragmentation, dehydration and condensation reactions are in involved in sugar pyrolysis process [9].

Returning back to scientific treatment of pyrolysis, the investigation of biomass and coal pyrolysis relies on 1970s in order to come across with an alternate for petroleum and chemical invention by extending the yield of liquid products [2]. Although, biomass resists prediction of its product yields and distribution because of their complex structure, the successful indications of coal pyrolysis products lead to development of numerous processes of coal conversion [10]. The process of bitumen, petroleum and oil sands provide pitch or a residue with high boiling point. The disposal problem of these residues rises with increasing dependency on heavy oil. Pitch is semi-liquid fraction of hydrocarbon that is a by-product of bitumen or cruel oil with a general boiling point above 500°C [2].

2.1.1   Types of Pyrolysis

The pyrolysis temperature, atmosphere, pressure, time, and feedstock affect the formation of products during process. For this reason, there are different pyrolysis methods for obtaining certain products. Six general types of pyrolysis are listed and explained below.

Fast Pyrolysis

Fast pyrolysis is the thermal degradation that occurs very rapid, such as in a few seconds, continuing with a rapid quenching at the end. Due to this rapid reaction mechanism of fast pyrolysis, phase transition and, heat and mass transport phenomena play important role besides chemical reaction kinetics of this process [11]. Optimizing the reaction temperature in order to synthesize desired products is the key point of fast pyrolysis. Another key point to approach desired products in this method is whether accomplishing size reduction and drying of feedstock or rapidly heating the particle surface that is in contact with heat source [11, 12].

The main products of the fast pyrolysis are liquid (oil), char and gas as listed in Table 2.1 [11, 12]. Fast pyrolysis is an appropriate process for producing liquids in high yields. The advantageous and disadvantages of this process can be listed as in Table 2.2 [11, 13].

Table 2.1: Properties and product yields of certain pyrolysis types

Pyrolysis Type	Heating Rate (K/s)	Residence Time (s)	Temperature (°C)	Product Yields		
				Liquid (oil)	Char	Gas
Slow	≪ 1	300-1800	400	x	✓	x
			600	✓	✓	✓
Fast	500-10^5	0.5-5	400-650	60-70 %	12-15 %	13-25 %
Flash	‹ 1	‹ 650	‹ 650	✓	x	x
	‹ 1	› 650	› 650	x	x	✓
	‹ 0.5	1000	1000	x	x	✓

6

Table 2.2: Advantages and disadvantages of fast pyrolysis

Advantages	Disadvantages
1. Feasible at moderate temperatures, so it is pyrolysis temperature can be controlled	1. Difficult storage due to the polymerization and phase separation of liquids as well as corrosion of containers
2. Operates under atmospheric pressure	2. Low-class hydrocarbon fuels because of high oxygen and water content of pyrolysis liquids
3. High production yields of oil	
4. Short residence times	

The fast pyrolysis is mostly dependent on the reactor. There are several types of reactors that can be used in fast pyrolysis processes. These main reactors are bubbling fluid beds [11, 12, 13, 14, 15], rotating cone pyrolyzer [11, 12, 13, 16], circulating fluidized beds, transport reactors, ablative pyrolyzer, auger and cyclonic reactors [11, 12, 13].

Slow Pyrolysis

Slow pyrolysis is the thermal degradation of organic molecules which processes very slowly. Slow pyrolysis reactions generally occur with low heating rates and high residence times as mentioned in Table 2.1. The feedstocks, reaction temperature, heating rate and residence times are the key parameters that affect the products of the pyrolysis that are char and volatile materials. As the heating rate of the pyrolysis reaction increases the formation of char reduces meaning that slower heating rates favors more char formation [12, 17, 18]. Also, Table 2.1 confirms that there is an effect of pyrolysis reaction temperature on the product formation in which as the temperature increases reaction mechanism favors liquid and gas formation as well as char.

Slow pyrolysis is usually carried out in rotary kilns and static furnaces supplied with screws and blades in order to mix the samples and increase heat transport [19]. Slow pyrolysis has a simpler process mechanism and equipment than fast pyrolysis [20].

Flash Pyrolysis

The faster stage of fast pyrolysis can be called as flash pyrolysis. Flash pyrolysis has highest heating rate that results with high yield of volatile materials as products. The distribution of the volatile materials, gases and oils, depends on the pyrolysis temperature, heating rate, and residence time as listed in Table 1.1. As in fast pyrolysis, the kinetic mechanism of flash pyrolysis is very complex. For example in flash pyrolysis of wood, oil and gas-solid products are degraded in two parallel reactions and then oil fractions goes through homogenous degradation reactions in order to form gas fractions [20].

Vacuum Pyrolysis

In vacuum pyrolysis, feedstock is thermally decomposed under vacuum. The main purpose to use vacuum pyrolysis is decreasing boiling point in order to prevent adverse chemical reactions during heating of organic materials. This method is also known as procycling process. When it is compared to slow pyrolysis, it reduces formation of the secondary reactions and produces more liquid material and when compared to flash or fast pyrolysis it has longer residence time and it can process larger particles [7, 13, 21].

Pressure Pyrolysis

In pressure pyrolysis, the change in product formation with change in pressure of the reaction mechanism at constant temperature is studied in literature. In coal pyrolysis field, Suuberg et al. investigated the yield of products at 1000°C. They resulted that as pressure increase yield of volatile material, especially tar, decreases whereas yield of gas formation increases [7, 22]. Also, at higher pyrolysis pressures the weight loss increases as shown in Figure 2.2.

Pyrolysis in Different Gas Environment

Although pyrolysis reactions usually occur under inert atmospheres such as nitrogen, argon, or helium [12, 23, 24], they can take place under reactive gas atmosphere. The effect of change in pyrolysis atmosphere in weight loss is illustrated in Figure 2.2 [7, 25]. The usage of reactive gas during pyrolysis strongly affects the results. As a fact the oxidative pyrolysis of coal is equivalent to combustion of coal [7, 4]. Also pyrolysis under hydrogen atmosphere or hydro-pyrolysis is in interest due to the reaction of hydrogen with coal fragment products, which are the free radicals. As Anthony et al. demonstrated in their study, this reactivity between the free radicals and hydrogen results with higher yield of volatile materials [7, 25].
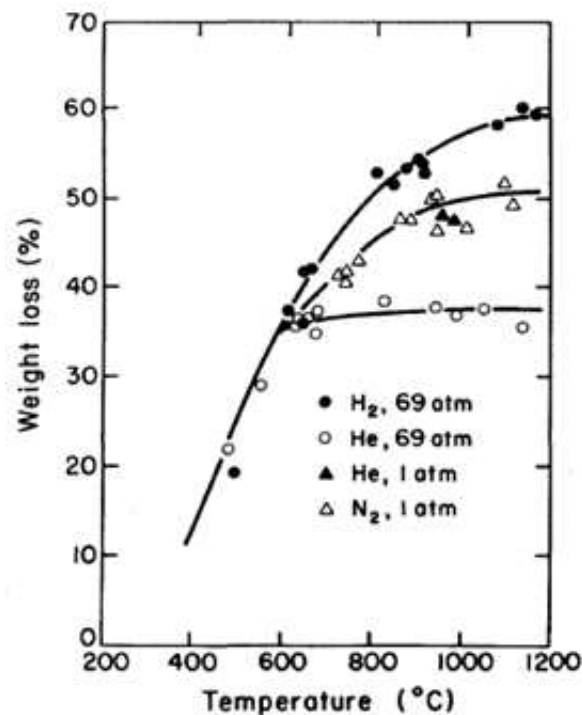
Figure 2.2: Weight loss vs. temperature graph of bituminous coal under different atmospheres and pressures

9

2.1.2 Pyrolysis and Constitution

Elemental Composition

The elemental composition of feedstock changes through pyrolysis process. As pyrolysis temperature increases [H/C] ratio of the feedstocks like coal or wood decreases during pyrolysis process. This indicates that hydrogen content reduces as the reaction temperature increases [7, 26]. Another study shows that [O/C] ratio also decreases with increasing temperature [7, 27]. In 1980s, Perry and Grint analyzed the functional group composition during carbonization process. They concluded that first decomposition of the carboxyl groups occurs at pyrolysis temperatures around 350°C, then decomposition of carbonyl groups takes place at temperatures up to 500°C and ether oxygen groups are the most stable functional groups at temperatures higher than 500°C due to their formation by condensation of hydroxyl groups [28].

Carbonization and Aromaticity

Aromaticity is another important parameter in discussion of elemental constitution of pyrolysis products. Especially f_{aC} and f_{aH} are the important key parameters [7]. Studies at the past years proved that polycyclic aromatic carbons are not volatile physically so aromatic carbon is left in the coke after pyrolysis process [7, 29] There are several methods for aromaticity calculation. Wang et al. calculated the aromaticity, f_{aH}, by using proximate analysis data [30];

$$f_a = \frac{1200 \times (100 - V_{daf})}{1240 C_{daf}} \tag{1}$$

Another useful method is calculating the fraction of aromatic carbons by directly integrating the nuclear magnetic resonance spectra. The aliphatic carbons region is 0 to 90 ppm whereas aromatic carbon region is 100 to 200 ppm, and if the total integrated area is calibrated as 100 [31], f_a can be

defined as:

$$f_a = \frac{\text{aromatic carbon}}{\text{aromatic carbon} + \text{aliphatic carbon}} \tag{2}$$

2.2 Pitch

The main raw material of this work, pitch, is a black, sticky to solid material with very high viscosity. International Union of Pure and Applied Chemistry (IUPAC) [6] defines pitch as a solid material at room temperature which is the residue obtained after pyrolysis of organic materials or distillation of tar. They also indicated that it is a complex form consisting of necessary aromatic hydrocarbons and heterocyclic compounds. The feedstock affects aromatic to aliphatic hydrogen ratio of pitch that indicates the hydrogen aromaticity which is reported as a variation from 0.3 to 0.9 [6]. Although pitch does not have a definite melting temperature, due its molecular weight [1] and composition, it has a broad softening range from 320K to 570K. So when it is cooled after melting it directly solidifies without crystallization [6]. According to Yue and Watkinson [2] pitch is the general term of liquid to semi-liquid fractions of hydrocarbon that have boiling point usually higher than 524°C. In their study they emphasized formation of pitch occurs as a by-product of crude oil, bitumen or coal-tar processes [2].

Depending on the production methods, pitch can be characterized as either coal-tar or petroleum pitch. Coal-tar pitches are residues formed by distillation or heat-treatment of coal-tar from by product recovery coke ovens [6, 32]. Petroleum pitches are residues formed from distillation and heat-treatment of petroleum fractions or formed as by-products of oil refining [6, 32, 33]. Both pitch types are complex mixtures of organic molecules that mainly consist of polycyclic aromatic hydrocarbons (PAH). Coal-tar pitch includes hetero-aromatic compounds in addition to PAHs, while petroleum pitch includes numerous alkyl-substituted PAHs [32]. This polycyclic aromatic structure of pitches results in isotropic or anisotropic coke formation

---

[1]relative molecular mass

with high yields during heat treatment processes. Due to this chemical property of pitch, their main applications rely on its chemical characteristic structure. The main application fields of pitch as a raw material are manufacturing of carbon and graphite materials like graphite electrodes for electric steel industry and carbon anodes for aluminum smelters [32, 33, 34] production of carbon fibers [32, 33, 35], poligranular and nuclear graphites [32], carbon composites [33, 34, 36], manufacturing of electric brushes and contactors, heat exchangers, etc. [32, 33].

Pitches can be also classified as isotropic and mesophase pitches. Mesophase pitches are high molecular weight aromatic pitches that have mainly an anisotropic nature. The pitch precursor is usually converted to mesophase pitch by thermal treatment, as a result the product (mesophase pitch) contains both isotropic and anisotropic phases in its structure. Mesophase pitches contain a mixture of numerous aromatic hydrocarbons that have anisotropic liquid-crystalline particles (carbonaceous mesophase) in its complex form. The aromatics of high molecular mass in mesogenic pitches, which have not yet been aggregated to particles detectable by optical microscopy within the apparently isotropic pitch matrix, form these carbonaceous mesophase particles [6, 37]. On the other hand, isotropic pitches contain a small amount of hydrogen and after carbonization of them mesophase spheres can be formed. Furthermore, after that pitches can reach up to total anisotropic structure [38]. Isotropic pitches are generally considered as cheap materials for manufacturing high performance carbon fibers. Both coal-tar and petroleum pitches contain high molecular weight carbonaceous materials. Due to its lower proportion of unwanted light components, petroleum pitches are preferred to coal-tar pitches [37]

2.2.1 Coal-Tar Pitch

Coal carbonization process, which occurs at temperatures between 1000-1200°C and residence times between 14-20 hours, gives rise to coke, coal-

tar, light oil e.g. benzene, ammonia liquor, water, and gas production [32]. From these by-products, coal-tar is used for pitch production. Distillation of coal-tar is mainly performed in central filtration plants that have capacities around 750 000 tons per year. The distillation process consists of certain procedures that are tar denaturation, inorganic chloride neutralization by Na_2CO_3 or NaOH followed by vacuum rectification [39, 40]. Due to the vacuum rectification method used in process, crude tar can be divided into 3 to 5 primary fractions [32]. These primary fractions are tar oils used for carbon black production and pure chemical compounds used for chemical industry [40]. Depending on the raw tar, the yield of coal-tar pitch at the end of distillation process is around 50-55% (w/w) [32].

Coal-tar pitch is a complex material with a broad molecular weight distribution from around 200 to more than 3000 amu [32, 41]. Zander demonstrated that depending on the pitch, coal-tar pitches consist of around 40% (w/w) of polycyclic aromatic hydrocarbons that have molecular masses lower than 330 amu, around 50% (w/w) of larger aromatic molecules having molecular masses between 330 and 1500 amu, and around 10% (w/w) of high molecular weight compounds with molecular masses from 1500 to 3000 amu [32, 42]. Fetzer and Reichsteiner detected the largest aromatic molecules in coal-tar pitch were a dimer of coronene with a molecular mass of 596 amu and dibenzocoronene [43]. Coal-tar pitches contain carbons that are 97% aromatic carbons. IUPAC indicates that hydrogen aromaticity in coal tar pitch is generally between 0.7 and 0.9 [6]. These aromatic compounds consist of PAHs, heteroaromatic compounds and their derivative compounds. Although coal-tar pitch consists of many different compounds, the complexity of coal-tar pitch is balanced with similarity of these different compounds [32]. This is a very important effect in applicability of coal-tar pitches in industry because of the necessity of converting pitch constituent into utilized solid carbon materials [41, 44]. Zander listed the main types of compounds that can be obtained in the coal-tar pitch are [45];

- PAHs,

- Alkylated PAHs

- PAH with cylopenteno moieties,

- Partially hydrogenated PAHs,

- Oligo-aryl methane, Oligo-aryls,

- Hetero-substituted PAH: NH_2, OH,

- Carbonyl derivatives of PAHs, and

- Polycyclic hetero-aromatic compounds such as benzologs of pyrrole, furan, thiophene, and pyridine.

Although these large numbers of aromatic hydrocarbons present in the coal-tar pitch give capability of converting into graphitic carbons by pyrolysis reactions, emission of these polycyclic aromatic hydrocarbons have some negative aspects [46]. Various studies and reports demonstrated that emissions during pyrolysis reactions of coal-tar pitch are highly toxic and carcinogenic, so there is a limitation in use of coal-tar pitch at some places of North America and European Union countries as well as closing of some coking plants in USA [46, 47, 48]. These environmental restrictions forced industrial market to come up with an alternative raw material; petroleum pitch [46, 49, 50].

2.2.2 Petroleum Pitch

Due to the less toxic and carcinogenic behavior of petroleum pitch during pyrolysis processes, it is becoming a popular alternative for market exclusively dominated by coal-tar pitches [49, 50, 51]. In addition to its less toxic and carcinogenic properties, petroleum pitches have less metal, ash and heteroatom, especially sulfur, content [46, 49, 51], they are capable to produce highly oriented graphitic carbon materials and high-density carbon precursors [49, 52], and its raw material production's accessibility and standardization is warrant in medium to long term [51].

14

Petroleum pitches can be produced by several methods such as thermal treatment, distillation, vacuum/steam stripping, oxidation, or blend of these processes [6, 32, 49]. There are various feedstocks that can be used for petroleum pitch manufacturing through these processes. Decant oil (with a molecular weight distribution from 100 to 500 amu) [32] from catalytic cracking of fluids and pyrolysis tars from steam cracking of naphtha are the important feedstock for petroleum pitch production. Aromatic by-products from lube-oil extraction, and asphalt as residue of vacuum stills and hard asphalt obtained from solvent deasphalting units are also feedstocks for petroleum pitch manufacturing [32]. These feedstocks and production methods have strong effect on the quality of the petroleum pitch and its products. Peréz et al. demonstrated three different petroleum pitches produced by three different methods: distillation formed PP-1; thermal treatment in a batch reactor with stirring formed PP-2; and continuous non-stirring visco-reduction process formed PP-3 followed by rapid distillation in order to raise softening point (SP) of the pitch by removing the light molecules [49]. They illustrated the effects of production methods on pitch pyrolysis in the Table 2.3.

Table 2.3: Properties of petroleum pitch

	[C]/[H]	SP (°C)	Toluene insolubles (wt. %)	Quinoline insolubles (wt. %)	Carbon Yield (wt. %)	I_{Ar}^a	I_o^b
PP-1	1.23	193	0.2	0.2	46	0.38	0.34
PP-2	1.31	91	18.8	0.7	51	0.45	0.30
PP-3	1.34	126	30.6	0.5	45	0.45	0.30

Petroleum pitch occurs as a residue from heat treatment of petroleum fractions that generated through certain reaction of dealkylation, dehydrogenation followed by condensation and polymerization of hydroaromatics, medium-sized aromatic hydrocarbons and their alkyl by-products [32].

Just like coal-tar pitch, petroleum pitch is also a complex material but it has a broader molecular weight distribution and higher average molecular

---

a=aromaticity factor index determined by FTIR, b=Orthosubstitution index determined by FTIR

weights than coal-tar pitch [53, 54]. Özel and Bartle demonstrated in their study at Figure 2.3 and Figure 2.4 [54].

Figure 2.3: Size exclusion chromatograms of Ashland-240 petroleum pitch, extract and residue (1 ml toluene, 400 atm, 200°C and 30 minutes dynamic extraction)

Figure 2.4: Size exclusion chromatograms of coal tar pitch, extract and residue (1 ml heptane, 400 atm, 200°C and 30 minutes dynamic extraction)

In addition to these, the most important difference between petroleum and coal-tar pitches originates from profusion sp^3 carbon interactions included in these materials [32]. Gemmeke et al. reported the difference of

16

weights than coal-tar pitch [53, 54]. Özel and Bartle demonstrated in their study at Figure 2.3 and Figure 2.4 [54].

Figure 2.3: Size exclusion chromatograms of Ashland-240 petroleum pitch, extract and residue (1 ml toluene, 400 atm, 200°C and 30 minutes dynamic extraction)

Figure 2.4: Size exclusion chromatograms of coal tar pitch, extract and residue (1 ml heptane, 400 atm, 200°C and 30 minutes dynamic extraction)

In addition to these, the most important difference between petroleum and coal-tar pitches originates from profusion sp^3 carbon interactions included in these materials [32]. Gemmeke et al. reported the difference of

16
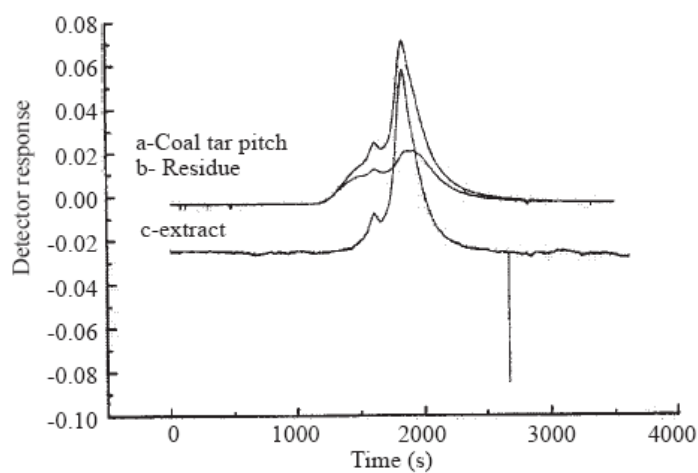
these two types of pitches in Table 2.4 [54] depending on their fa, degree of substitution of the average aromatic molecule $(S)^2$, the [C]/[H] ratio of the aromatic molecule (M), and C/H ratio of the entire material [32].

Table 2.4: Statistical structural data of a petroleum and coal-tar pitch

	Petroleum Pitch	Coal-Tar Pitch
f_a	0.88	0.97
S	0.19	0.08
M	1.77	1.77
[C]/[H]	1.46	1.70

As Table Table 2.4 indicates, petroleum pitch has lower aromaticity but higher S values than coal-tar pitch. Also IUPAC reported that hydrogen aromaticity of petroleum pitches has a range from 0.3 to 0.6 [6]. An additional difference of petroleum pitch than coal-tar pitch is emphasized by Zander; heterocyclic compounds are less in petroleum pitches than in coal-tar pitches [32].

2.3 Pitch Pyrolysis

Petroleum and coal-tar pitches turned from worthless wastes into important raw materials of aromatic and carbonaceous materials production. Manufacturing of graphite electrodes (for aluminum and steel industry), PAHs (for lithium ion batteries and hydrogen storage), carbon fibers, carbon-carbon composites, nuclear graphites, activated carbons, mesophase carbon fibers, and mesocarbon microbeds can be approached by pyrolysis and carbonization processes of pitches [51, 50, 55]. Formation of graphitic carbons and cokes can be achieved in high yields during pitch pyrolysis reactions [32].

It is very difficult to explain mechanism of pitch pyrolysis and carbonization, because of the complex chemical structure of it. There are thousands of different types of molecules with various molecular sizes and functions in pitch structure. For this reason, there is a potential for each different

---

^{2}S=C (aromatic, substituted) / C (aromatic, substitutable)

molecule to react distinctively. However, Figure 2.5 [32] still gives a reliable general idea of the carbonization process of pitches. Just like the complex
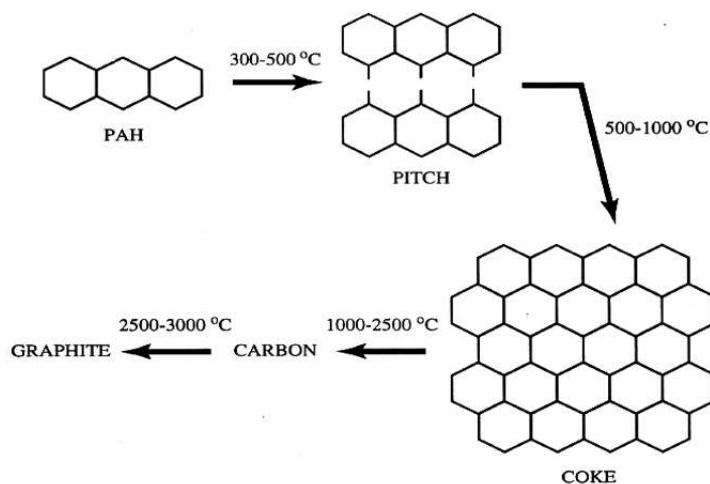
Figure 2.5: General reaction mechanism of pitch carbonization

chemistry of pitches, a complex thermal chemistry occurs during pyrolysis of pitches. According to Zander, among various chemical reactions, dehydrogenative polymerization reactions followed by dehydrocyclization dominate the pyrolysis processes. Dehydrogenation polymerization of aromatic compounds is also known as aromatic growth. Zander illustrated the mechanism of aromatic growth in Figure 2.6 [32].
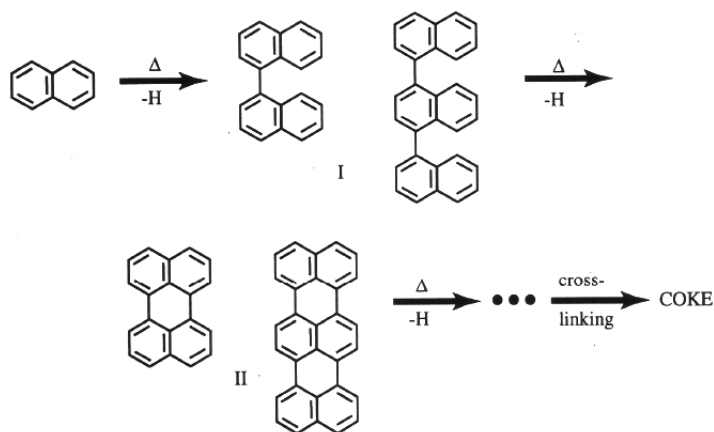
Figure 2.6: Mechanism of aromatic growth

18

The formation of type I compound (biaryls and oligo-aryls) is the rate determining step that continues with the next step of formation of type II (peri-condensed aromatic compounds) by intramolecular dehydrocyclization reactions. After the repetition of these reactions steps, cross-linking occurs which gives rise to coke formation finally [42]. Harsh et al. summarizes that cokes formed through deformable or fluid semicokes occurs by intermolecular and intramolecular reactions including molecular growth during pyrolysis of pitches [55]. Beside these dominating reactions of pitch pyrolysis process, there are other reactions leading to the formation of fragmentation compounds. The smaller molecules of hydrocarbons are formed by transfer of hydrogen in order to stabilize polycyclic aromatics followed by breaking up C-C single bonds during pyrolysis of pitches [32].

In addition to these reactions, dealkylation occurs in petroleum pitches due to their alkyl-aromatic rich structure [32]. Since the distinctive feature of pyrolysis reactions is the formation of mesophase when the molecules grow large enough [55], dehydrogenative polymerization of aromatic compounds appear to be more important than dealkylation reactions based on the studies of Greinke [56]. Mesophase is the phase that is anisotropic between isotropic pitch and anisotropic semicoke during the pyrolysis process [32].

To summarize, pyrolysis and carbonization reactions of petroleum and coal-tar pitches cause an increase in the molecular size via polymerization and volatile removal reactions. Greinke and Singer emphasized in their study that this molecular increase can be recognized by increase in the average molecular weight and by change in molecular weight distribution of the products [32, 57].

2.4 Non-isothermal Kinetics of Pitch Pyrolysis

Thermal analysis methods have been extensively used in recent years, because they offer a quick quantitative technique for the assessment of pyrolysis or combustion processes under non-isothermal conditions and allow guess-

ing the effective kinetic parameters for the various decomposition reactions [58, 59, 60].

The reaction kinetics parameters of pitch pyrolysis under inert N_2 atmosphere at different heat rates can be calculated according to the method given in Sanchez et al. [61] and Dumanli and Yürüm [62]. The rate of heterogeneous solid-state reactions can generally be explained as,

$$\frac{d\alpha}{dt} = k(T)f(\alpha) \tag{3}$$

where f(α) is a function that describes the reaction model, t is time, and k(T) is the temperature-dependent constant. The function f(α), states the dependence of the reaction rate, β, on the extent of reaction. Arrhenius equation describes the relation between rate constant and the temperature. As a result, the rate of a solid-state reaction can generally be explained as,

$$\frac{d\alpha}{dt} = Ae^{\frac{-E}{RT}}f(\alpha) \tag{4}$$

In this equation, A is the pre-exponential Arrhenius factor, E is the activation energy, and R is the gas constant. To convert equation 4 to the non-isothermal rate expressions, constant heating rate as expressed below can be inserted into equation 4.

$$\beta = \frac{dT}{dt} = constant \tag{5}$$

This placement will result in equation below with non-isothermal rate expressions, which describes reaction rates as a function of temperature at a constant β.

$$\frac{d\alpha}{dT} = \frac{1}{\beta}Ae\frac{-E}{RT}f(\alpha) \tag{6}$$

By integrating equation 6 up to conversion, α, it becomes,

$$\int_0^\alpha \frac{d\alpha}{f(\alpha)} = g(\alpha) = \frac{A}{\beta}\int_{T_0}^T e^{\frac{-E}{RT}}dT) \tag{7}$$

20

Vyazovkin [63], Khawam and Flanagan [64], and Dumanli and Yürüm [62] revealed that isoconversional methods need a series of experiments at different heating rates, β. According to the isoconversional methods applied by Ozawa [65, 66], Flynn and Wall [67] using the Doyle's approximation of p(x), which involves measuring the temperatures corresponding to fixed values of α from experiments at different heating rates [68], the activation energies from dynamic data can be estimated. In order to make this estimation of activation energy, the following equation is required,

$$ln(\beta) = ln[\frac{AE}{Rg(\alpha)}] - 5.331 - 1.052\frac{E}{RT} \tag{8}$$

From this equation, the activation energy E may be estimated by plotting $ln(\beta)$ versus 1/T.

The reaction orders of pitch pyrolysis reactions can be figured out by applying Avrami's theory for non-isothermal case description [69, 70, 71]. In the theory of Avrami, degree of conversion (α) changes with respect to heating rate (β) and temperature. This theory can be illustrated by the following equation,

$$\alpha(T) = 1 - exp[-\frac{k(T)}{\beta^n}] \tag{9}$$

Taking the double natural logarithm of both sides of equation 9, with k (T) = $Ae^{-E/RT}$, gives

$$ln[-ln(1 - \alpha(T))] = lnA - \frac{E}{RT} - \mathbf{nln}\beta \tag{10}$$

From this equation, reaction orders, n, of the pyrolysis reactions can be estimated by plotting ln [-ln (1- α (T)] versus ln β, which were obtained at the same temperature from a number of isotherms taken at different heating rates. The plot of ln [-ln (1- α (T)] versus ln β should give in straight lines whose slope will have the value of the reaction order or the Flynn-Wall-Ozawa exponent n [65, 72]. Extra aspects of the technique applied to examine the

21

process are explained by Ozawa [66].

2.5 Carbon Materials

Carbon is considered to be one of the most important elements for all living things because all organic compounds are composed of carbon-networks [73]. Carbon has a broad range of allotropes. Diamond crystals, graphite, carbon black, graphite electrodes, and activated carbons are known to be classical carbon allotropes whereas, carbon fibers, glassy carbons, turbostratic carbons, pyrolytic carbons, mesophase spheres in pitches, fullerenes, graphene and carbon nanotubes are considered to be the new members of carbon scicence. Some of these carbon allotropes, graphite, graphene, PAHs, and turbostratic carbons, can be obtained by pitch pyrolysis.

2.5.1 Graphite, Graphene, and Hydro-graphene

Graphite is one of the most common allotropes of carbon. Although, graphite crystallizes in hexagonal system in play form by construction of sp^2 hybrid orbitals of carbon-carbon bonding, it is rare to find it as perfect crystals. Depending on its occurrence and origin, graphite can be graded into three forms such as flake, crystalline, and cryptocrystalline (amorphous). Flake graphite can be found in metamorphosed rocks like vein deposits. Crystalline or lumpy graphite can be found as fissure filled veins whereas cryptocrystalline (amorphous) graphite can be found in metamorphosed coal beds [74].
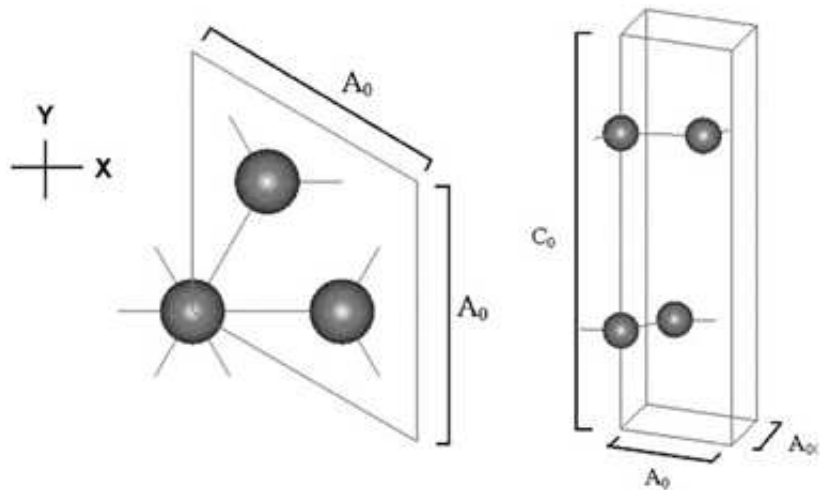
Figure 2.7: Unit cell of graphite
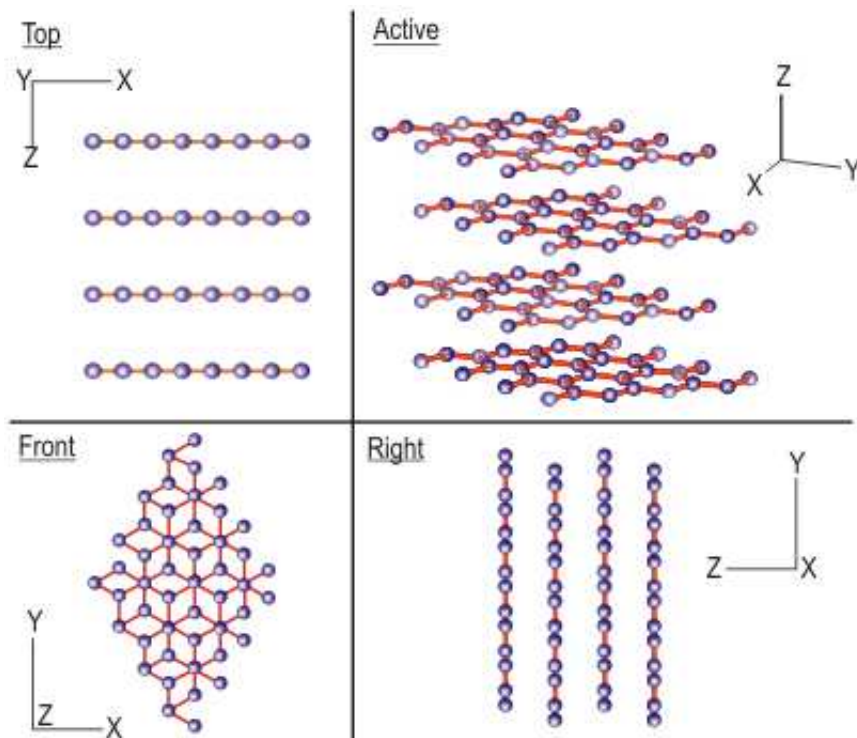
Figure 2.8: Crystal structure of graphite from different views

Graphite has a layered structure along c-axis in a staggered array that is mainly indicated as ABABAB.... The carbon atoms, which are placed in each layer of the graphite, are arranged in a hexagonal lattice structure with a distance of 1.42 $\mathring{A}$ as a result of the covalent bonds in carbon atoms. Since van der Waals forces determine the spacing between elemental planes, the distance between them is larger, 3.35 $\mathring{A}$ [75, 76, 77]. Figure 2.7 [77] and Figure2.8 [78] illustrate the unit cell and crystal structure of graphite respectively. Due to the difference between the bond strength in two directions (phonons can propagate very quickly along the tightly-bound planes whereas they can propagate slower from one plane to another), graphite has highly anisotropic properties such as, thermal conductivity [79]. The vast electron delocalization within the carbon layers makes graphite to be able to conduct electricity. The free movement of the valence electrons is the reason for the conductivity within the plane of the layers of graphite.

Each layer constructing the three dimensional crystallographic structure of graphite is a graphene sheet. Graphene is the one-atom thick monolayer of sp^2 bonded carbon atoms. Graphene, the two dimensional honeycomb arranged monolayer, is the structural element of fullerenes, carbon nanotubes, and PAHs as well as graphites [80, 81, 82]. Through the sheets of graphene, electrons can move very fast at ambient conditions what makes it an important material for electronics. The two dimensional structure of graphene and how it contributes to construction of other carbon allotropes are illustrated in Figure 2.9 [83]
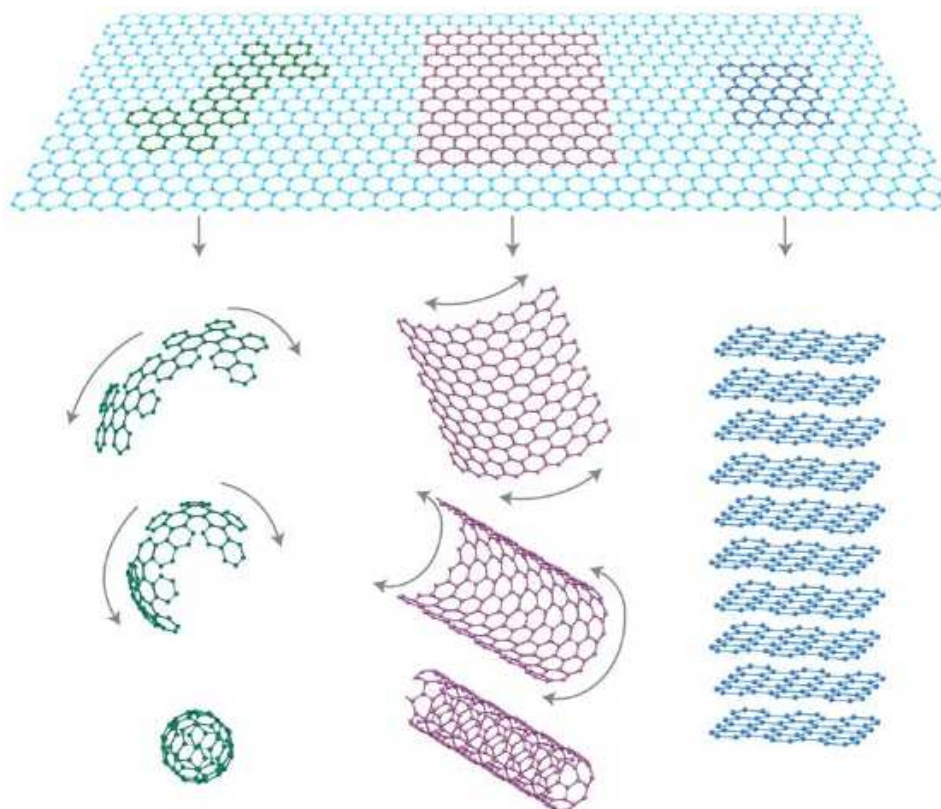
Figure 2.9: (a) Two dimensional graphene sheet forming (b) Zero dimensional fullerenes, (c) One dimensional carbon nanotubes, and (d) Three dimensional graphites

According to the statement of IUPAC, graphene is a six-member carbon ring structure of PAH [84]. As explained in previous sections, PAHs can be synthesized via pitch pyrolysis. Yamabe et al. denoted that PAH materials produced from pitch pyrolysis have significant [H]/[C] ratio and they are generally composed of different sizes of graphite sheets that are terminated by hydrogen atoms. Since one single layer of graphite is graphene, these graphene layers with terminating hydrogen atoms can be called as "hydro-graphene" [80]. The hydro-graphene's crystal structural model is illustrated in Figure 2.10 [80].

In addition to these explanations, IUPAC made the following statement about graphene: "Previously, descriptions such as graphite layers, carbon layers, or carbon sheets have been used for the term graphene...it is not correct to use for a single layer a term which includes the term graphite, which would imply a three-dimensional structure. The term
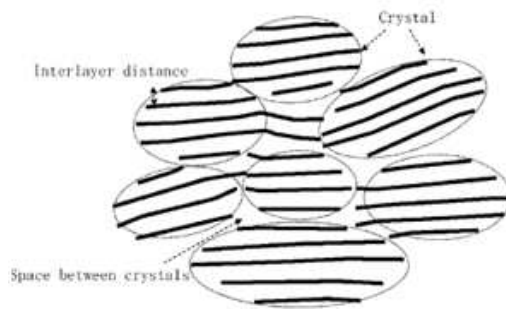
Figure 2.10: Crystal structural model of hydro-graphene

2.5.2 Turbostratic Carbons

When the regular ABAB...stacking of hexagonal crystal layered structure of graphite becomes randomly stacked, the name of the new structure is called as turbostratic carbon. Just like the hexagonal graphite, turbostratic carbon has a regular stacking of layer but only difference is the change in stacking degree [85]. Figure 2.11 [73] clearly illustrates the difference between graphitic and turbostratic carbons.
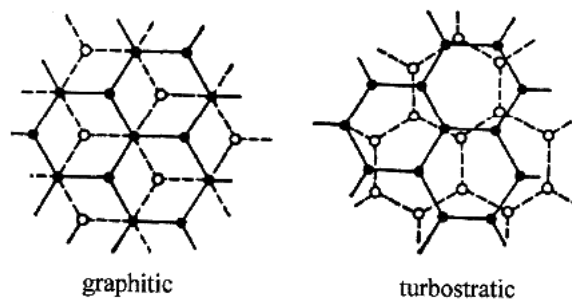
Figure 2.11: (a) Graphitic and (b) turbostratic stacking of carbon layers

The parallel stacking of the layers with complete randomness in turbostratic carbons can be obtained at lower pyrolysis temperatures. At temperatures below 1300°C, formation of hexagonal layers are small and their parallel stacking is incomplete. Application of a higher heat treatment will

graphene should be used only when the reactions, structural relations or other properties of individual layers are discussed"[84]

cause an increase in number and size of the hexagonal layers. Also this application will improve the regularity of the stacking degree in carbon structure [73]. So during heat treatment both graphitic and turbostratic carbon structures occur until all the stacking in the crystallite is approached in complete graphitic form. This random stacking of hexagonal layers is illustrated in Figure 2.12 [73].
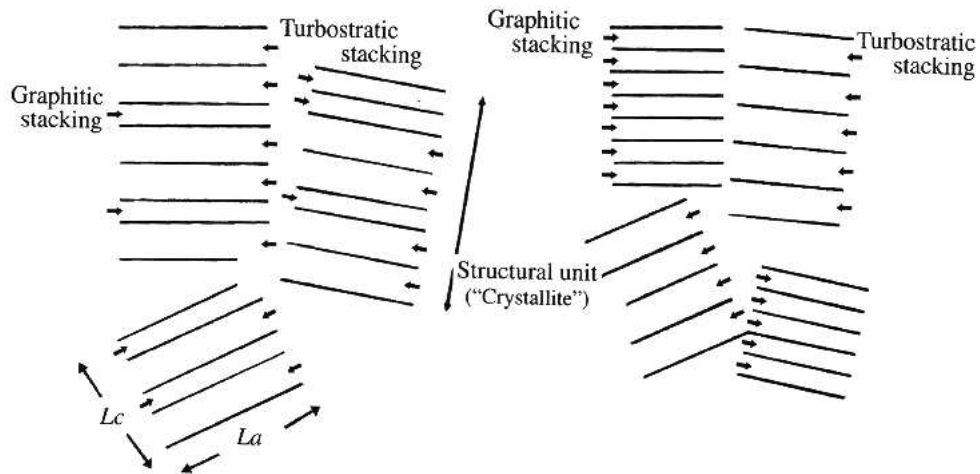
Figure 2.12: (a) Random formation of graphitic stacking in a crystallite and (b) coexistence of two crystallites with graphitic and turbostratic staking of hexagonal carbon layers

Chapter III

3   Experimental

This work consists of four main parts: pyrolysis of petroleum pitches under various conditions, non-isothermal kinetic studies of the pyrolysis of petroleum pitches, characterization of the produced hydrocarbons, and oxidation and expansion reactions of produced hydrocarbons.

3.1   Materials

The main raw materials of this study were two petroleum pitches. One of them was obtained from Turkish Petroleum Refineries Co. (TÜPRAŞ), Batman Refinery and it was named as pitch A. The other petroleum pitch was obtained from TUBITAK Marmara Research Center, Gebze and it was named as pitch B. Both petroleum pitches were used as they received. The analyses of the pitches used are given in Table 3.1 Ar (99.99%) and N_2 (99.99%) received from Karbogaz. Acetic anhydride (Merck, extra pure), Sulfuric acid (Fluka, 95-97%), Potassium dichromate (Chempur, 99.9%), Hydroquinone (Acros, 99%), and Sodium hydroxide (Merck, 97%) were used in oxidation and reduction experiments of hydro-graphenes. They were all used as received.

3.2 Pyrolysis of Petroleum Pitches

Two different petroleum pitches-pitch A and pitch B- were chosen as raw materials for hydro-graphene preparation by pyrolysis process. The different samples of hydro-graphene materials were produced by pyrolysis of two types of pitches. Pitches were placed in a ceramic boat, and then placed in a quartz tube which was finally put into the tube furnace. The pyrolysis experiments were carried in a tube furnace under argon atmosphere with a flow rate of 2.5 l/min. In order to investigate the effect of pyrolysis temperature and time on the formation of products, various temperature and time sets were performed during experimental studies. The pyrolysis temperature was in the range of 500-1000°C and the pyrolysis times were 30, 60, and 120 minutes.

3.3 Non-isothermal Kinetics of Pitch Pyrolysis

Non-isothermal kinetics of pitch pyrolysis experiments were performed in a Netzsch STA 449 C Jupiter differential thermogravimetric analyzer (precision of temperature measurement $\pm 2^{o}$C, microbalance sensitivity <5 μg), with which the sample weight loss and rate of weight loss as functions of time or temperature were recorded continuously, under dynamic conditions, in the range 25-1100°C. The experiments were carried out at atmospheric pressure, under inert (N_2) atmosphere, with a flow rate of 60 ml/min, at a linear heating rate of 10°C/min. Pyrolysis of the pitches was performed in the furnace of the thermobalance under controlled temperature to obtain the corresponding thermogravimetric (TG) curves with heating rates (β) of 5 K/min, 10 K/min, 20 K/min and 30 K/min. Preliminary tests with different sample masses and sizes and gas flow rates were carried out, in order to check the influence of heat and mass transfer. In experiments, it was found appropriate to use small masses around 20 mg of each pitch that were distributed as finely as possible in the in order to eliminate the effects of eventual side reactions and mass and heat transfer limitations. The experi-

ments were replicated at least twice to determine their reproducibility, which
was found to be very good.

3.4 Characterization

3.4.1 Elemental Analyses

Elemental analyses (C, H, N, and S) of pitch A and pitch B were con-
ducted at the Instrumental Analysis Laboratory of the TUBITAK Marmara
Research Center, Gebze by using a standard C-H-N-S analyzer. Data of the
elemental analyses of the pitch samples are presented in Table 3.1.

Table 3.1: Elemental analysis data for pitch A and pitch B (wt. %)

	%N	%C	%H	%S	H/C
Pitch A	0.68	82.85	9.72	6.44	1.40
Pitch B	0.61	85.40	10.26	4.03	1.44

3.4.2 Fourier Transform Infrared Spectroscopy (FTIR)

Chemical bonding (molecular structure) of the two pitches and samples
produced by their pyrolysis were examined by using a Bruker Equinox 55
FTIR spectrometer equipped with an ATR system by co-adding 20 scans
over the range 600-4000 cm^{-1} performed at 1 cm^{-1} of digital resolution.

3.4.3 Nuclear Magnetic Resonance (NMR)

Characterization of the molecular structure of the pitch A and pitch B were
done by ^{1}H-NMR spectroscopy utilizing Unity Inova 500 spectrophotometer
(Varian) and benzene-d6 as a solvent. Also, the change in the molecular
structure and aromaticity of the samples formed through pitch pyrolysis were
conducted by solid-state ^{13}C-NMR spectroscopy utilizing Unity Inova 500

spectrophotometer (Varian) with cross polarization (CP) and magic angle spining (MAS) .

3.4.4 Raman Spectroscopy

Structural changes in the hydro-graphenes were analyzed by Renishaw InVia Reflex Raman Microscopy System (Renishaw Plc., New Mills, Wotton-under-Edge Gloucestershire, UK) using a 514 nm argon ion laser in the range of 100 to 3200 cm^{-1}.

3.4.5 X-Ray Diffractometry (XRD)

Investigation of the change in the crystal structure and graphene layers of hydro-graphenes due to change in pyrolysis condition were examined by Bruker AXS advance powder diffractometer fitted with a Siemens X-ray gun, using Cu K_{α} radiation ($\lambda = 1.5406$ Å). The hydro-graphene samples were rotated at 10 rpm and swept from $2\theta = 10°$ through to $90°$ using default parameters of the program of the diffractometer that was equipped with Bruker AXS Diffrac PLUS software. The X-ray generator was set to 40 kV at 40 mA. All the XRD measurements were repeated at least two times and the results were the average of these measurements.

The XRD patterns were analyzed for the stuctural parameters by using the by using the classical Debye-Scherer equations:

$$t = 0.90\lambda/\beta_{002}cos\theta 002 \tag{11}$$

$$n = t/d_{002} \tag{12}$$

where t represents the thickness, β the full width half maxima (FWHM), d the interlayer spacing, and n is the number of graphene sheets.

The peak positions of the (002) peak and d_{002} were measured. FWHM values of the (002) peaks were calculated by the Bruker axs Diffrac PLUS software provided with the Bruker axs advance powder diffractometer.

3.4.6 Scanning Electron Microscopy (SEM)

Investigation of morphology of hydro-graphenes obtained from pitch pyrolysis, hydro-graphenes oxides, expanded hydro-graphenes oxides, and their reduced forms were carried out with Scanning Electron Microscope (SEM) analyses (Supra 35VP Field Emission SEM, Leo).

3.5 Oxidation, Expansion, and Reduction of Hydro-graphenes

3.5.1 Oxidation of Hydro-graphene

According to graphite oxidation method of Jia and Demopoulos [86], hydro-graphene oxide was prepared. Hydro-graphene obtained from pyrolysis of pitch A at 700°C for 2 hours was used in this process. With regard to work of Jia and Demopoulos, potassium dichromate was used as oxidizing agent [86]. In oxidation experiment, first chromic acid was prepared by stirring potassium dichromate and sulfuric acid in weight ratios of 2.1: 55 and 1.5 ml distilled water. Then 1.0 g of hydro-graphene was added to flask and the mixture was stirred gently. Finally, 1.0 g of acetic anhydride, which used as an intercalate, was slowly dropped into the solution. The solution was stirred at 45°C for 50 minutes. Oxidized hydro-graphenes were filtered and neutralized with 0.1 M NaOH. Then they were washed with distilled water until the solution becomes neutral. After washing step, hydro-graphene oxides were dried in a vacuum oven at 60°C overnight. In order to exfoliate hydro-graphene oxide into dispersed hydro-graphene oxide sheets, they were sonicated in distilled water for 1 h at room temperature via ultrasonic vibration.

3.5.2 Expansion of Hydro-Graphene Oxides

After ultrasonic bath, hydro-graphene oxide was expanded by thermal treatment up to 900°C rapidly in a tube furnace for 15 min under argon

atmosphere. After expansion step, hydro-graphene oxides were exposed to ultrasonic water vibration again for 1 h for dispersion. Sonicated hydro-graphene oxides were dried at 60°C in a vacuum oven overnight.

3.5.3 Reduction of Expanded Hydro-Graphene Oxides

Reduction and exfoliation of the expanded hydro-graphene oxides were achieved by refluxing in them in a mixture of hydroquinone and distilled water under N_2 atmosphere for 1 day. The graphene-based sheets were separated by filtration and washed with methanol and water three times and, dried in a vacuum oven at 60°C overnight.

Chapter IV

4 Results and Discussion

4.1 Elemental Analyses

Due to complex structure of pitches, each pitch may show different properties. Although both pitch types are complex mixtures of organic molecules consisting of polycyclic aromatic hydrocarbons (PAH), coal-tar pitch includes hetero-aromatic compounds in addition to PAHs, while petroleum pitch includes numerous alkyl-substituted PAHs [32]. In addition to this, the most important difference between petroleum and coal-tar pitch is the less toxic and carcinogenic properties petroleum pitches. Petroleum pitches have less metal, ash and heteroatom, especially sulfur, content than coal-tar pitches [46, 49, 51]. However, petroleum pitches (also coal-tar pitches) differ among themselves due to their production method and feedstock.

The elemental analyses of the pitches in Table 3.1 demonstrated that the carbon percentages of the pitch A and pitch B were 82.85 and 85.40, respectively. Hydrogen content of the pitch B was slightly higher than that of pitch A, 10.26 and 9.72, respectively. The H/C atomic ratios of the pitches were larger than 1. This indicated the liquid nature of the pitches. The significant difference between the two pitches was in their sulfur contents. While pitch A contained 6.44% sulfur, the sulfur content of pitch B was

4.03%. This difference in sulfur content points out to the variation of the origin of the pitches.

4.2 Pyrolysis of the Pitches

Pyrolysis of pitches A and B were carried out in a tube furnace by using the combination of methods of slow pyrolysis and pyrolysis under different gas environment. Slow pyrolysis method was used because the main aim of this study was to investigate the solid carbon structures formations. So both pitches were heated up with an uncontrolled slow heating rate and their residence times were between 15-120 minutes under an Ar atmosphere with a flow rate of 2.5 l/min. Sample mass of 10-15 g of pitches were distributed uniformly in alumina (Al_2O_3) crucibles, in order to obtain more accurate results.

After the pyrolysis reactions there were a serious mass loss in both pitches, and there were formations of tars on the surface of quartz tube, as well as solid carbon structures formations. It is observed that there were exclusions of gaseous products up to 600°C. The intense exclusion of yellow colored volatile materials at temperatures around 500-550°C indicated there was a removal of sulfur containing volatile matter. Also it was observed that during the removal of these gases, they were condensing at the end of the tube which remained outside the furnace. Due to these condensations, there was formation of tars at the edge of the tube. Furthermore, there was formation of tars in the inside of the tube as products. There was more tar formation at lower heat treatments due to the gasification of tar at higher pyrolysis temperature. Another evidence for this was cleaning up tubes being able at only high temperatures of >900°C, for at least 1 hour.

The sample weights of pitches before and after pyrolysis were recorded in each experiment. However, the problem of weighing products after the pyrolysis was stuck solid products inside the tube. It was almost impossible to collect all solid products without brushing the tube, so in each experiment

there was some sample loss which could not be measured. Tables 4.1 and 4.2 represent the weight of the pitches A and B (respectively) before the pyrolysis, and the weight of their products after the pyrolysis reaction.

Table 4.1: Solid product yield, sample weight before and after pyrolysis of pitch A

		1000°C	900°C	800°C	700°C	600°C	500°C
	Before	6.6	10.8	11.0	9.0	13.7	15.5
120 min	After	1.0	0.5	1.6	1.6	0.7	0.6
	Yield, %	14.4	4.7	14.7	19.4	5.3	3.9
	Before	13.3	7.7	8.0	12.6	10.5	12.3
60 min	After	1.3	1.3	1.6	1.1	1.2	1.6
	Yield, %	9.6	16.7	19.4	9.0	11.3	13.1
	Before	13.5	8.2	11.2	12.6	11.6	10.9
30 min	After	1.3	0.9	2.1	1.0	1.5	1.3
	Yield, %	9.2	10.6	18.5	7.9	12.7	12.2

Table 4.2: Solid product yield, sample weight before and after pyrolysis of pitch B

		1000°C	900°C	800°C	700°C	600°C	500°C
	Before	12.8	12.2	13.9	14.5	10.4	13.5
120 min	After	0.7	0.6	1.1	1.5	0.6	1.3
	Yield, %	5.4	4.9	7.9	10.3	5.8	9.6
	Before	10.7	9.7	8.7	9.6	8.4	10.1
60 min	After	0.8	0.9	0.9	1.13	1.1	0.3
	Yield, %	7.5	9.3	10.3	11.8	13.1	3.0
	Before	11.1	9.4	9.8	9.8	9.3	9.9
30 min	After	1.5	1.0	0.9	1.0	0.6	1.4
	Yield, %	13.5	10.6	9.2	9.7	6.5	14.1

4.3 Non-Isothermal Kinetic Analysis of Pitch Pyrolysis

Non-isothermal kinetic studies of pyrolysis of the pitches were based on the thermogravimetric measurements. The TG curves measured from the temperature programmed pyrolysis of the pitch A and pitch B at the heating rates (β) of 5 K/min, 10 K/min, 20 K/min and 30 K/min were illustrated in Figure 4.1 and 4.2, respectively. As it might be examined, on raising the temperature, both pyrolysis of pitch A and pitch B occurred with a related

mass loss. Once the volatile content of the pitches were consumed, the mass corresponding to the formed carbon structures stayed almost constant. Given the small sample amounts and relatively slow heating rates, the weight loss versus temperature curves showed one main zone, as in the examples for pyrolysis of two biomass fuels (wood chips and pine seed shells) [87] and pitch pyrolysis [2] under inert atmosphere. This main zone of weight loss, temperatures below 500°C and conversion up to 75%, was the pyrolysis (or devolatilization) stage. The sequel zone after the main pyrolysis zone showed very low conversion value indicating that the exclusion of volatile matters occurred in the first zone.
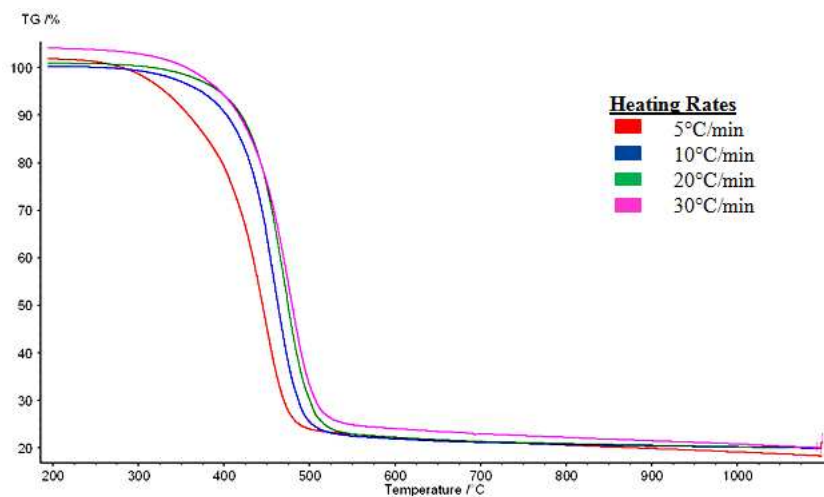
Figure 4.1: TGA tracings obtained during the pyrolysis of pitch A with different heating rates in the temperature range of 25-1100°C.

Figure 4.1 and 4.2 respectively shows the TG mass loss curve of the pyrolysis of pitch A and pitch B with at various heating rates (β) (5, 10, 20 and 30 K/min) in order to study the effect of heating rate on non-isothermal kinetics. As Figure 4.1 and 4.2 indicated the main temperatures for mass losses for every heating rate for both pyrolysis of pitch A and pitch B, respectively. For pitch A, the temperature range was 479-515°C; as the heating rate was increased the lower mass losses were detected at higher temperatures. For pitch B, the temperature range was 489-533°C; in this range higher heating rates caused lower mass losses at more elevated temperatures. Residual
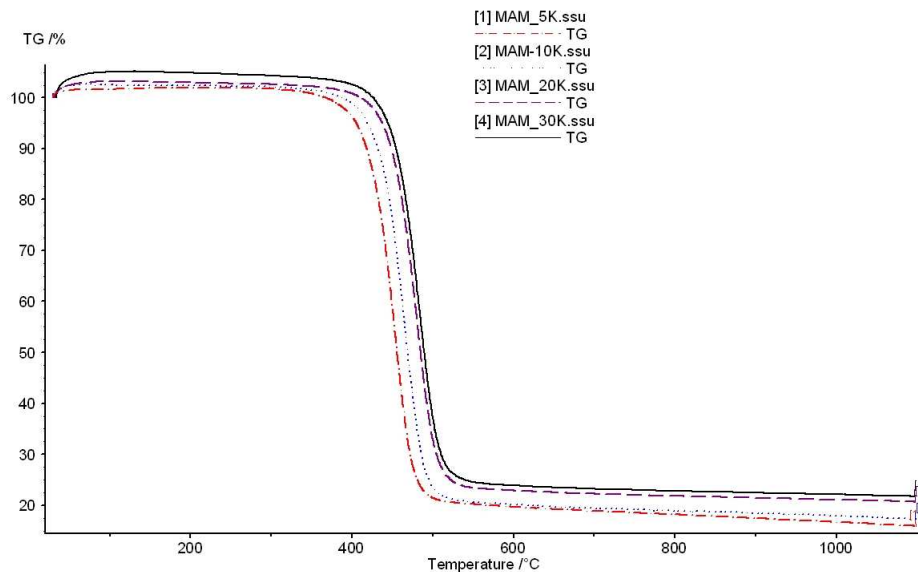
Figure 4.2: TGA tracings obtained during the pyrolysis of pitch B with different heating rates in the temperature range of 25-1100°C.

masses of pitch A pyrolysis in the range of 18.3-20.0% were obtained at about 1098-1099.3^{o}C, while residual masses of pitch B pyrolysis in the range of 15.8-21.7% were obtained at about 1097.1-1099.3^{o}C. The TG curves of pitch A and pitch B also demonstrated that there was a main step for mass loss in each graph. Pyrolysis of pitch A showed, depending on the heating rate at about 479-515°C, 72.3-73.4% of the volatiles were lost. On the other hand, pyrolysis of pitch B showed, depending on the heating rate at about 489-533°C, 74.6-77.2% of the volatiles were lost. At the end of the measurements, the total material lost of pitch A and pitch B were in the range of 80.0-81.8% and 78.3-84.2%, respectively. Higher heating rates caused less material loss compared to the loss of material at lower heating rates in both pyrolysis of pitches. Since small masses of pitches (20-25 mg) were utilized in each experiment, mass and heat transfer limitations were eliminated. The data obtained using different heating rates during pyrolysis experiments therefore did not contain any restrictive resistances. As the heating rate was increased, the maximum mass loss shifted to higher temperatures. This was attributed to the changes in the rate of heat transfer with the increase in the heating

38

rate and the short exposure time to a particular temperature at high heating rates, as well as the effect of the kinetics of pyrolysis.

Seven different percentages of conversion (α) were pointed out in each curve of pitch A pyrolysis mechanisms; 10, 20, 30, 40, 50, 70, and 80%. Figure 4.3 illustrates the indication of temperatures with respect to conversion values of pyrolysis of pitch A with a heating rate 30K/min. Depending on the TG curve, six different percentages of conversion (α) are pointed out in each curve of pitch A pyrolysis mechanisms; 10, 20, 30, 40, 50, and 70%. Figure 4.4 illustrates the indication of temperatures with respect to conversion values of pyrolysis of pitch B with a heating rate 30K/min.
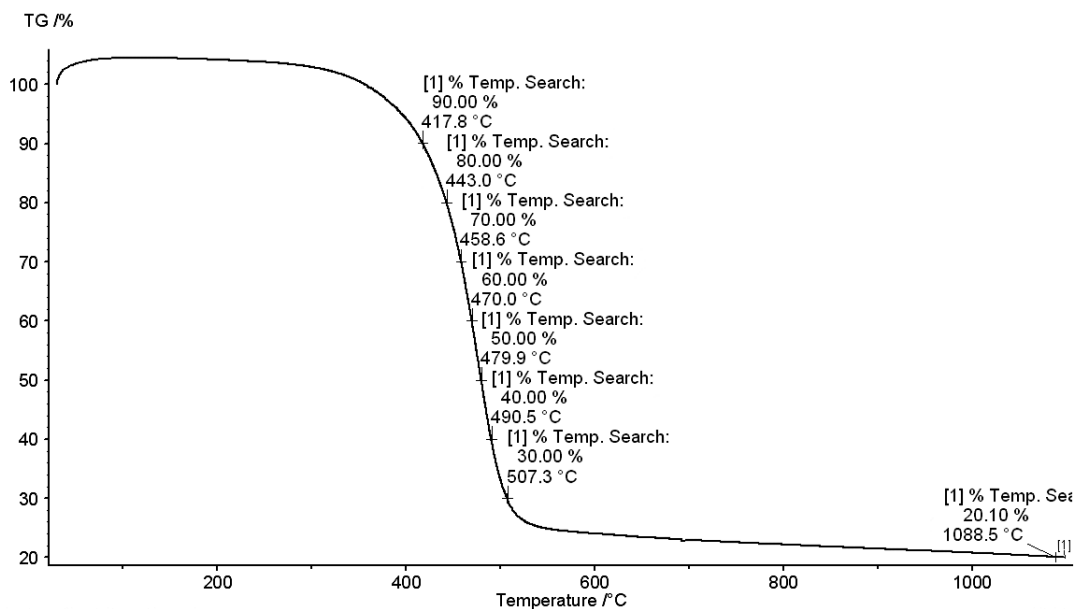
Figure 4.3: Indication of the temperatures with respect to conversion in TGA tracings of pyrolysis of pitch A at a heating rate of 30K/min.

TG /%

[1] % Temp. Search:
90.00 %
455.1 °C
[1] % Temp. Search:
80.00 %
467.3 °C
[1] % Temp. Search:
70.00 %
475.8 °C
[1] % Temp. Search:
60.00 %
483.1 °C
[1] % Temp. Search:
50.00 %
490.1 °C
[1] % Temp. Search:
40.00 %
497.9 °C
[1] % Temp. Search:
30.00 %
510.8 °C
[1] % Temp. Search:
23.00 %
745.8 °C
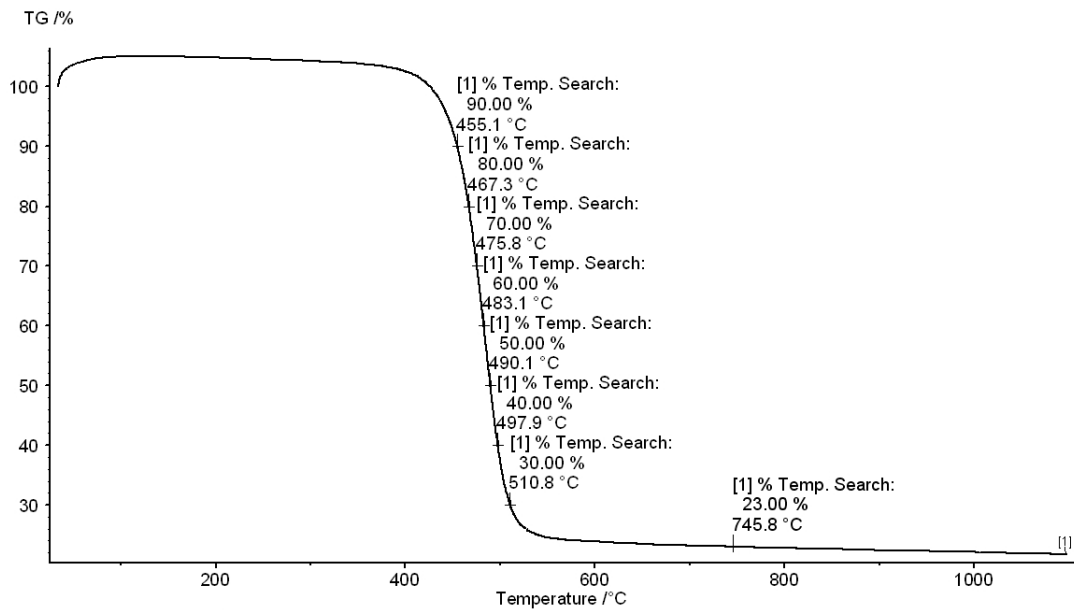
Temperature /°C

Figure 4.4: Indication of the temperatures with respect to conversion in TGA tracings of pyrolysis of pitch B at a heating rate of 30K/min.

By plotting ln (β) versus 1/T, we estimated activation energy, E. Figure 4.5 and 4.6 illustrated the kinetic model proposed by Ozawa-Flynn-Wall to various conversion percentages corresponding to the pyrolysis of pitch A and pitch B at different heating rates for the calculation of activation energies, respectively.

40
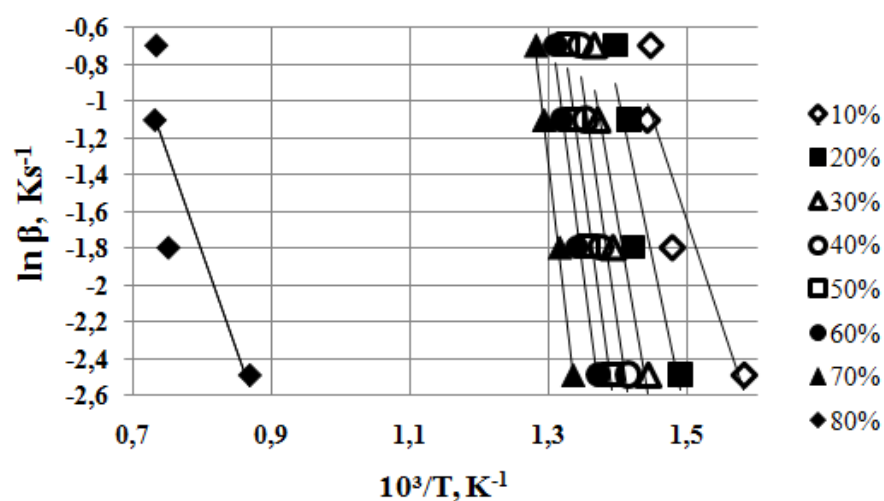
Figure 4.5: Curves of fitting to kinetic model proposed by Ozawa-Flynn-Wall to various conversion percentages corresponding to the pyrolysis of pitch A at different heating rates for the calculation of activation energies
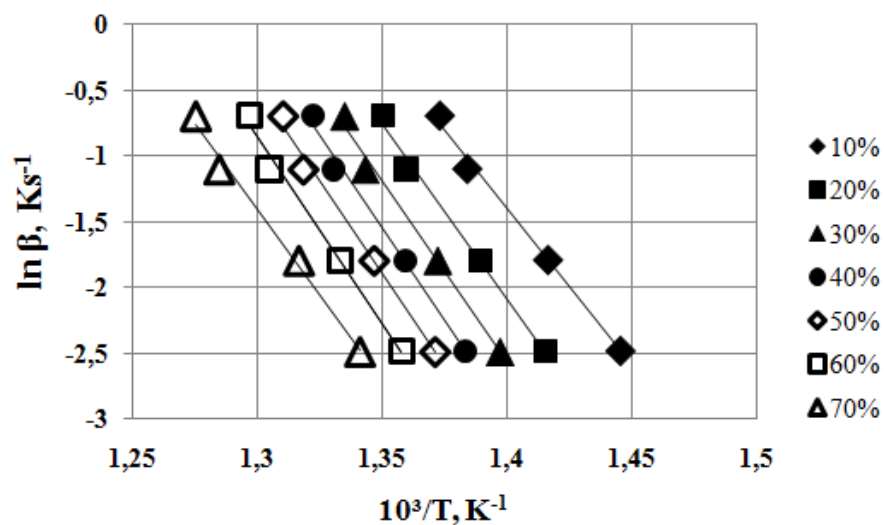
Figure 4.6: Curves of fitting to kinetic model proposed by Ozawa-Flynn-Wall to various conversion percentages corresponding to the pyrolysis of pitch B at different heating rates for the calculation of activation energies

After the plotting of these graphs, it was clear that there were linear relations for the conversion percentages. So the activation energies of both

41

pitches were calculated from the corresponding slopes according to the Ozawa-Flynn-Wall kinetic method. The results for the estimations of activation energies of pyrolysis of pitch A and pitch B are illustrated in Table 4.3 and 4.4, respectively

Table 4.3: Slopes and correlation coefficients (R^2) corresponding to linear fittings to kinetic model proposed by Ozawa-Flynn-Wall to various conversion percentages corresponding to the pyrolysis of pitch A at different heating rates together with the resultant activation energy (E) values.

Conversion, %	R^2	Slope	Activation Energy, kJ/mol	Average Activation Energy, kJ/mol
10	0.841	-11.12	87.9	
20	0.854	-17.85	141.1	Rate determining
30	0.915	-21.36	168.9	reactions
40	0.955	-25.09	198.3	
50	0.973	-27.38	216.4	185.7
60	0.982	-28.46	224.9	
70	0.998	-33,24	262.7	
80	0.773	-10,61	83.9	Fast reactions 83.9
Overall Average Activation Energy, 173 kJ/mol				

Raising the temperature, pyrolysis of the pitch A occurred with mass losses and related decrease in activation energies at the second zone. Activation energy calculated at 10% conversion was 87.9 kJ/mol and steadily increased until 70% conversion to a value of 262.7 kJ/mol then as the material loss increased beyond this point, the again activation energy decreased to 83.9 kJ/mol at conversion of 80%. It seemed that the first phase of reactions constituted the rate determining set of reactions with average activation energy of 185.7 kJ/mol. The overall average activation energy of the pyrolysis of the pitch A was calculated to be 173 kJ/mol. This value calculated for pitch A was higher than the activation energy of pyrolysis of pitch (produced from bitumen) by Yue and Watkinson [2].

Table 4.4: Slopes and correlation coefficients (R^2) corresponding to linear fittings to kinetic model proposed by Ozawa-Flynn-Wall to various conversion percentages corresponding to the pyrolysis of pitch B at different heating rates together with the resultant activation energy (E) values.

Conversion, %	R²	Slope	Activation Energy, kJ/mol
10	0.994	-23.96	189.4
20	0.992	-26.61	210.3
30	0.991	-27.64	218.4
40	0.991	-28.07	221.8
50	0.991	-28.30	223.7
60	0.991	-28.15	222.5
70	0.991	-26.12	206.4
Overall Average Activation Energy, 213.2 kJ/mol			

For pyrolysis of pitch B there was only one reaction zone that was available to be calculated for estimation of activation energy. Due to the raising the temperature, pyrolysis of the pitch A occurred with mass losses in the reaction zone with a continuous increase in activation energies, and then a slight decrease in the last conversion step. Activation energy calculated at 10% conversion was 189.4 kJ/mol and steadily increased until 60% conversion to a value of 222.5 kJ/mol. Then due to the material loss, at conversion of 70% activation energy slightly decreased to 206.4 kJ/mol. The overall average activation energy of the pyrolysis of the pitch B was calculated to be 213.2 kJ/mol. According to these values, overall average activation energy of pitch B was higher than both the overall and the average rate determining activation energy of pitch A. In order to make a more accurate comparison, we compared only the activation energies of both pyrolysis up to a conversion 70%. The activation energy of pitch B, 213.2 kJ/mol, was higher than activation energy of A, 185.7 kJ/mol. These results indicated that pitch B contained probably structures that were harder to pyrolyze relative to those present in pitch A. So that pitch B was harder to pyrolyze whereas pitch A had probably more degradable compounds in its structure. Activation energies of both pitches A and B were higher than the activation energy measured

by Yue and Watkinson [2] in pyrolysis of a pitch produced from a bitumen.

Our next step was figuring out the reaction orders of pitch pyrolysis reactions. For this purpose, we applied Avrami's theory for non-isothermal case description [69, 70, 71]. The plots of ln [-ln (1- α (T)] versus ln β is represented in Figure 4.7and 4.8 for the computation of the reaction orders of pitch A and B, respectively.
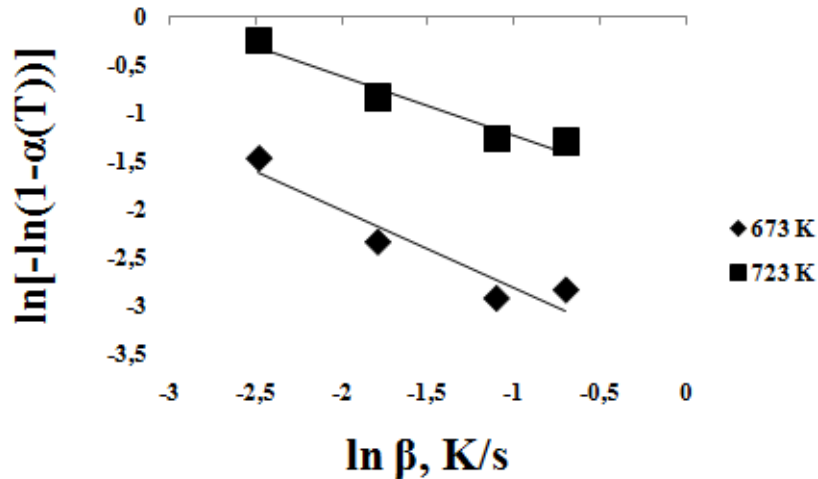
Figure 4.7: Straight lines fitting to Ozawa-Flynn-Wall kinetic model for various conversion percentages corresponding to the pyrolysis of pitch A at different heating rates for the determination of reaction order n.

The n values as a function of temperature for pyrolysis of pitch A and B are represented in Table 4.5. The reaction order values of pitch A changed from 1.12 to 1.56 with increasing temperature. However, the reaction order for the pyrolysis of pitch B was lower value, 0.91. Variations of these reaction orders were dependent on the complex structure of pitches. Reaction order of pitch A was dependent on the extent of the reaction, i.e., not constant during the reaction, which was an evidence of the multiple step process. Reaction orders closer to zero in the case of pitch B, indicated that the pyrolytic reactions might probably occurred in more heterogeneous media, such as solid-liquid or solid-gas.

44
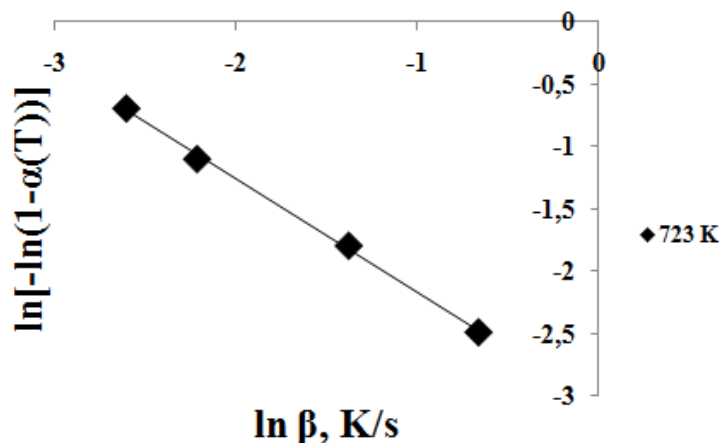
Figure 4.8: Straight lines fitting to Ozawa-Flynn-Wall kinetic model for various conversion percentages corresponding to the pyrolysis of pitch B at different heating rates for the determination of reaction order n.

Table 4.5: Reaction order (n) as a function of temperature for the pyrolysis of pitch

	T, K	R^2	Reaction Order, n	Average Reaction Order, n
Pitch A	673	0.898	1.1	1.3
	723	0.949	1.6	
Pitch B	723	0.998	0.9	0.9

4.4 Characterization

4.4.1 FTIR Analyses

FTIR spectra recorded in the 400-4000 cm^{-1} region of original pitch A and pitch B are presented in Figure 4.9 and 4.10, respectively. FTIR spectrum of the pitch A contained a strong stretching of aliphatic groups (-CH$_3$ and >CH$_2$) attached to aromatic at 2850-2920 cm^{-1}, ring vibration of aromatic compounds at 1540-1576 cm^{-1}, a strong peak belonging to aliphatic compounds at 1460 cm^{-1} and methylbenzene derivatives at 1375 cm^{-1}, several distinct peaks of C-H bending and a possible sulfur stretching in the finger print region between 700 and 810 cm^{-1}. More specifically, the bands represented -CH$_3$ asymmetric stretching of methyl or methylene groups at

2919 cm^{-1}, >CH$_2$ symmetric stretching of saturated hydrocarbons at 2850 cm^{-1}, ring vibrations of aromatic compounds (-N=N- stretching of aromatic azo compounds were also possible in this region) at 1540-1576 cm^{-1}, -CH$_3$ asymmetric and symmetric bending of aliphatic hydrocarbon chains respectively at 1460 cm^{-1} and 1375 cm^{-1}, C-H bending at 724 and 810 cm^{-1}, and a possible -C-S-C- stretching of dialkyl sulphide between 600-750 cm^{-1} [88].

FTIR spectra of pitch A was a demonstration of its complex structure and its content. Most of these bands have contribution from both aromatic and aliphatic compounds and methyl derivatives. More specifically, the bands occurred at 1400-1460 cm^{-1} (characteristic of aliphatic chains), 1550-1600 cm^{-1} (aromatic compounds), 2850-2920 cm^{-1} (CH$_3$ and CH$_2$ stretching of methyl or methylene groups) [88].
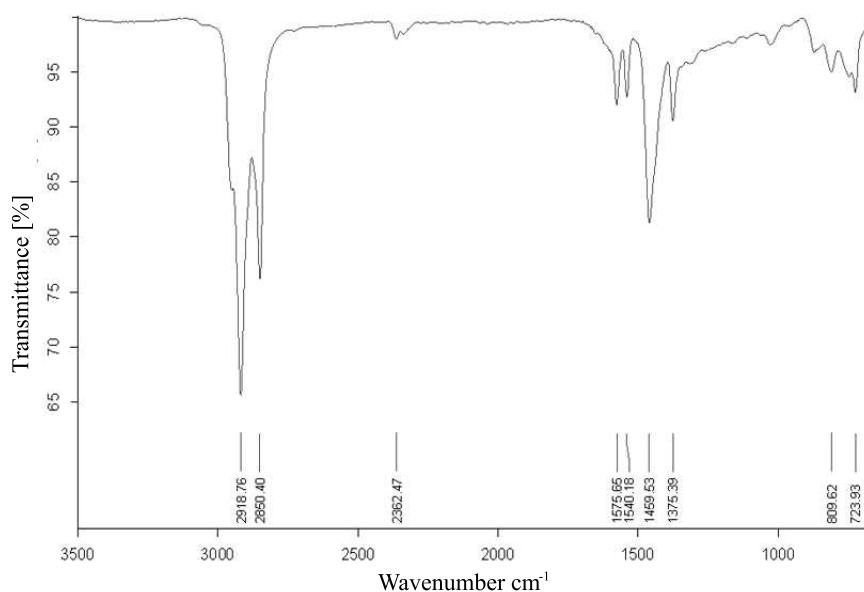
Figure 4.9: FTIR spectrum of pitch A

46
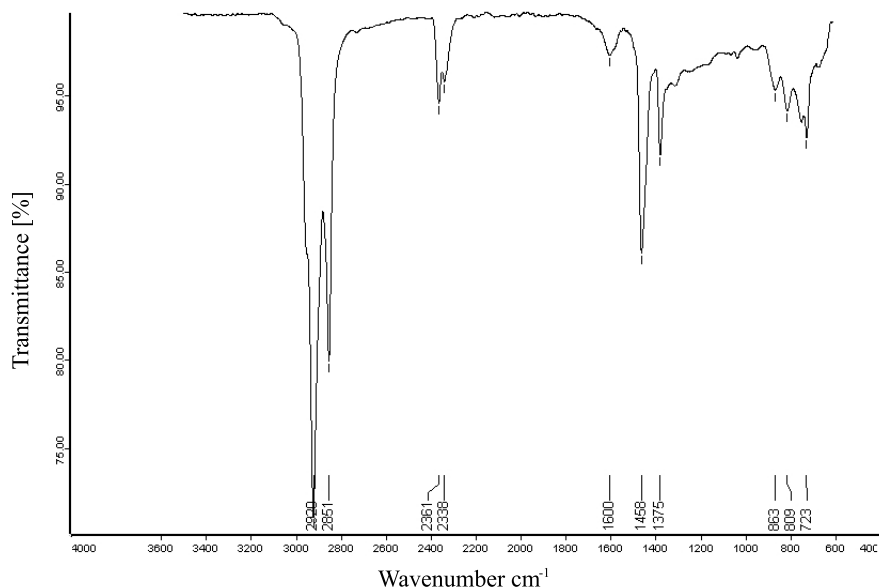
Figure 4.10: FTIR spectrum of pitch B

FTIR spectrum of the pitch B included a strong stretching of aliphatic groups attached to aromatic compounds at 2850-2900 cm^{-1}, ring vibration of aromatic hydrocarbons at 1600 cm-1, a strong peak of aliphatic hydrocarbon chains at 1458 cm^{-1}, and methylbenzene derivatives at 1375 cm^{-1}, several distinct peaks of C-H bending and probably a sulfur stretching in the finger print region between 700 and 865 cm^{-1}. More precisely, the bands represented -CH and >CH$_2$ symmetric stretching of saturated hydrocarbons, respectively at 2919 and 2850 cm^{-1}, ring vibrations of aromatic compounds ant 1600 cm^{-1}, -CH$_3$ asymmetric and symmetric bending of aliphatic hydrocarbon chains respectively at 1458 cm^{-1} and 1375 cm^{-1}, C-H bending at 723, 809 and 863 cm^{-1} [88]. Comparison of spectra of pitch A and pitch B demonstrated that pitch A probably had a more aromatic structure due to the ratio of the aliphatic and aromatic peaks (in the range of 1400-1450 cm^{-1} and 1550-1650 cm^{-1}, respectively). FTIR spectrum of pitch B illustrated the peaks aliphatic compounds' intensities were stronger than aromatic peaks relative to strong of aliphatic peaks in spectrum of pitch A.

The FTIR spectra of the carbon structures (hydro-graphenes) obtained

47

from the 2 h pyrolysis of pitch A at 500, 700, and 900°C are presented in Figure 4.11, 4.12, and 4.13 respectively.
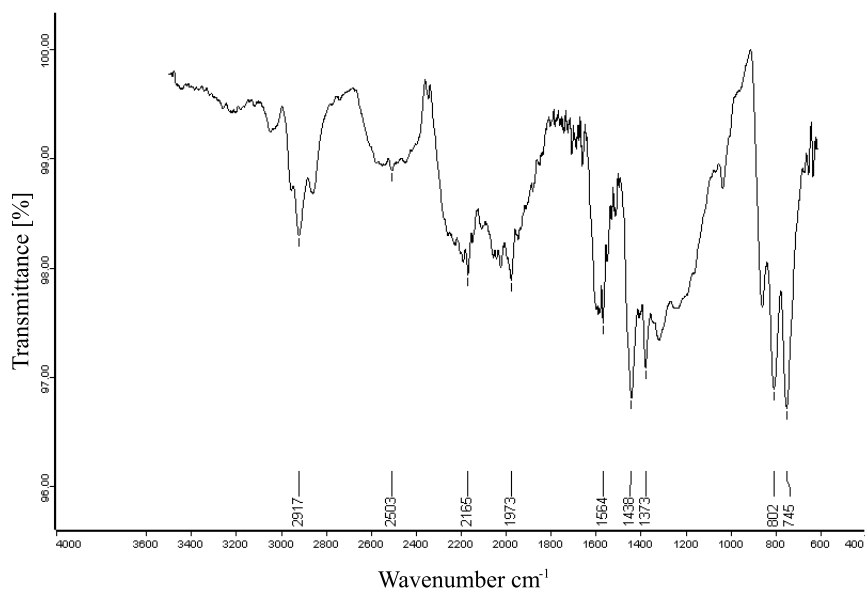
Figure 4.11: FTIR spectra of hydrographenes from pyrolysis of pitch A at 500°C for 2h
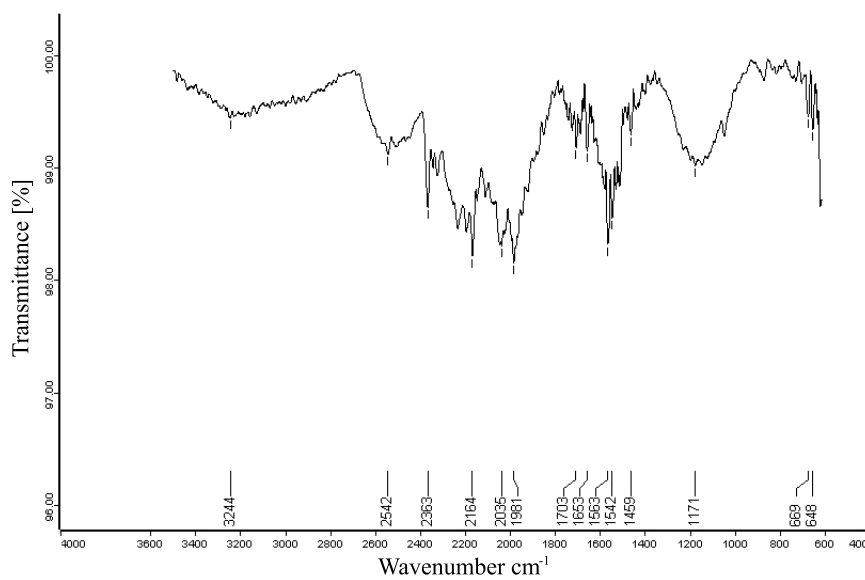
Figure 4.12: FTIR spectra of hydrographenes from pyrolysis of pitch A at 700°C for 2h
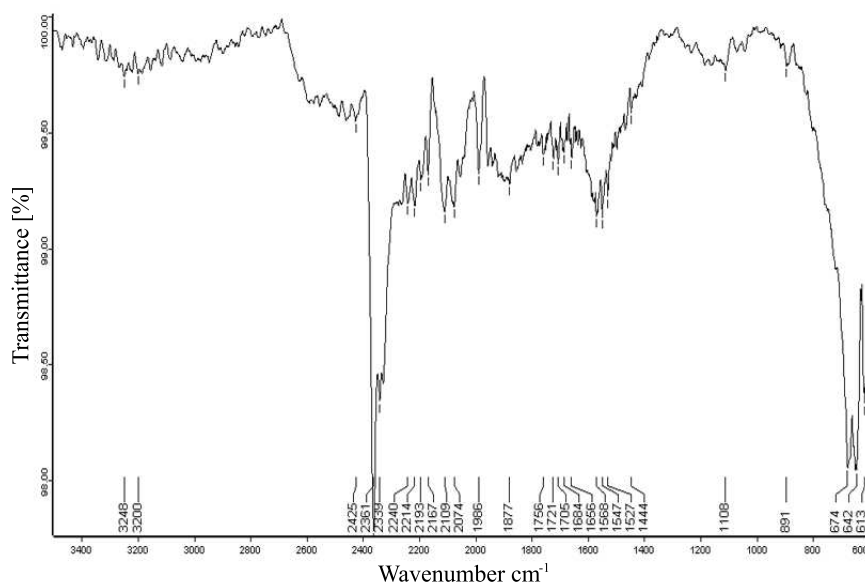
Figure 4.13: FTIR spectra of hydrographenes from pyrolysis of pitch A at 900°C for 2h

There were significant changes in the spectra of hydrographenes with respect to increasing pyrolysis temperature. When pyrolysis temperature was increased to 500°C, the band of -CH$_3$ asymmetric stretching at 2919 cm^{-1} shifted to 2017 cm^{-1} with a weaker intensity, >CH$_2$ symmetric stretching of saturated hydrocarbons at 2850 cm^{-1} was lost, the difference between intensities of ring vibration of aromatic compounds at 1564 cm^{-1} and bending of CH in aliphatic compounds at 1400-1450 cm^{-1} was decreased indicating there was a loss in aliphatic compounds. Also, there was formation of overtone and combination bands at 1650-2000 cm^{-1} and a shifting of -CH bending in the finger print region at 750-800 cm^{-1}. Increasing the temperature to higher degrees, 700°C, spectrum demonstrated that stretching of aliphatic groups attached to aromatic compounds were lost (at 2850-2920 cm^{-1}), more peaks of ring vibration of aromatic compounds formed at 1540-1650 cm^{-1} (indicating increase in the aromatic structure), a steady decrease in the intensity -CH bending in aliphatic compounds continued at 1459 cm^{-1}, and formation of oxidation peak at 1703 cm^{-1} and methyl rocking at 1171 cm^{-1} occurred.

49

The spectrum of hydrographenes formed at 900°C for 2 hours contained an increase in the overtones and combination bands of benzene derivatives at 1650-2000 cm^{-1}, increase in the oxidation peaks around 1700 cm^{-1}, decrease in bending of aliphatic hydrocarbons at 1444 cm^{-1}, and most importantly increase in the ring vibration of aromatic hydrocarbons at 1550-1650 cm^{-1}. Also, similar to Figure 4.12, it contained formation of methyl rocking at 1108 cm^{-1}. The spectra of hydrographenes clearly demonstrated the change in the chemistry of products as the pyrolysis temperature was increased. The significant decrease in the peaks and intensities of aliphatic groups at 2850-2920 cm^{-1} and 1400-1450 cm^{-1}, and increase in the ring vibrations of the aromatic hydrocarbons at 1550-1650 cm^{-1} was an important result. The decrease in the aliphatic hydrocarbons with increasing pyrolysis temperature was the expected result, because higher pyrolysis temperatures favor formation of aromatic carbons [32].

The FTIR spectra of the carbon structures (hydro-graphenes) obtained from the 2h pyrolysis of pitch B at 600 and 1000°C are presented in Figure 4.14 and 4.15, respectively. Similar to product spectra of pitch A, there were significant changes in the spectra of hydrographenes from pitch B with respect to increasing pyrolysis temperature. Increasing pyrolysis temperature up to 600°C with a residence time of 2 hours caused loss of stretching of aliphatic groups attached to aromatic compounds at 2850-2900 cm^{-1}, formation of more ring vibrations of aromatic compounds at 1500-1600 cm^{-1}, a decrease in the intensities of aliphatic hydrocarbon chains a 1375-1460 cm^{-1}, and formations of oxide peaks and overtone/combination of bands of benzene derivatives around 1702 cm^{-1} and 1800-2000 cm^{-1}, respectively. Also, there was a formation of methyl rocking at 1150 cm^{-1}. When pyrolysis temperature of pitch B was increased to 1000°C, the bands of ring vibrations of aromatic hydrocarbons increased in number at 1500-1650 cm^{-1} with stronger intensities than aliphatic hydrocarbon chains at 1400-1450 cm^{-1}, the methyl rocking shifted from 1150 cm^{-1} to 1107 cm^{-1}, and oxidation

peaks increased in number at 1700-1750 cm^{-1} with a stronger intensity. The spectra of samples from pyrolysis of pitch B demonstrated that ratio of intensities of aliphatic groups (1380-1450 cm^{-1}) to aromatic groups (1480-1650 cm^{-1}) decreased with increasing pyrolysis temperature. Also, the bands of aliphatic groups attached to aromatic compounds (2850-2920 cm^{-1}) disappeared totally. These are the evidences that higher heat treatment favors the formation of more aromatic structures in pitch pyrolysis products, as well as degradation of aliphatic compounds.
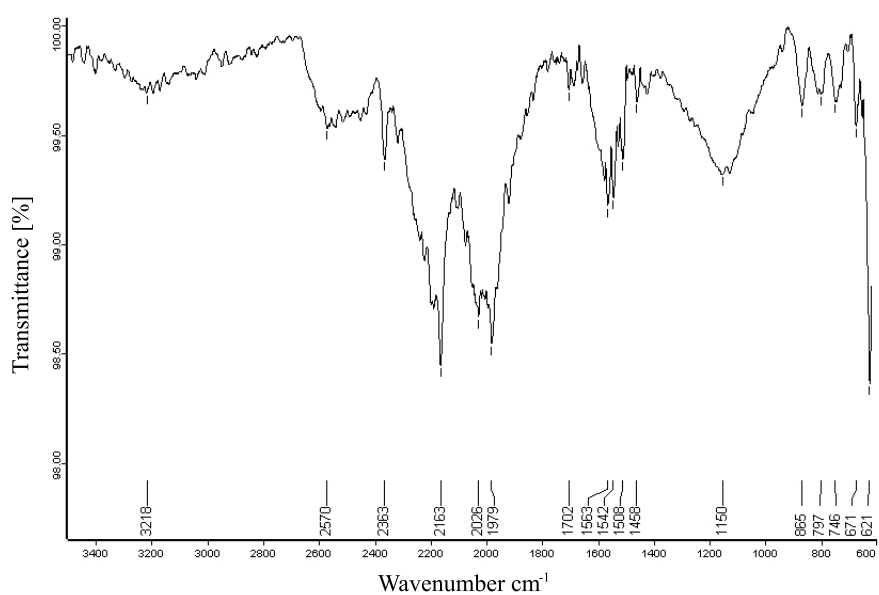
Figure 4.14: FTIR spectra of hydrographenes from pyrolysis of pitch B at 600°C for 2h
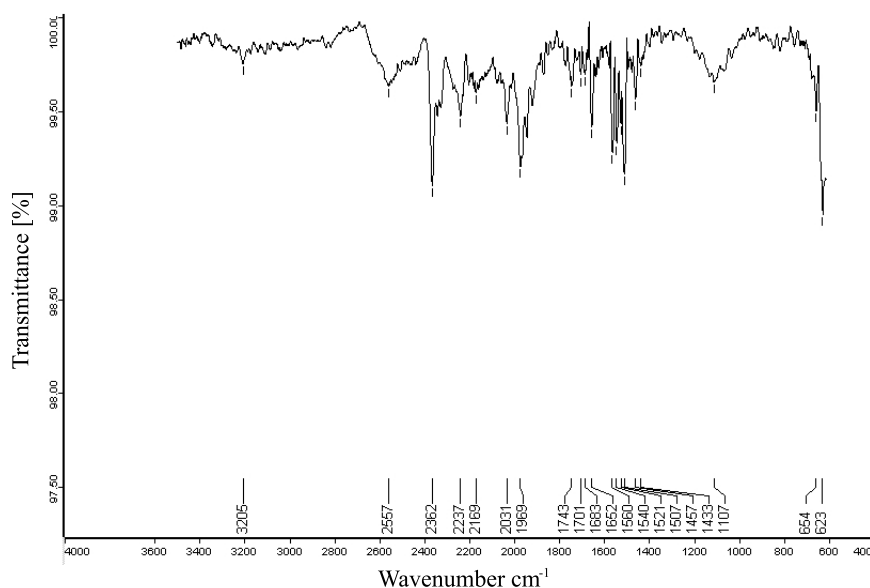
Figure 4.15: FTIR spectra of hydrographenes from pyrolysis of pitch B at 1000°C for 2h

In addition to temperature effect on molecular structure, time effect on pyrolysis products were investigated. The FTIR spectra of the carbon structures (hydro-graphenes) obtained from pyrolysis of pitch A at 800°C for 30, 60 and 120 minutes are presented in Figure 4.16, 4.17, and 4.18, respectively. There were significant changes in the spectra with respect to time. It was apparent that stretching of aliphatic groups attached to aromatic compounds at 2850-2920 cm^{-1} was lost, range of ring vibrations of aromatic hydrocarbons increased from 1540-1575 cm^{-1} to 1500-1660 cm^{-1} with stronger intensities, aliphatic hydrocarbon chains were lost (it occurred at spectrum of 2 hour pyrolysis with one peak, but with a lower intensity than the aromatic hydrocarbons), oxidation bands around 1700 cm^{-1} occurred after 1 hour heat treatment, and methyl rocking around 1120-1150 cm^{-1} formed after 1 hour treatment. As a result, aromatic structure formation was favored with increasing pyrolysis time (ratio of aliphatic intensities to aromatic intensities decrease continuously and aliphatic groups attached to aromatic were eliminated with increasing time).
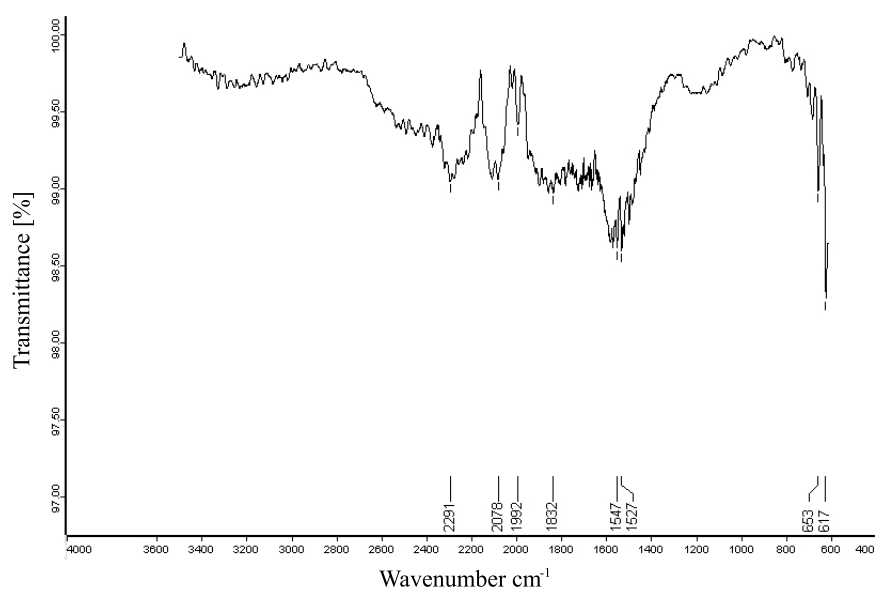
Figure 4.16: FTIR spectra of hydrographenes from pyrolysis of pitch A at 800°C for 30 minutes
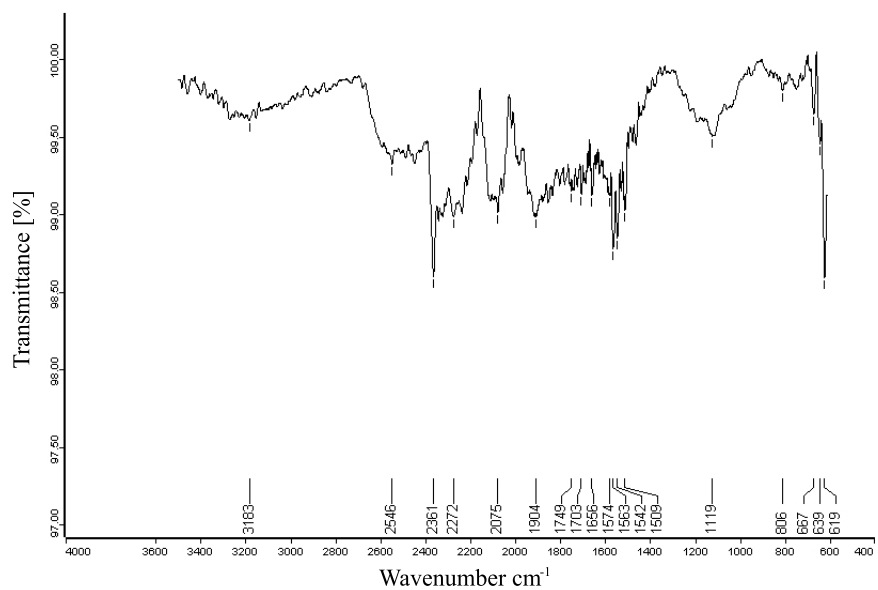
Figure 4.17: FTIR spectra of hydrographenes from pyrolysis of pitch A at 800°C for 1 h
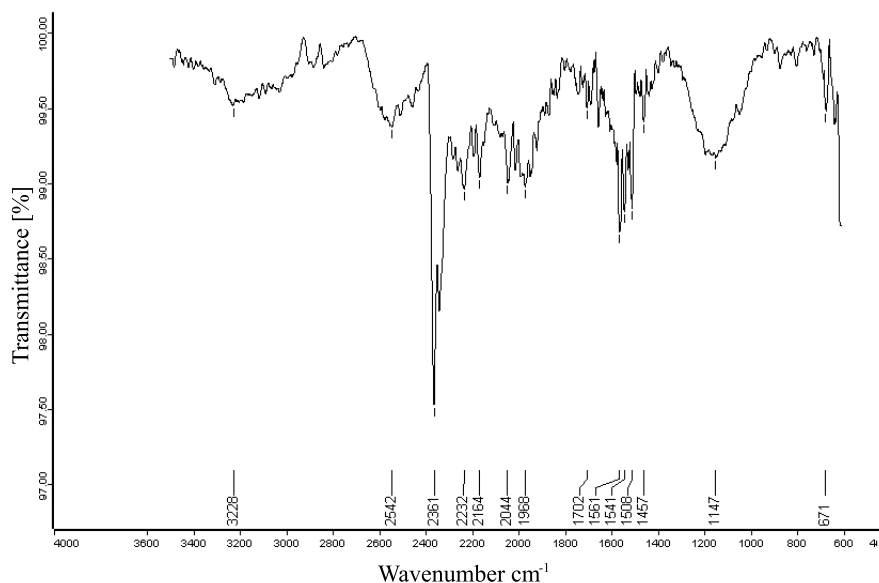
Figure 4.18: FTIR spectra of hydrographenes from pyrolysis of pitch A at 800°C for 2 h

4.4.2 NMR Analyses

The molecular structures of pitch A and pitch B were examined ^{1}H-NMR in addition to FTIR analyses. Figure 4.19 represents the ^{1}H-NMR spectra of pitch A and pitch B from 0 to 7 ppm. Both spectra of pitch A and pitch B contained chemical shifting of saturated hydrocarbons between 0.5-1.3 ppm. More specifically, there were chemical shifts of primary hydrocarbons (R-CH$_3$) at 0.9 ppm, secondary hydrocarbons (R$_2$-CH$_2$) at 1.3 ppm, and probably cyclohydrocarbons around 0.5 ppm in the both spectra of pitch A and pitch B [89]. When the range between 4-7 ppm was magnified, we obtained the spectra in Figure 4.20. Magnified spectra showed that pitches had aromatic structures also. ^{1}H-NMR spectrum of pitch A contained chemical shifts of vinylic (C=C-H) compounds at 5.0-5.3 ppm and aromatic compounds at 6.5-7.0 ppm [89]. ^{1}H-NMR spectrum of pitch B contained the similar chemical shifts with spectrum of pitch A however, spectrum of the pitch B contained smaller integrated values of the chemical shifting areas

54

with respect to pitch A. the ^{1}H-NMR spectra both pitch A and pitch B indicated that they contained both aliphatic and aromatic compounds in their structure. According to the intensity ratios of the peaks, aliphatic structures seemed to be dominating over the aromatic structures. Also, ^{1}H-NMR spectra of pitches between 4-7 ppm indicated that pitch A contained probably more aromatic structures than pitch B.
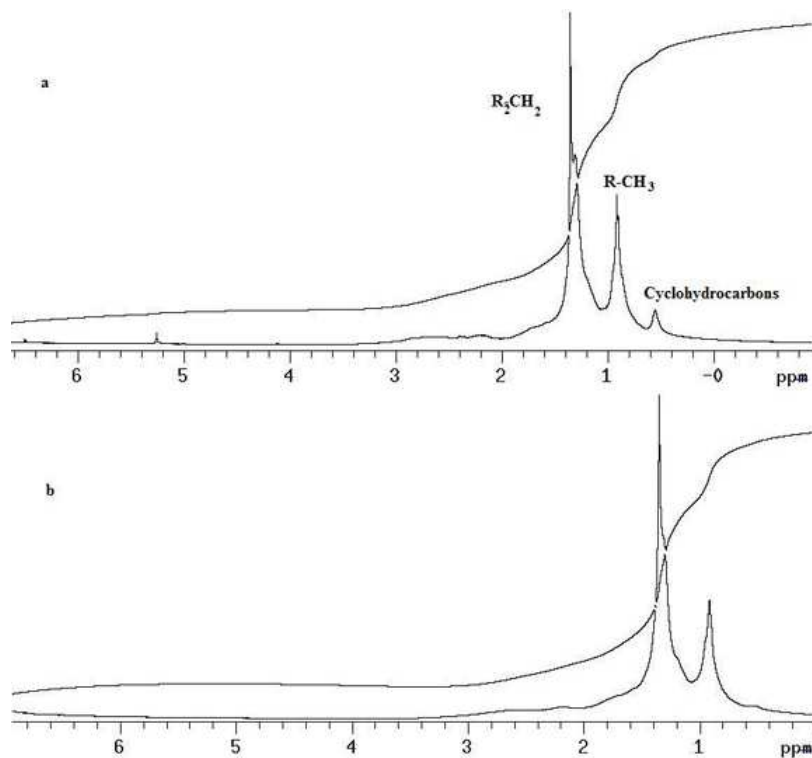
Figure 4.19: ^{1}H-NMR spectra of (a) pitch A and (b) pitch B in range of 0-7 ppm

55
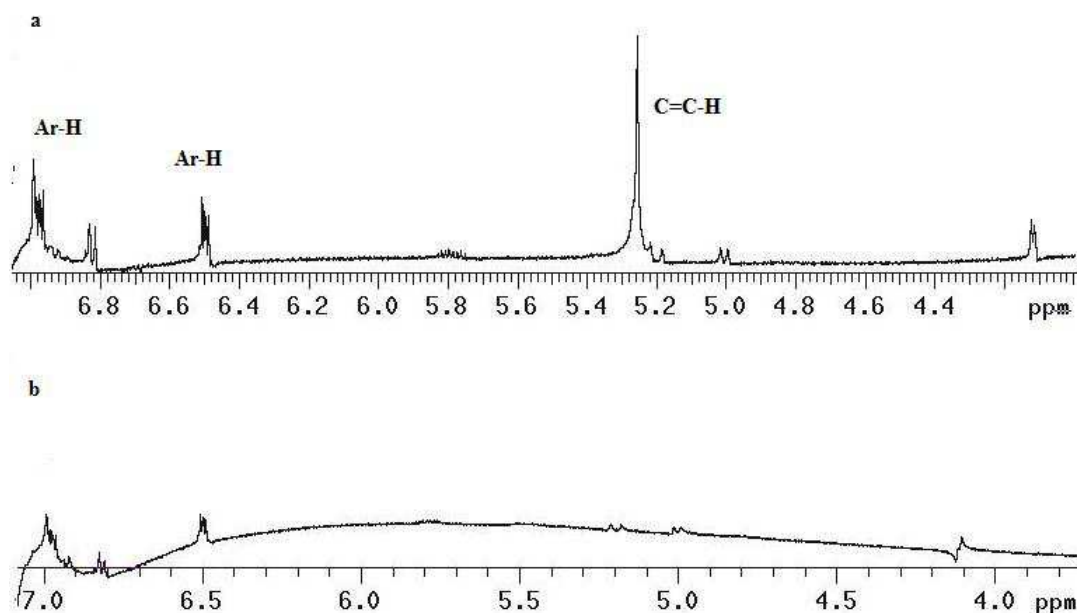
Figure 4.20: ^{1}H-NMR spectra of (a) pitch A and (b) pitch B in range of 4-7 ppm

The molecular structures of the hydrographenes were analyzed by solid-state ^{13}C-NMR. Figure 4.21 represents the solid-state ^{13}C-NMR spectra of hydrographenes from pyrolysis of pitch A for 2 hours. The spectra contained chemical shifting of carbonyl groups at 200-215 ppm, aromatic C-O at 150-200 ppm, aromatic C-H and C-C at 100-150 ppm, branched aliphatic ethers at 60-100 ppm, and a broad shifting of aliphatic groups at 0-60 ppm [90]. The chemical shifting of carbonyl group was lost at temperature 700°C. As the temperature increased chemical shifting of aliphatic compounds were lost prior to aromatic compounds. Until 900°C, the intensity of aromatic groups was higher than that of aliphatic groups, indicating that it was harder to degrade aromatic structures. These were the stronger supporting results that were consistent with the FTIR spectra of increasing aromaticity with increasing pyrolysis temperature. According to study of Bandara et al. [31], the aromaticity estimated from the integrals of the peaks showed that it increased from 0.69 to 0.81 as temperatures increased from 500 to 800°C, respectively. This proved that higher heat treatments favored formation of

aromatic structures which was consistent with FTIR results.
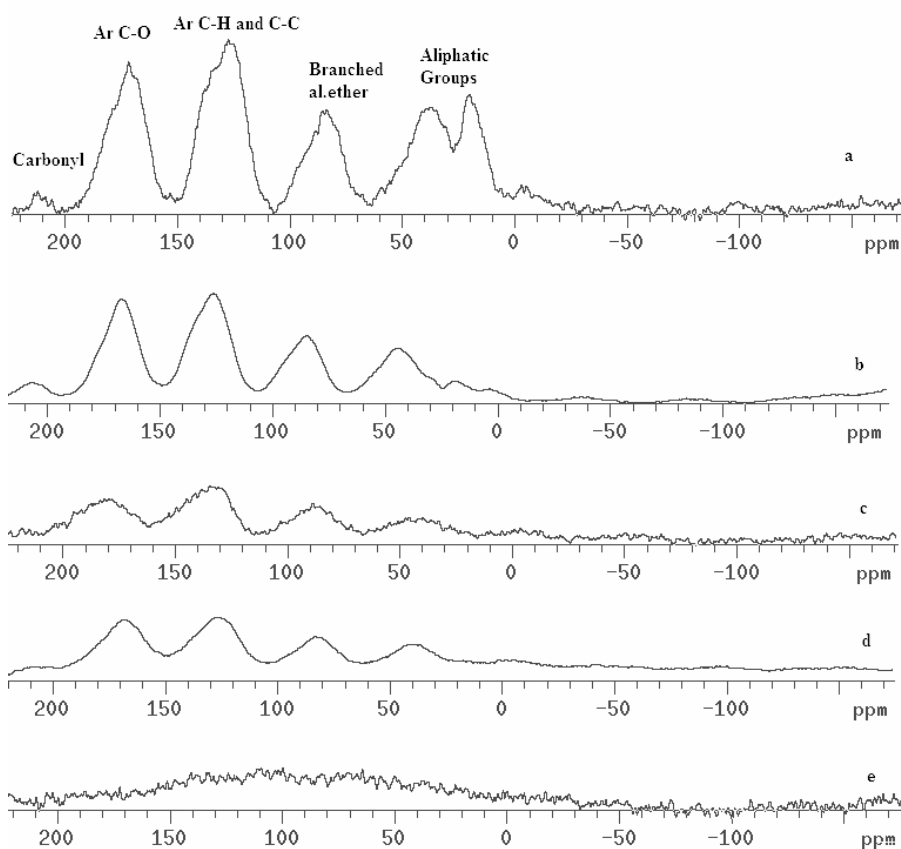
Figure 4.21: Solid-state ^{13}C-NMR spectra of hydrographenes from pyrolysis of pitch A for 2 hours at (a) 500°C, (b) 600°C, (c) 700°C, (d) 800°C, and (e) 900°C

The solid-state ^{13}C-NMR spectra of hydrographenes from pyrolysis of pitch B for 2 hours (Figure 4.22) contained chemical shifting of carbonyl groups at 200-215 ppm, aromatic C-O at 150-200 ppm, aromatic C-H and C-C at 100-150 ppm, branched aliphatic ethers at 60-100 ppm, and aliphatic groups at 0-60 ppm [90]. This time chemical shifting of carbonyl group was lost after 800°C whereas it was lost at 700°C in pitch A pyrolysis. Also the intensities of the peaks were lower in pitch B pyrolysis with respect to pyrolysis of pitch A. These explained there was effect of feedstock on pyrolysis products. Similar to pitch A pyrolysis, intensities of all the chemical shifting

57

were decreased with increasing pyrolysis temperature. More specifically, the aliphatic shifting was lost prior to aromatic groups and at 1000°C there was a broad peak of joined aromatic shifting. The aromaticity estimations by integrating the peaks [31] were 0.64 and 0.67 for 600 and 800°C, respectively. Pitch B pyrolysis, also favored aromatic structure formation due to both higher intensities and late loss of aromatic peaks as well as the ratio of integration of aromatic shifts to total shifts.
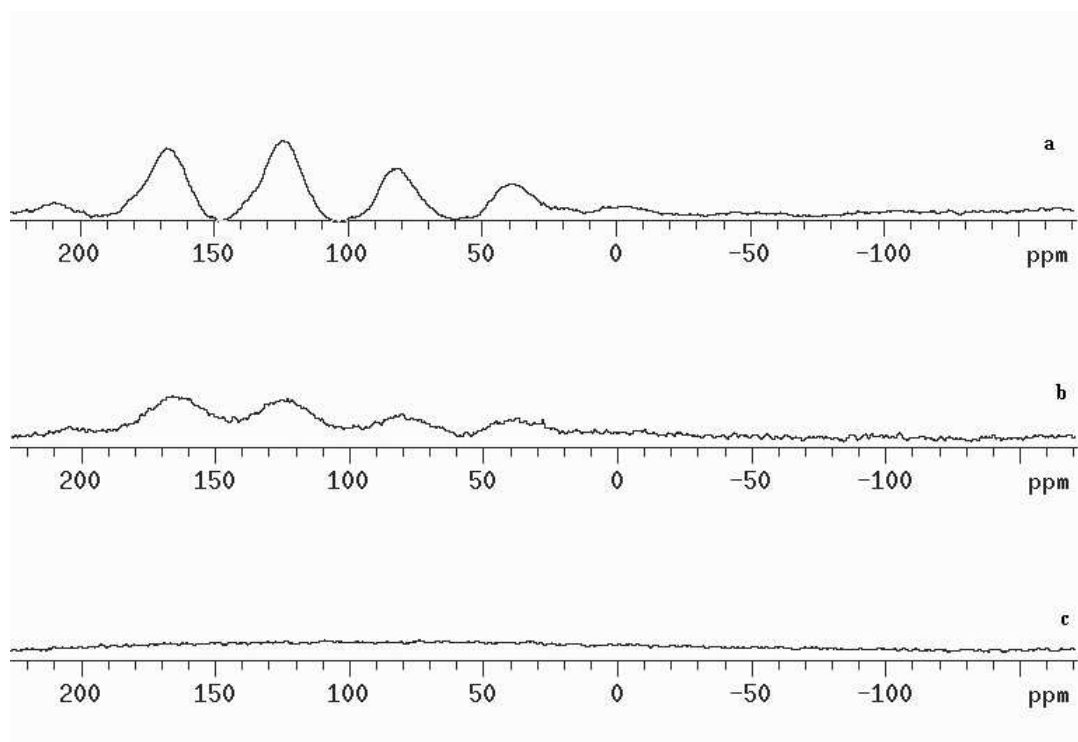
Figure 4.22: Solid-state ^{13}C-NMR spectra of hydrographenes from pyrolysis of pitch pitch B for 2 hours at (a) 600°C, (b) 800°C, and (c) 1000°C

The change in the molecular structures of the pitch A based hydrographenes with respect to pyrolysis time at low (500°C) and high (800°C) temperatures were presented in solid-state ^{13}C-NMR spectra in Figure 4.23 and Figure 4.24, respectively. The solid-state ^{13}C-NMR spectra of hydrographenes from pyrolysis of pitch A at both 500°C and 800°C contained chemical shifts of carbonyl groups at 200-215 ppm, aromatic C-O at 150-200 ppm, aromatic C-H and C-C at 100-150 ppm, branched aliphatic ethers at

60-100 ppm, and a broad shifting of aliphatic groups at 0-60 ppm [90]. Both solid-state ^{13}C-NMR spectra at high and low temperatures indicated that the molecular structure was changing with respect to time. Although comparison of spectra related to pyrolysis temperature demonstrated a definite decrease in the intensities with increasing temperature, Figure 4.21 and 4.22 demonstrated that there was an increase in the intensities of the chemical shift as pyrolysis time was longer. In order to make a more accurate conclusion, the aromaticities of the hydrographenes were estimated at each time case. The aromaticities of hydrographenes from pyrolysis at 500°C for 30, 60, and 120 minutes were calculated as 0.59, 0.62, and 0.69, respectively. So this showed that longer pyrolysis times favored formation of aromatic structures at low pyrolysis temperatures. On the other hand aromaticities of the hydrographenes formed at 800°C for 30, 60, and 120 minutes were 0.64, 0.60, and 0.81, respectively. These results also indicated there was increase in aromatic structure at longer pyrolysis times at high temperatures. However, the aromaticity value of 0.60 calculated for 60 minutes pyrolysis was lower than 30 minutes pyrolysis at 800°C. This was a possible outcome of working with natural raw material.
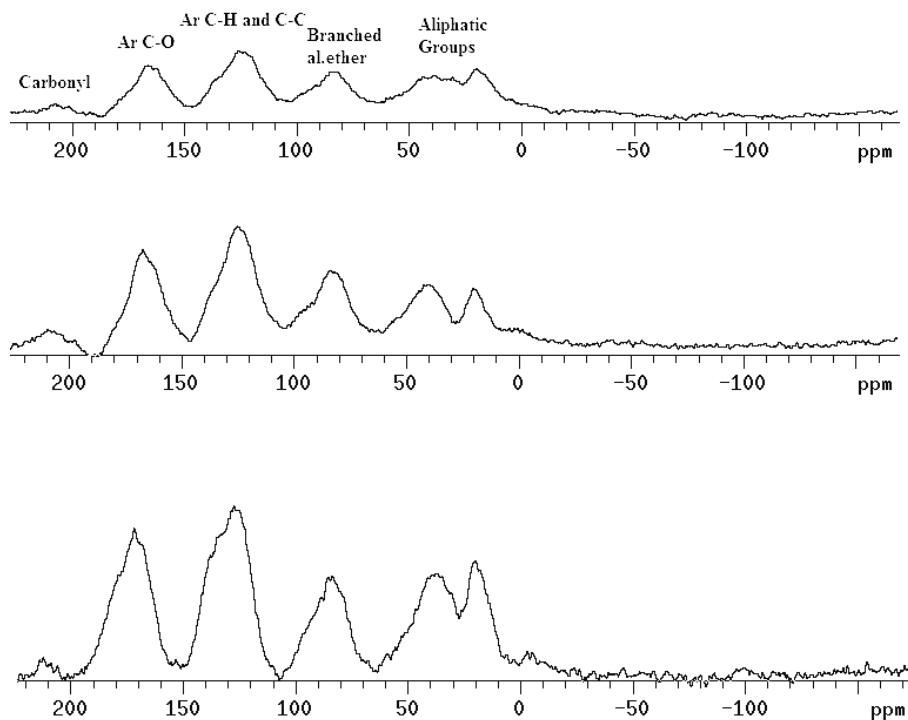
Figure 4.23: Solid-state ^{13}C-NMR spectra of hydrographenes from pyrolysis of pitch pitch A at 500°C for (a) 30, (b) 60, and (c) 120 minutes
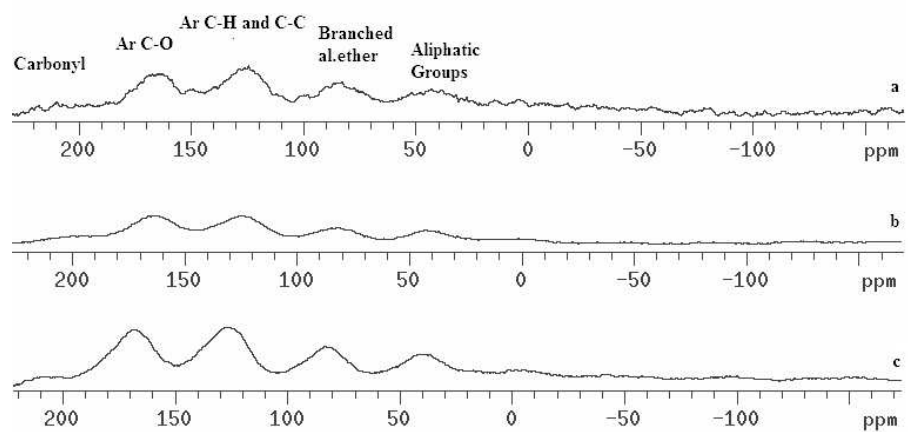
Figure 4.24: Solid-state ^{13}C-NMR spectra of hydrographenes from pyrolysis of pitch pitch A at 800°C for (a) 30, (b) 60, and (c) 120 minutes

4.4.3 Raman Spectroscopy Analyses

Raman spectroscopy is an accurate technique to determine the crystalline structure of materials. It is a powerful method due its sensitivity not only to the crystalline structure but also to the molecular structure of the compounds [91]. Nowadays, Raman spectroscopy also used for determination of the number of graphene layers [92]. Raman spectra of carbon materials usually divided in to two regions of first and second order [88]. For perfect graphite, there is only one peak called as G band at 1580 cm^{-1} in the first region. The other important three peaks of graphite are the G' band (the overtone of the G line) around 3248 cm^{-1}, the D band around 1350 cm^{-1} and the D' band (the overtone of the D line) around 2700 cm^{-1} [92]. The intensity ratio of the D band and G band are related to the degree of carbon structural order [91]. So, D band depends on the amount of the disorderness of the graphitic materials. The G peak is due to the bond stretching of all pairs of sp^2 atoms in both rings and chains. The D peak is due to the breathing modes of sp^2 atoms in rings [93].

Raman spectra of carbon structures after pyrolysis of pitch A for 2 hours at 900, 700, and 500°C and after pyrolysis of pitch B for 2 hours at 1000, 700, and 500°C are presented in Figure 4.25 and 4.26, respectively. Significantly, D and G bands occurred in both spectra of pitch A and pitch B products.
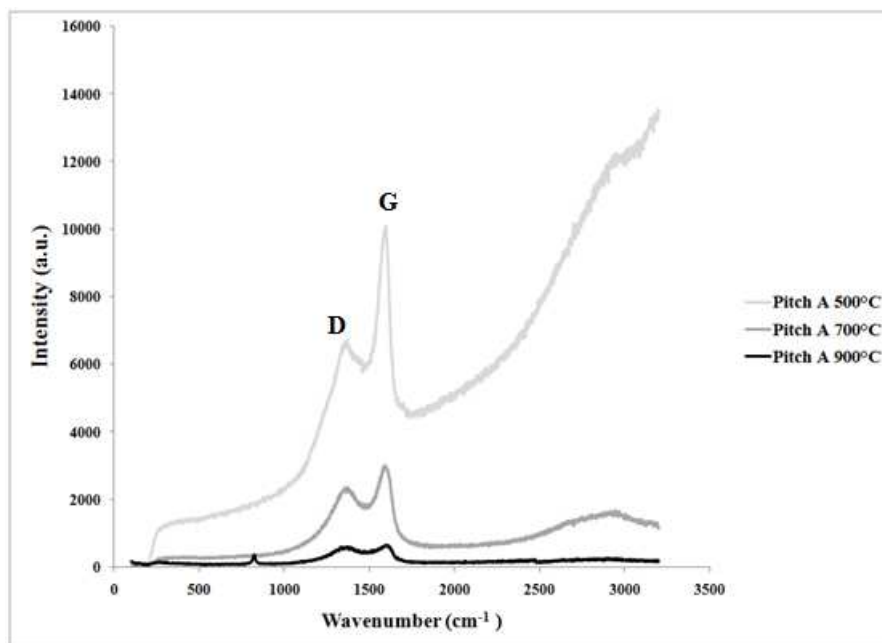
Figure 4.25: Raman spectra of carbon structures by pyrolysis of pitch A for 2 hours at 500, 700 and 900°C

In Raman spectra of carbon structures, obtained from pitch A for two hours at 500°C, contained a strong G peak at 1590 cm^{-1}, and a weaker D band at 1354 cm^{-1}. As the pyrolysis temperature increased, the intensity of D band decreased with a shifting towards 1360 cm^{-1} (at 700°C) and 1332 cm^{-1} (at 900°C), and intensity of G band decreased with shifting towards 1597 cm^{-1} (at 700°C) and 1604 cm^{-1} (at 900°C). The changes in the spectra clearly indicated that there was a change in the crystalline structure with respect to increasing pyrolysis temperature. The two important properties of D band are shifting to higher wavenumbers due to increasing incident laser excitation energies and relative intensity dependency to amount of disorderness [94]. So, as spectra indicated with increasing temperature the crystallite size increased with a decreasing disorderness due to the decreasing intensity of D band [94, 95]. Since G band is due to bond stretching of sp^2 atoms in both ring and chains, a decrease in the G band intensity is related to the decreasing of number of layers in graphitic structure [94]. For this reason, spectra indicated

62

a decrease of graphene layers with increasing pyrolysis temperature. Also, the intensity ratio of D and G bands are depended on the disorderness of carbon structure [91]. As pyrolysis temperature increases, I_D/I_G increases from 0.65 to 0.79 and finally to 0.92 indicating that the disorderness of the structures was decreasing with increasing pyrolysis temperature.
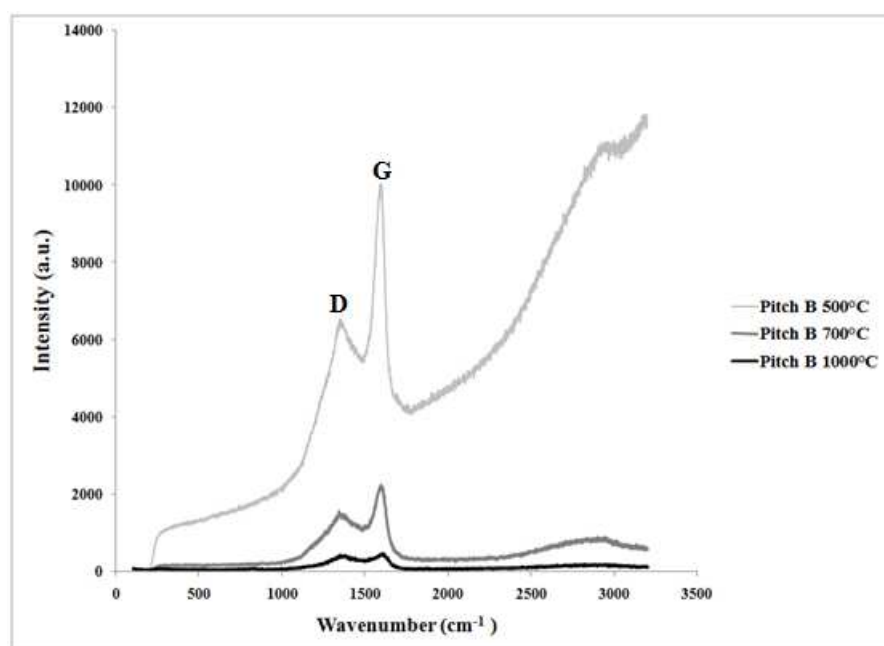
Figure 4.26: Raman spectra of carbon structures by pyrolysis of pitch B for 2 hours at 500, 700 and 1000°C

In Raman spectra of carbon structures, obtained from pitch B for two hours at 500°C, contained a strong G peak at 1597 cm^{-1}, and a weaker D band at 1354 cm^{-1}. As the pyrolysis temperature increased, D band shifted to 1342 cm^{-1} (at 700°C) and 1366cm^{-1} (at 1000°C) with a decreasing intensity, and G band shifted to 1592 cm^{-1} (at 700°C) and 1595 cm^{-1} (at 1000°C) with a decreasing intensity. The intensity of the D band decreased with increasing pyrolysis temperature, so that the disorderness in the graphitic structure is decreased at higher heat treatments. Also, decrease in the intensities of G band demonstrated a decrease in the number of layers with respect to increasing pyrolysis temperature. The spectra of carbon structures from

pyrolysis of pitch B for two hours showed the similar significant results of Figure 4.25. More specifically, D and G band parameters of both spectra in Figure 4.25 and 4.26 illustrated the decrease in number of layers and disorderness with respect to higher heat treatments. Table 4.6 and 4.7 present the parameters of D and G bands, respectively.

Table 4.6: Parameters of D Band

Sample	Wavenumber (cm^{-1})	Height	Width	Area	Absolute Intensity	I_D/I_G
Pitch A 500°C 2h	1354	1321	86	5.62×10^6	6677	0.65
Pitch A 700°C 2h	1360	822	108	1.34×10^6	2389	0.79
Pitch A 900°C 2h	1332	60	3	224516	610	0.92
Pitch A 900°C 1h	1408	71	4	23398	409	0.85
Pitch A 900°C 30 min	1344	355	47	246738	669	0.95
Pitch A 500°C 1h	1352	1636	105	3.49×10^6	5272	0.64
Pitch A 500°C 30 min	1354	822	64	3.44×10^6	4534	0.70
Pitch B 500°C 2h	1354	1954	103	5.56×10^6	7129	0.63
Pitch B 700°C 2h	1342	662	106	761031	1556	0.69
Pitch B 1000°C 2h	1366	72	4	90103	336	0.95

Table 4.7: Parameters of G Band

Sample	Wavenumber	Height	Width	Area	Absolute Intensity
Pitch A 500°C 2h	1590	4980	66	3.07x10^6	10283
Pitch A 700°C 2h	1597	1635	83	884398	3028
Pitch A 900°C 2h	1604	366	64	183513	666
Pitch A 900°C 1h	1600	97	7	80756	484
Pitch A 900°C 30 min	1600	424	78	170498	704
Pitch A 500°C 1h	1593	4619	64	2.28 x10^6	8298
Pitch A 500°C 30 min	1591	2248	67	1.87 x10^6	5759
Pitch B 500°C 2h	1597	5331	58	3.01 x10^6	11252
Pitch B 700°C 2h	1592	1429	70	500785	2242
Pitch B 1000°C 2h	1595	46	5	56681	354

In addition to the effect of pyrolysis temperature, the effect of pyrolysis time on the formation of crystalline structures in pyrolysis of pitch A at 900°C and 500°C were also demonstrated in Figure 4.27 and 4.28, respectively. At high pyrolysis temperatures, the lowest intensities of both D and G bands occurred at pyrolysis time of 1 hour and highest intensities of both D and G band occurred at 2 hours pyrolysis. The I_D/I_G ratios were 0.95, 0.85, and 0.92 as the pyrolysis times were 30, 60, and 120 minutes, respectively. However, as Figure 4.28 illustrated, at lower temperatures both D and G bands' intensities decreased with decreasing time. At lower temperatures, shorter residence time produced graphitic structures with less disorder. Also, I_D/I_G ratios were 0.70, 0.64, and 0.65 with respect to 30, 60, and 120 minutes pyrolysis.
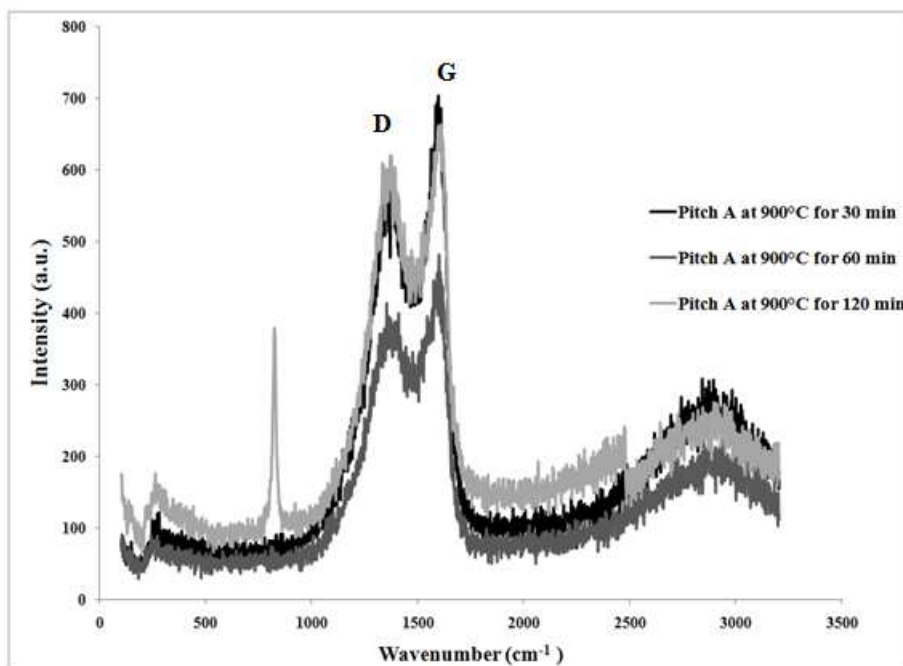
Figure 4.27: Raman spectra of carbon structures by pyrolysis of pitch A at 900°C for 30, 60 and 120 minutes.
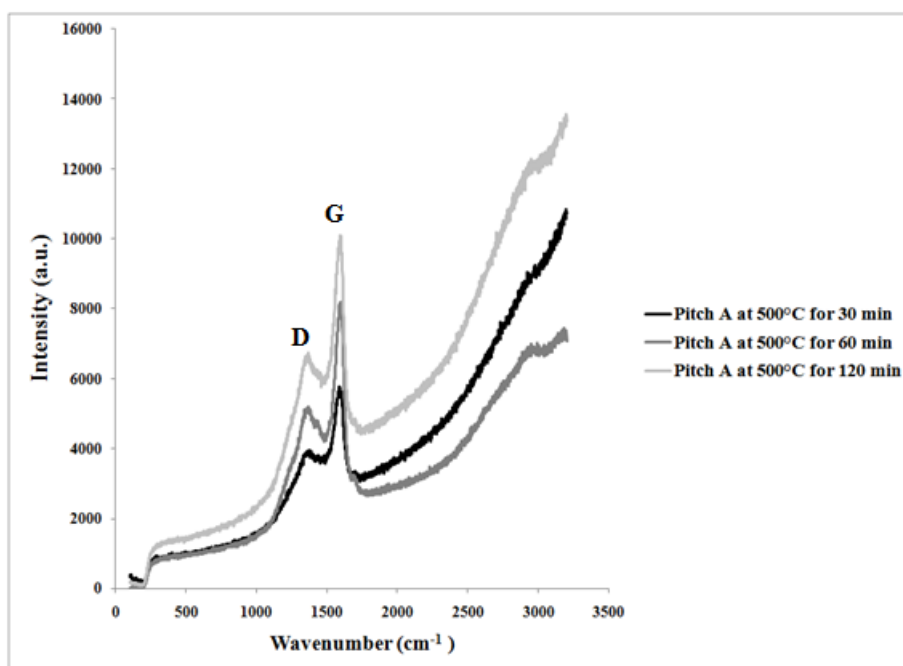
Figure 4.28: Raman spectra of carbon structures by pyrolysis of pitch A at 500°C for 30, 60 and 120 minutes.

4.4.4 XRD Analyses

On the other hand, microcrystalline structures of pyrolysis products were investigated by XRD. X-ray diffraction patterns of six hydrographene material produced from pitch A pyrolysis for 2 hours at 500°C, 600°C, 700°C, 800°C, 900°C, and 1000°C are shown in Figure 4.29 - 4.34. All of the patterns had broad peak around 2θ=25.0-25.7°, corresponding to (002) reflection of carbon structures due to the stacking of aromatic layers [1]. The broadness of the (002) peaks indicated that samples were highly amorphous [57] and there was a possible presence of crystallites perpendicular to aromatic layers [1]. At high temperatures of 800-1000°C, the intensity of the (002) peak increased clearly. The possible reason for this was the increasing crystalline structure at higher heat treatments.
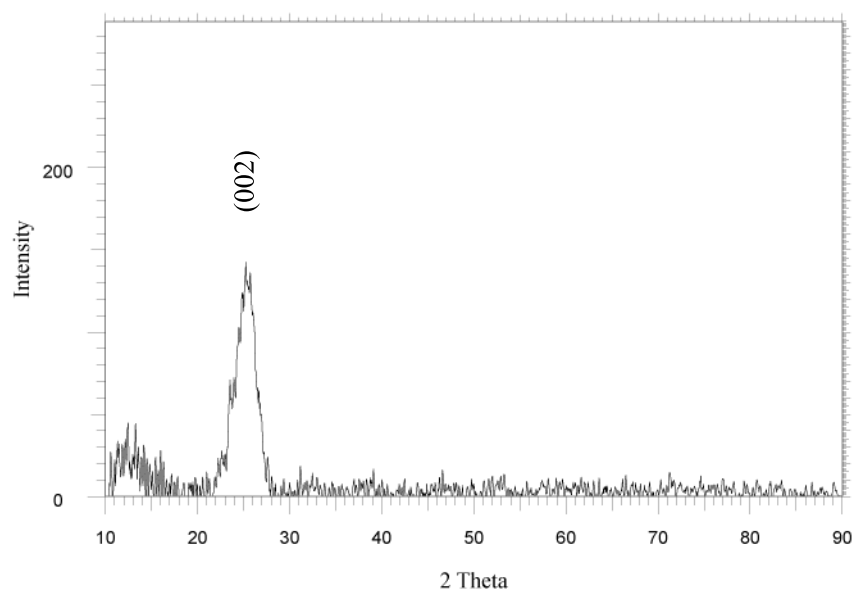
Figure 4.29: XRD of hydrographenes produced from pitch A pyrolysis for 2 hours at 500°C
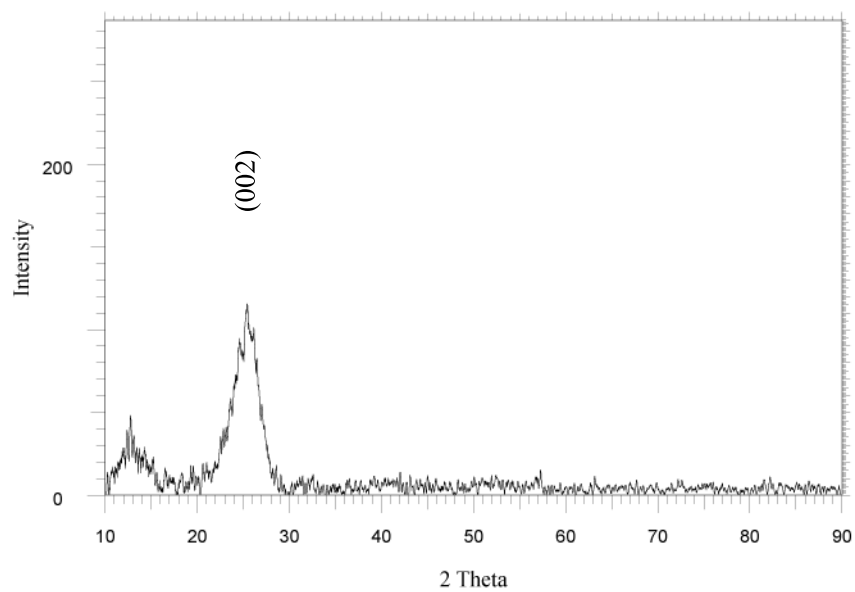
Figure 4.30: XRD pattern of hydrographenes produced from pitch A pyrolysis for 2 hours at 600°C
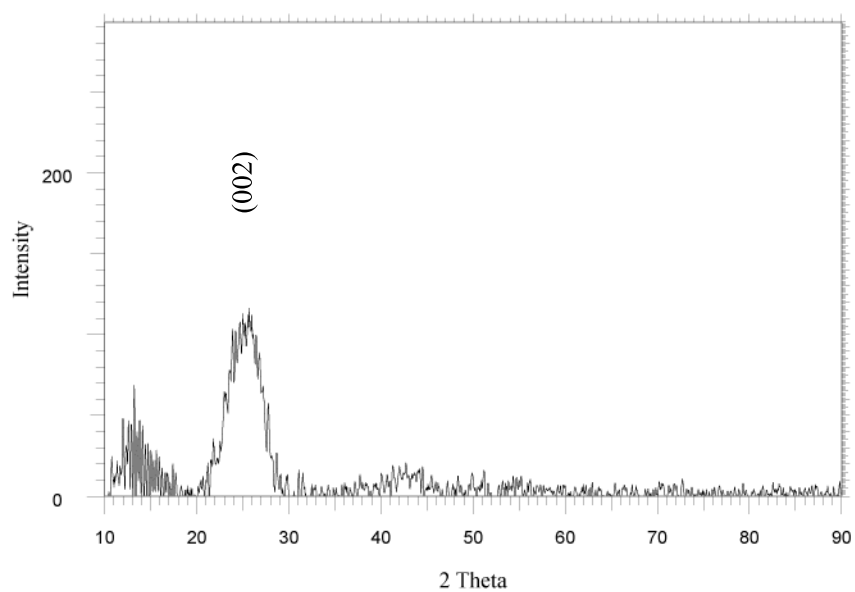
Figure 4.31: XRD pattern of hydrographenes produced from pitch A pyrolysis for 2 hours at 700°C
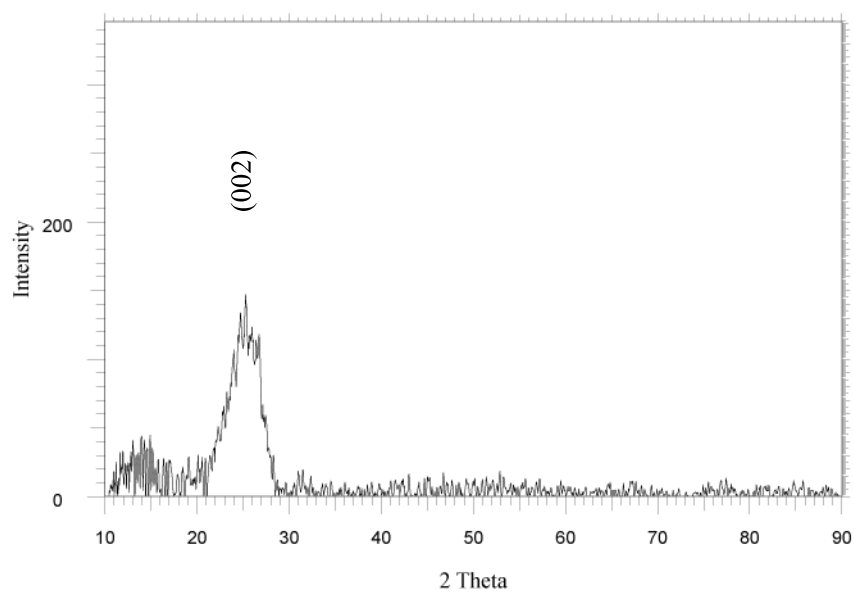
Figure 4.32: XRD pattern of hydrographenes produced from pitch A pyrolysis for 2 hours at 800°C
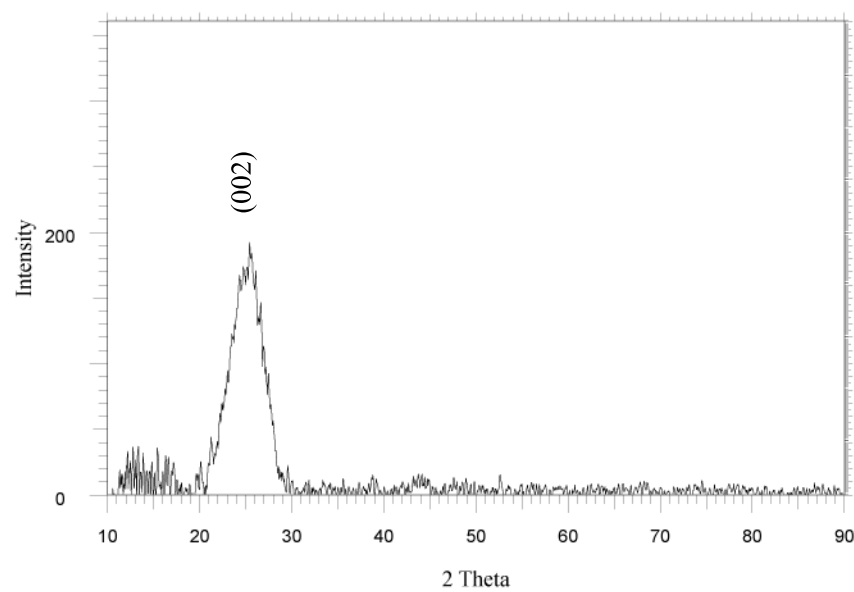
Figure 4.33: XRD pattern of hydrographenes produced from pitch A pyrolysis for 2 hours at 900°C
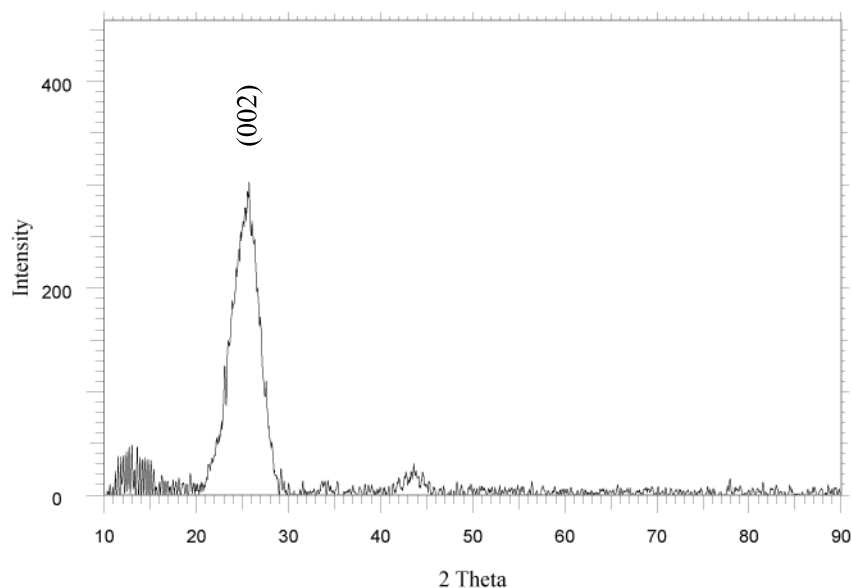
Figure 4.34: XRD pattern of hydrographenes produced from pitch A pyrolysis for 2 hours at 1000°C

X-ray diffraction patterns of three hydrographenes materials produced from pitch B for 2 hours at 500°C, 800°C, and 1000°C are shown in Figure 4.35, 4.36, and 4.37, respectively. Similar to above patterns, all three of the patterns of pitch B pyrolysis had broad (002) peak around 2θ=25.1-25.6°. These samples were amorphous due to their broad (002) peak, with a possible increasing crystallinity at higher heat treatments due to the increase in the intensity in the patterns. The diffraction pattern of all samples were similar to the pattern of graphite (Figure 4.38), however the intensity of the (002) peaks were so low indicating that samples were probably very poor in crystalline structure. Although the Raman results were supporting the amorphousity caused by possible turbostratic structures in hydrographenes, the poor crystallinity of the hydrographenes was a real problem due to the possible turbostratic structures leading to broad peaks of (002).
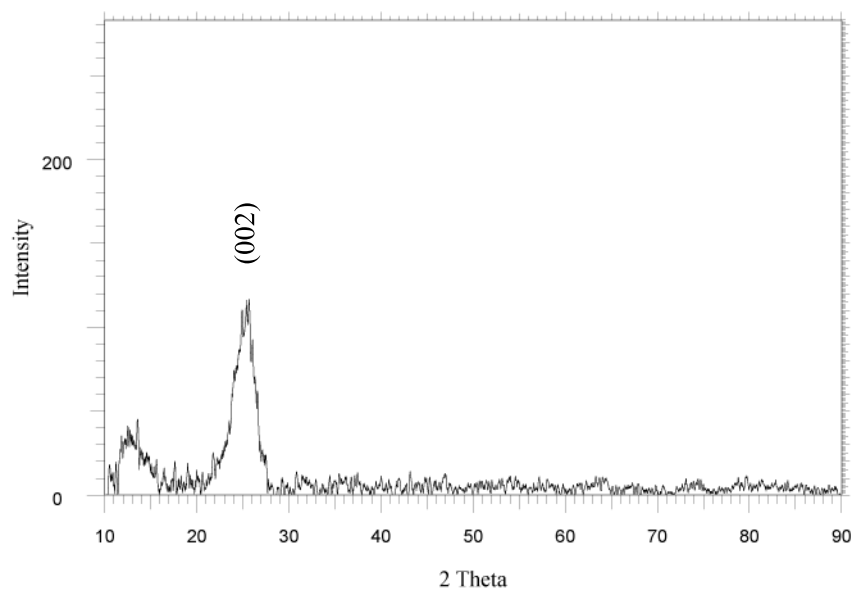
Figure 4.35: XRD pattern of hydrographenes produced from pitch B pyrolysis for 2 hours at 500°C
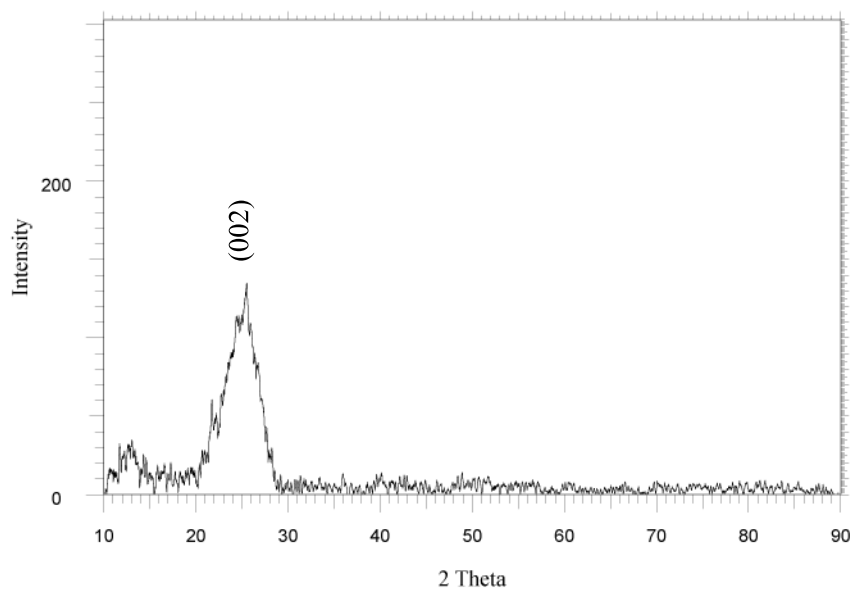
Figure 4.36: XRD pattern of hydrographenes produced from pitch B pyrolysis for 2 hours at 800°C
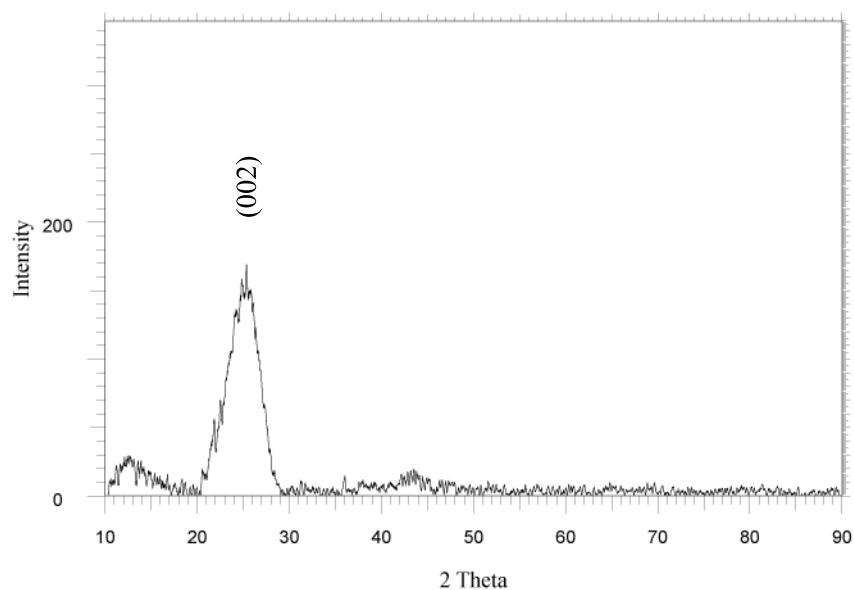
Figure 4.37: XRD pattern of hydrographenes produced from pitch B pyrolysis for 2 hours at 1000°C
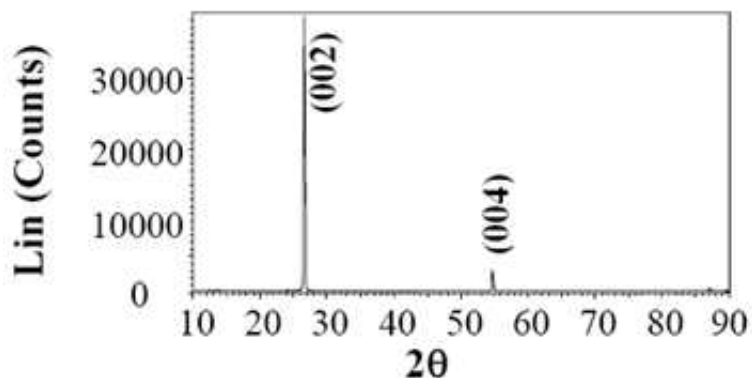
Figure 4.38: XRD pattern of raw graphite

Due to the broadness and low intensity of (002) peak, we estimated the crystallinity of the amorphous hydrographene materials with respect to ratio of the area (002) peak of a perfect graphite and area of the (002) peak of the samples relative to their masses. The results for the crystallinity estimations of pyrolysis of pitch A and pitch B are presented in Figures 4.39 and 4.40, respectively. In Figure 4.39, 0.84 was the highest percentage ob-

72

tained from the pyrolysis of pitch A at 1000°C for 2 hours whereas 0.10 was the lowest percentage obtained from the pyrolysis of pitch A at 500°C for 30 minutes. Figure 4.40 illustrated that for pitch B based hydrographenes 0.49 and 0.12 were the highest and lowest percentages of crystallinity, respectively obtained at 1000°C for 2 hours and 500°C for 30 minutes pyrolysis. The graphs supported the previous arguments of increasing crystalline structure at higher heat treatments. In both pyrolysis of pitch A and pitch B, crystallinity increased with respect to increasing both time and temperature. Also, reaction temperature effect of feedstock on the formation of crystalline structures was demonstrated in Figure 4.41. As Figure 4.41 clearly demonstrated, hydrographenes obtained from pyrolysis of pitch A had drastically more crystallinity at high temperatures. However, around 700°C almost same crystallinity percentage obtained from both feedstock and at temperature lower than 700°C pitch A based hydrographenes had slightly lower crystallinity than pitch B based hydrographenes.
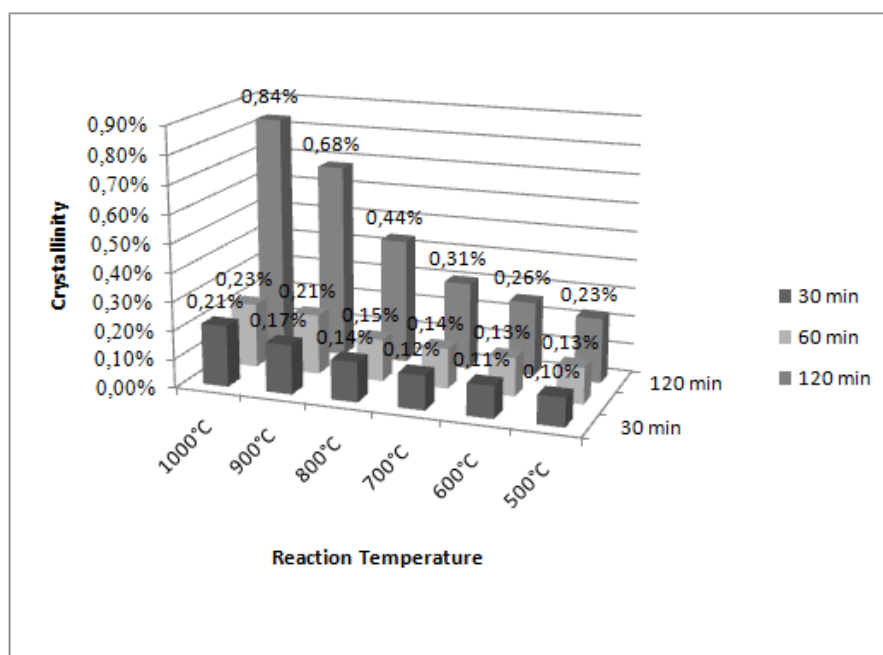
Figure 4.39: Crystallinity of hydrographenes from pyrolysis of pitch A
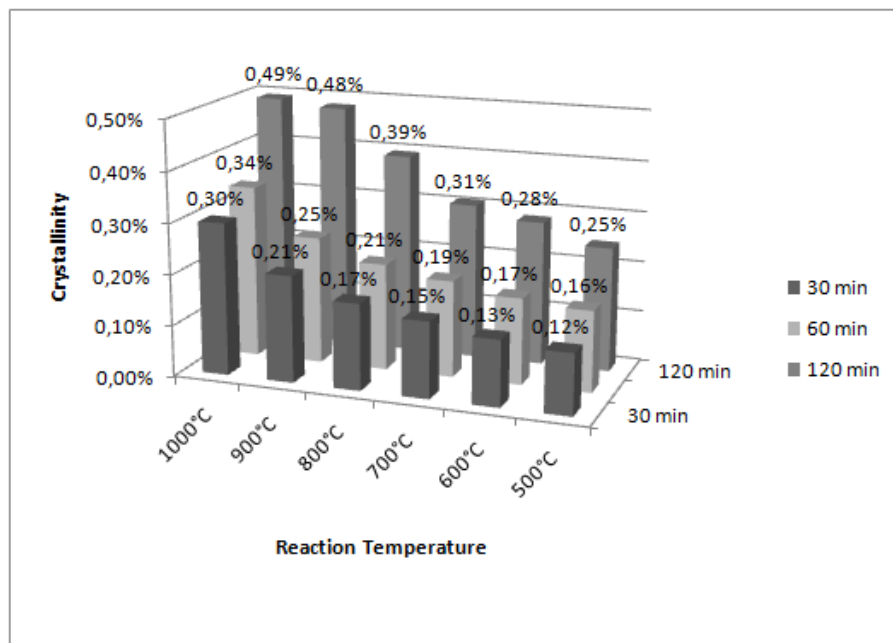
Figure 4.40: Crystallinity of hydrographenes from pyrolysis of pitch B
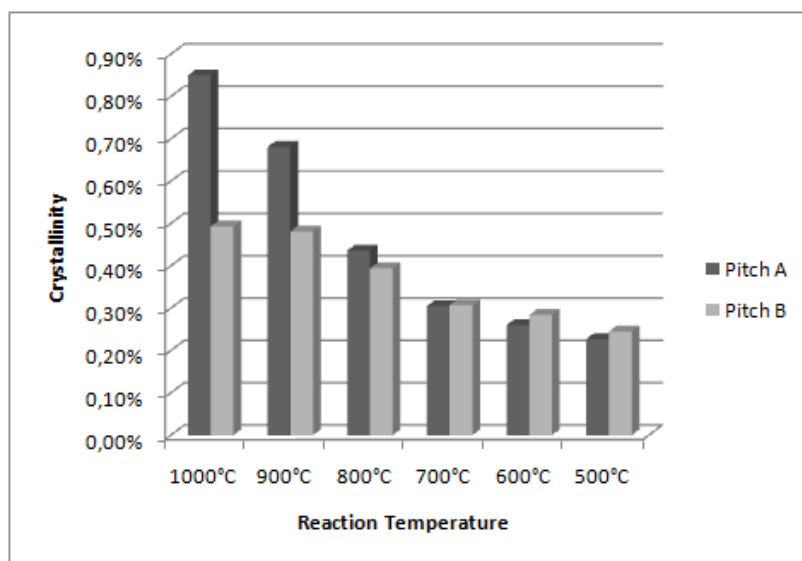
Figure 4.41: Comparison of crystallinity of pitch A and B at 2 hour pyrolysis

Figures 4.42 and 4.43 illustrated the interlayer spacing (d_{002}) with respect to temperature and time of the pyrolysis reactions of pitch A changed in the range of 3.46-3.56 Å, where as d_{002} of pitch B changed in the range of 3.47-3.62 Å, respectively. However, a correlation between d_{002} values and

74

pyrolysis parameters could not be done due to the turbostratic structure of the products and complex structure of the pitches. Also, the comparison of d_{002} of pitch A and B for 2 hours pyrolysis, demonstrated in Figure 4.44, indicated that there is not a correlation between d_{002} values and these pitch types. Generally, heat treatment of carbons below 1800°C results in very disordered carbons containing turbostratic structures. The presences of local stacking faults, random shifting between layers, unorganized carbon structures, strain in the layers, and unsteady interlayer spacings are the main reasons for the disorderness [1]. For this reason the results presented in the graphs with respect to change in time, temperature, and pitch type were the signs of high disorderness probably caused by the turbostratic structures in hydrographenes materials.
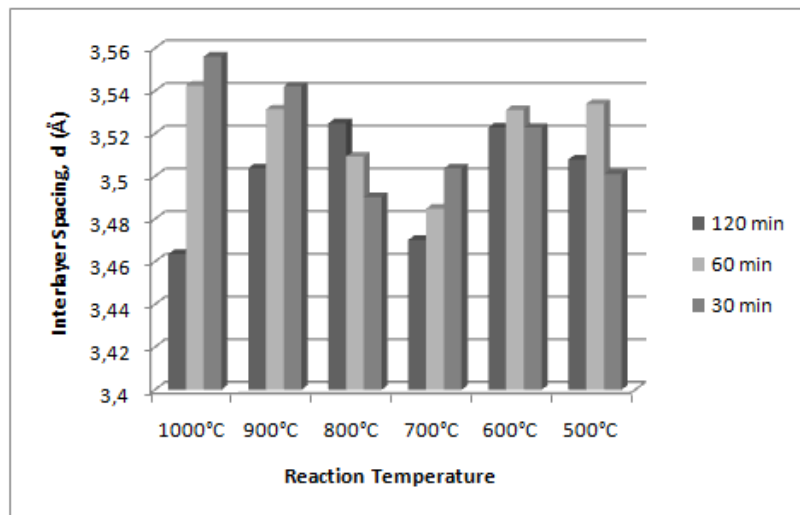
Figure 4.42: Interlayer spacing of pitch A products with respect to temperature and time
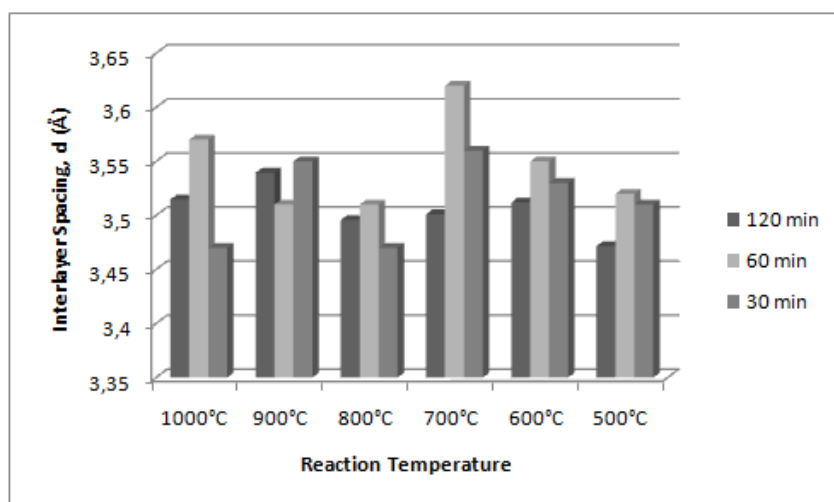
Figure 4.43: Interlayer spacing of pitch B products with respect to temperature and time
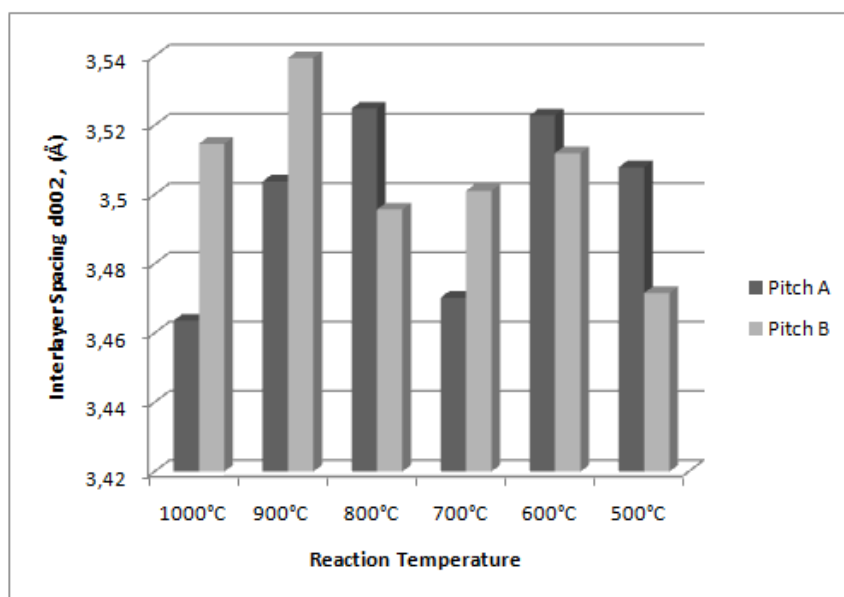
Figure 4.44: Interlayer spacing of pitch A and pitch B for 2 hours pyrolysis

XRD patterns obtained from the pyrolysis of pitch A and pitch B under different time and temperature were analyzed to obtain the structural parameters of FWHM, Lc, and d_{002} in order to make estimations on changing number of graphene layers with respect to varying conditions. Figure 4.45

76

and 4.46 are presented to show effect of temperature and time on the number of graphene layers of pitch A and of raw material on the number of graphene layers of hydrographenes produced from 2 hours pyrolysis, respectively. In these figures average numbers of graphene layers, n, were calculated by using classic Debye-Scherer equations. However, calculated stacking height, Lc, and the number of layers were not exactly equal to exact values of the crystallites because these equations can be only derived for highly graphitized carbon materials [1]. So, these equations are not suitable for highly turbostratic carbons because the positive interference function from intralayer plane is too strong to be cancelled by the negative interference function becoming weak in the small numbers of stacking of carbon layers [96]. So that, calculated values of n were used as convenient relative estimates of actual crystallite sizes and layer numbers that were probably greater than the calculated values. Figure 4.45 presents the calculated average n values were changing between 5-10 graphene layers. Although, there was not a distinct correlation between experimental conditions and the calculated results, n values were 5 to 7 layers at temperature higher than 700°C and 7 to 10 at temperatures 500-600°C. The calculated values of average n were similar to values measured for pyrolzed lignin forming turbostratic carbons [1], and number of layers in turbostratic carbons simulated by Yang and Frindt [97]. Other than time and temperature effects on n values, type of pitches seemed to affect calculated values as presented in Figure 4.46. More specifically, hydrographenes seemed to have fewer layers in case of pitch B than hydrographenes in the case of pitch A.
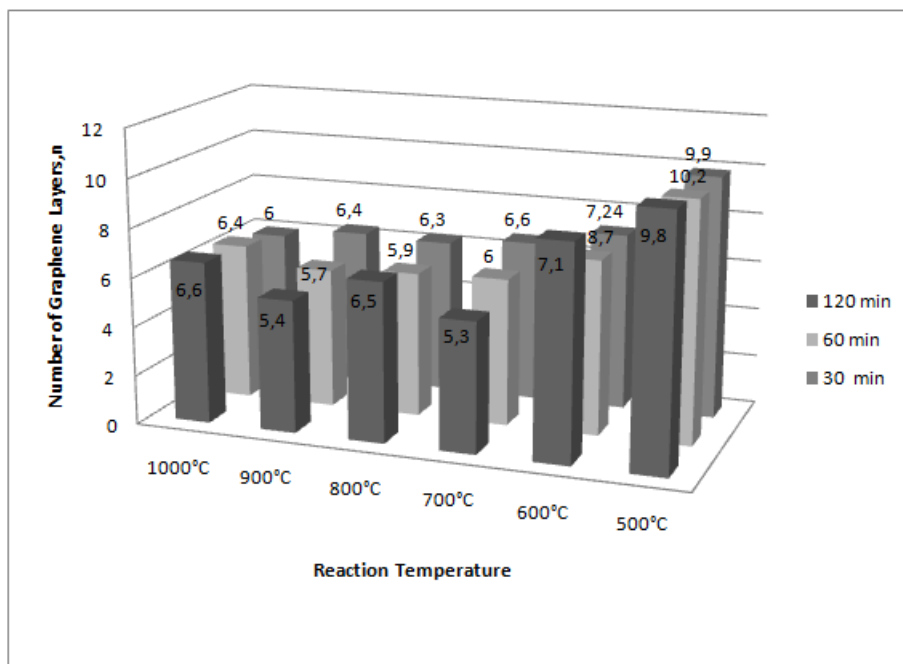
Figure 4.45: Calculated n values of pitch A based hydrocarbons with respect to time and temperature
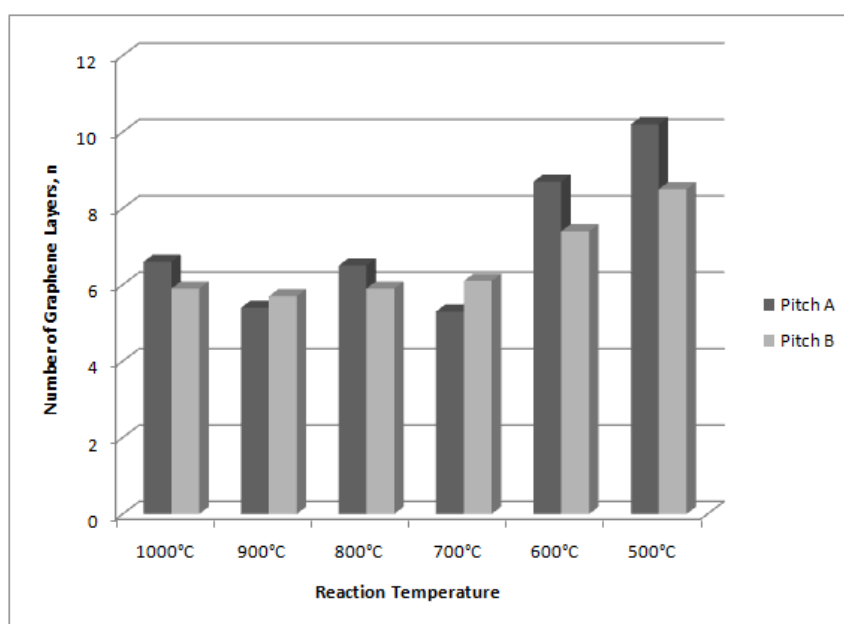
Figure 4.46: Change in calculated n values at two hours pyrolysis with respect to pitch type and pyrolysis temperature

4.4.5 SEM Analyses

Morphology of the hydrographenes obtained from pyrolysis of pitch A at 600°C for two hours were investigated by SEM in Figure 4.47. Physical appearances of hydrographenes were quite different in different spots during analyses. The SEM photographs clearly indicated that there was formation of pores and layering structure during the heat treatment process. The formation of pores was due to the devolatilization reactions taking place in the pyrolysis process. So, SEM micrographs of hydrographenes obtained at 600°C for two hours visualized remaining effect of the volatile matter exclusion observed by naked eye around 500-600°C during pyrolysis reactions. The effect of increasing temperature to higher values were also examined by SEM. SEM micrographs of hydrographenes produced at 700°C in Figure 4.48 showed different morphology than the hydrographenes at lower temperatures. Both images at low and high magnifications clearly indicated that there were the formation of turbostratic structures and expansion of carbon layers sequel to formation of layering at 600°C [1]. Figure 4.49 represents the morphologies of hydrographenes when the pyrolysis temperature was increased to 800°C. The micrographs demonstrated that there was increase of turbostratic content in hydrographenes at higher temperatures.
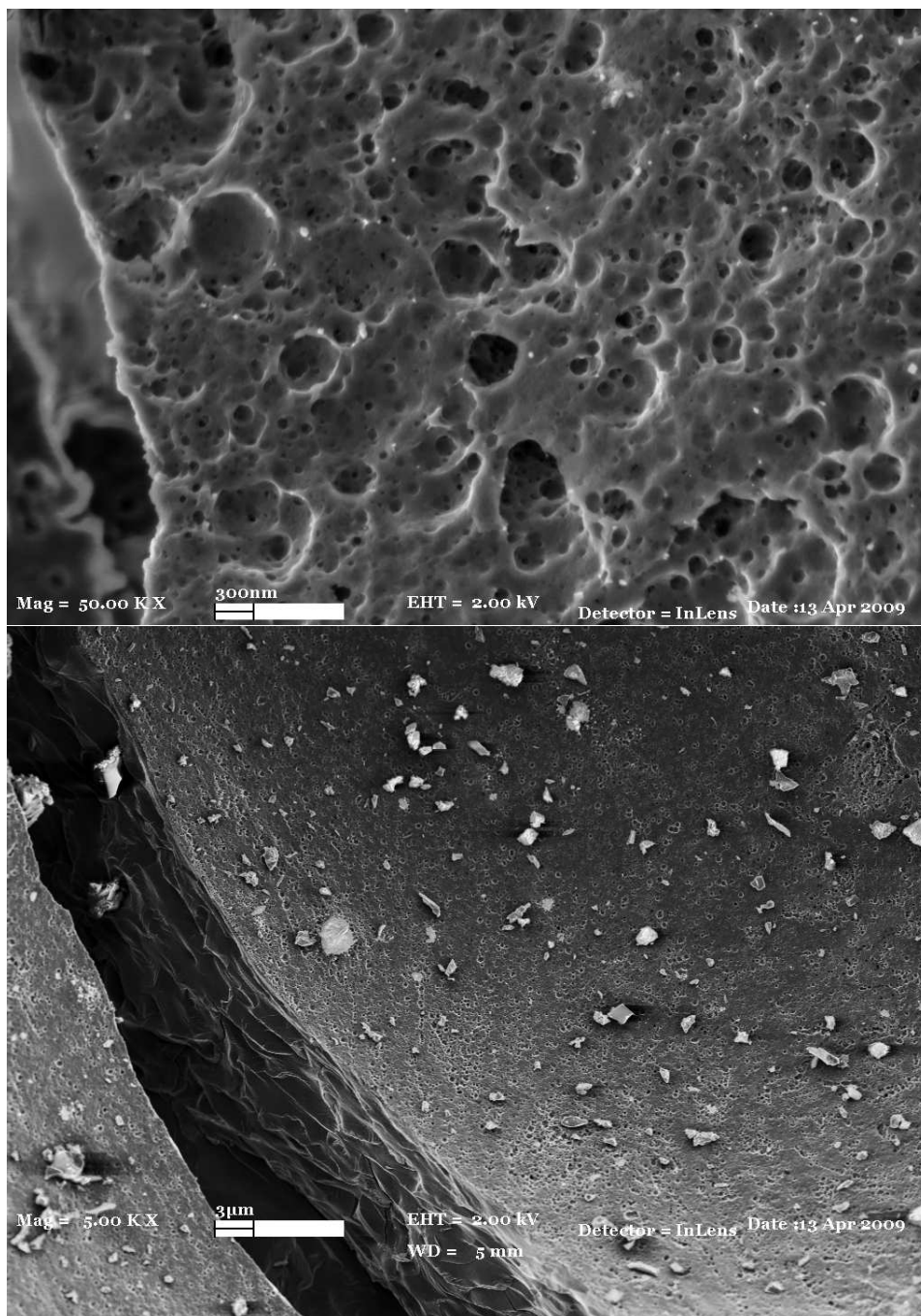
Figure 4.47: SEM micrographs of pitch A based hydrographenes obtained at 600°C for two hours showing (a) pores and (b) layering structures
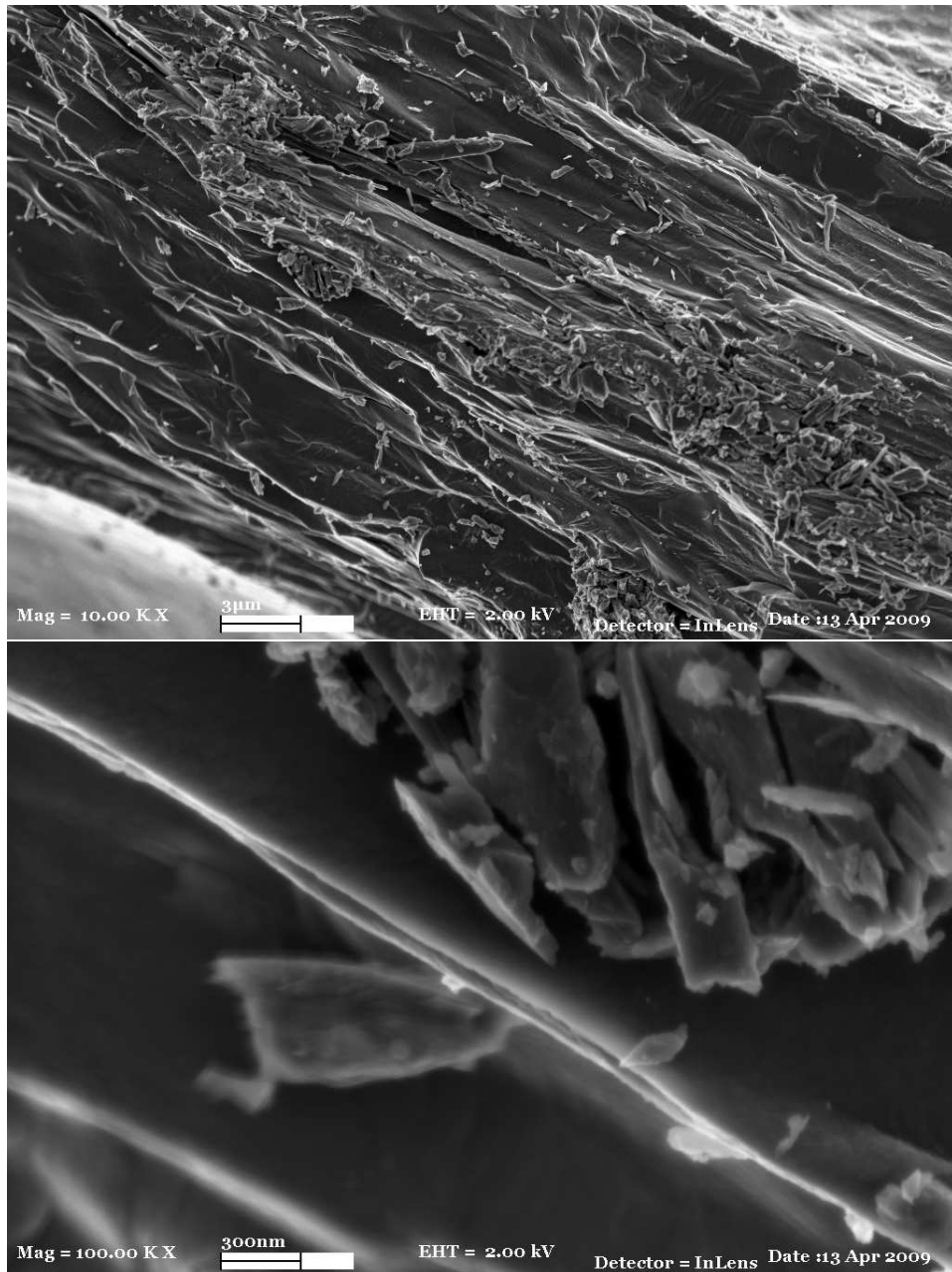
Figure 4.48: SEM micrographs of pitch A based hydrographenes obtained at 700°C for two hours showing (a) turbostratic structures and (b) expansion of layers
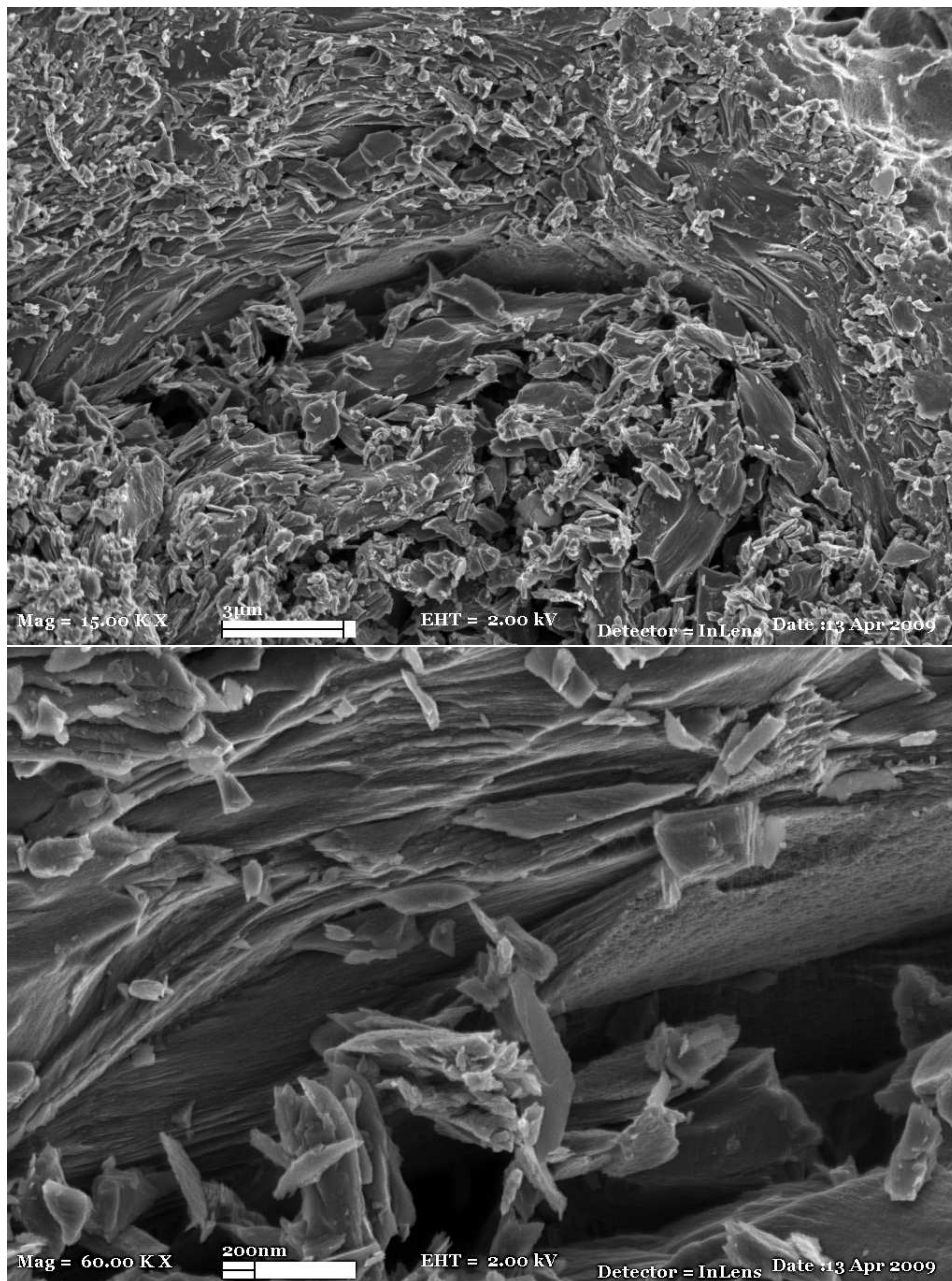
Figure 4.49: SEM micrographs of pitch A based hydrographenes obtained at 800oC for two hours showing high turbostratic structure content at (a) 15KX and (b) 60KX magnifications

4.4.6 Oxidation, Expansion, and Reduction of Hydro-graphenes

Although, our hydrographenes were highly amorphous with rich turbostratic carbon contents, we tried to examine the effect of oxidation and expansion

reactions on the structure of hydrographenes produced at 700°C for 2 hours pyrolysis of pitch A. SEM micrograph of hydrographenes used as raw materials of this demo experimental search is presented in Figure 4.50 in addition to Figure 4.48. Layers contained in the raw hydrographenes seemed to be expanded a little, however visualization of the porosity due to devolatilization reactions and amorphous structures were inevitable.
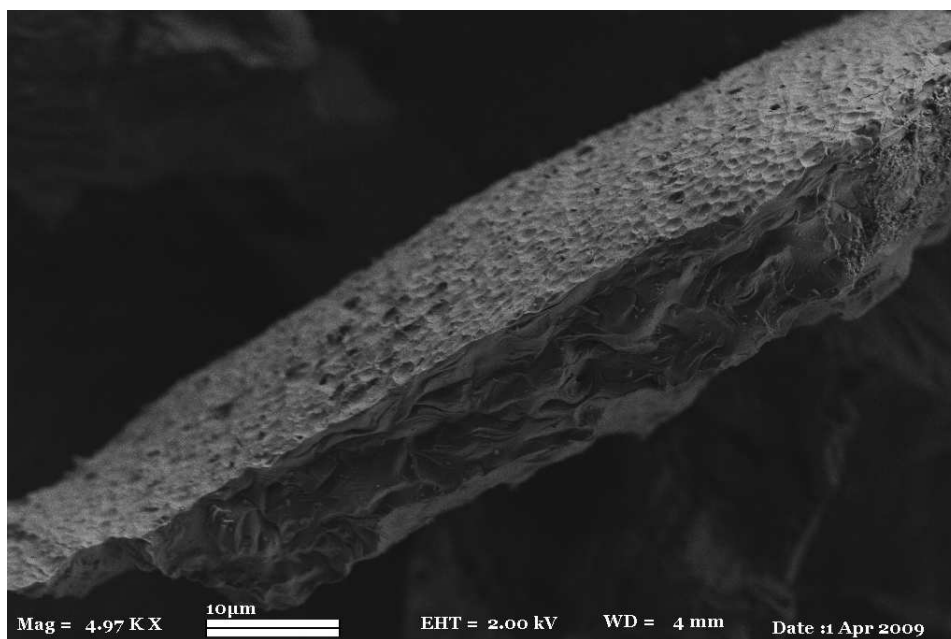
Figure 4.50: SEM micrograph of hydrographenes

SEM micrographs of oxidized hydrographenes are shown in Figure 4.51. It was expected to create oxygenated polar structures after cleavage of C-C bonds in aromatic layers which facilitated the diffusion of acetic anhydride into the layers by oxidation of hydrographenes with potassium dichromate. Amount of sulfuric acid highly affects the oxidation process [98], for this reason we used the sulfuric acid due to the amounts optimized in exfoliation of graphene-based nanosheets from graphite works [99]. After successful oxidation of the samples, thermal decomposition of acetic anhydride into CO_2 and H_2O vapor can lead to the expansion of the layered graphitic structure by heat treatments at elevated temperatures. Although, the success of oxida-

tion step was not obvious in our experiments we continued investigation by expansion treatment of oxidized hydrographenes. After the expansion treatment, the SEM micrographs of illustrated a slight expansion between layers in Figure 4.52. However, acquisition of graphene sheets failed to be observed due to the micrograph of expansion of oxidized hydrographenes.
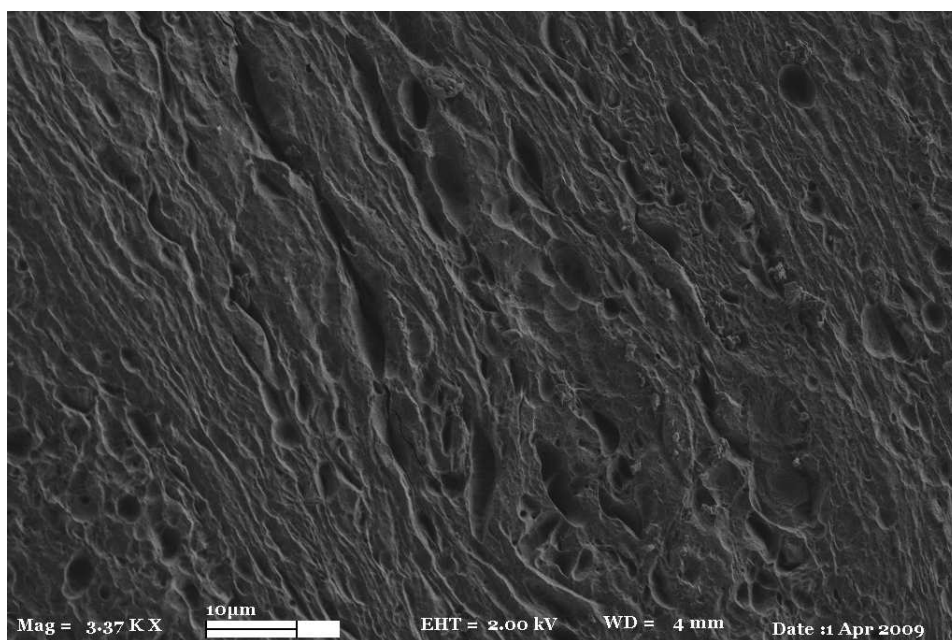
Figure 4.51: SEM micrograph of hydrographene oxides
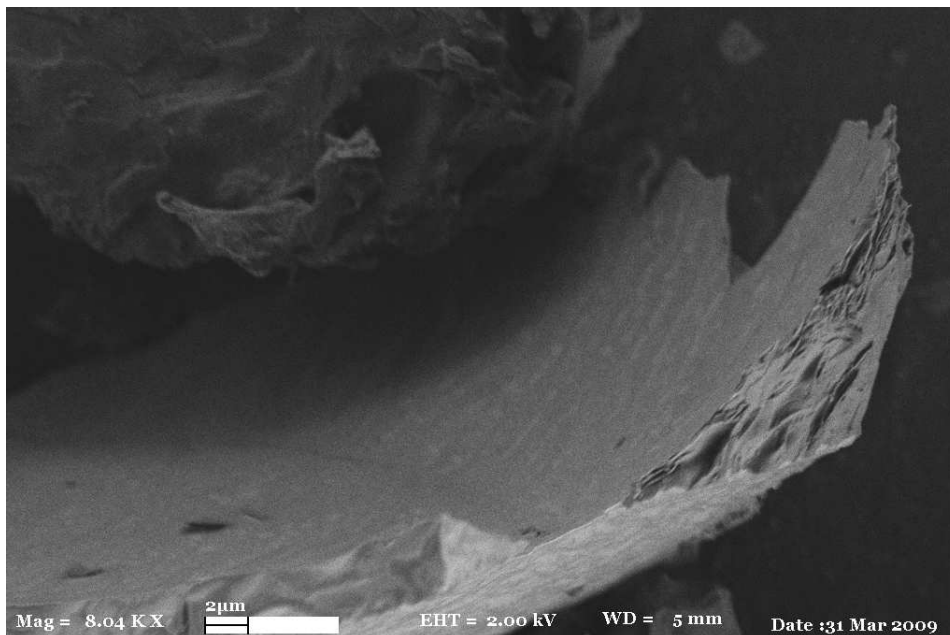
Figure 4.52: SEM micrograph of expanded hydrographene oxides

After expansion treatment samples were chemically reduced by hydro-quinone refluxing with in water. Main approach for the reduction process was acquisition of graphene-based nanosheets. Hydroquinone loses either one H^+ ion from one of its hydroxyls to form a monophenolate ion or two H^+ ions from both hydroxyls to form a diphenolate ion called as quinone, during reduction reaction by refluxing with hydroquinone [99]. It was observed that solution turned into yellowish color during reduction process by hydroquinone. The filtrated solid samples were washed with water, methanol and dried in 60°C overnight. SEM micrograph samples obtained after the chemical reduction experiment are presented in Figure 4.53. In this SEM micrograph it was still possible to observe the turbostratic structures present in the hydrographenes. The treatment of the pyrolyzed pitches seemed not to be very promising in terms of separating the graphene layers.
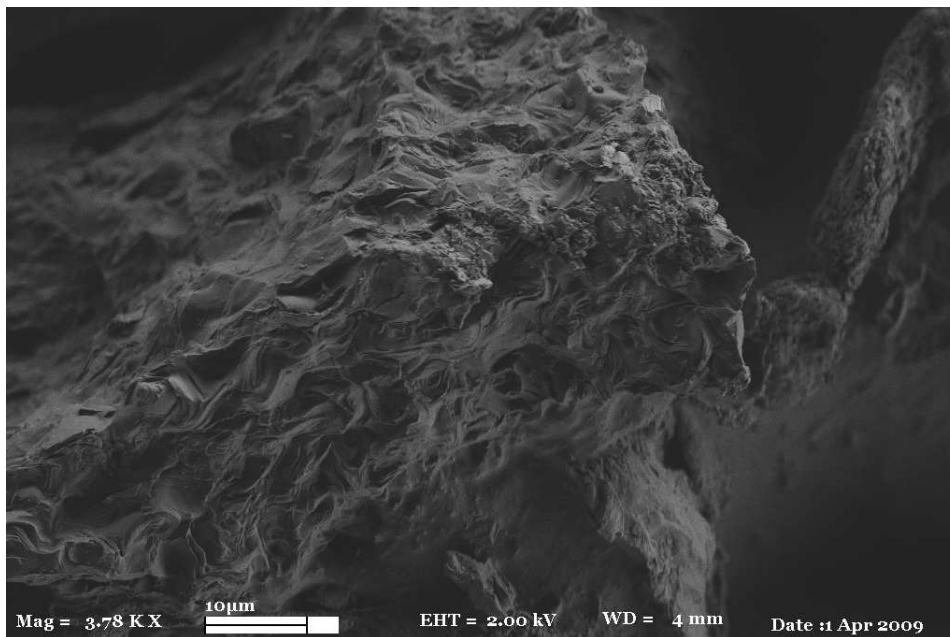
Figure 4.53: SEM micrograph of hydrographenes after reduction reactions

In addition to morphologic analysis, crystal structure evolution of hydrographenes with respect to oxidation, expansion, and reduction reactions were investigated by using powder XRD. X-ray diffraction patterns of hydrographenes, oxidized hydrographenes, expanded oxidized hydrographenes, and reduced hydrographenes are presented in Figures 4.54, 4.55, 4.56, and 4.57, respectively. XRD pattern of hydrographenes contained a broad (002) peak at $2\theta{=}25.5°$ with a low intensity (Figure 4.54). In Figure 4.55, XRD pattern of hydrographenes oxides showed that the intensity (002) peak was doubled at $2\theta{=}25.3°$ indicating there was a change in the crystal nature of hydrographenes due to oxidation. (002) peak at $2\theta{=}25.0°$ with a similar intensity to (002) peak was observed in the XRD pattern of expanded hydrographenes oxides in Figure 4.56. A broader (002) peak at $2\theta{=}25.1°$ was obtained in the XRD pattern of reduced expanded hydrographenes oxides in Figure 4.57.
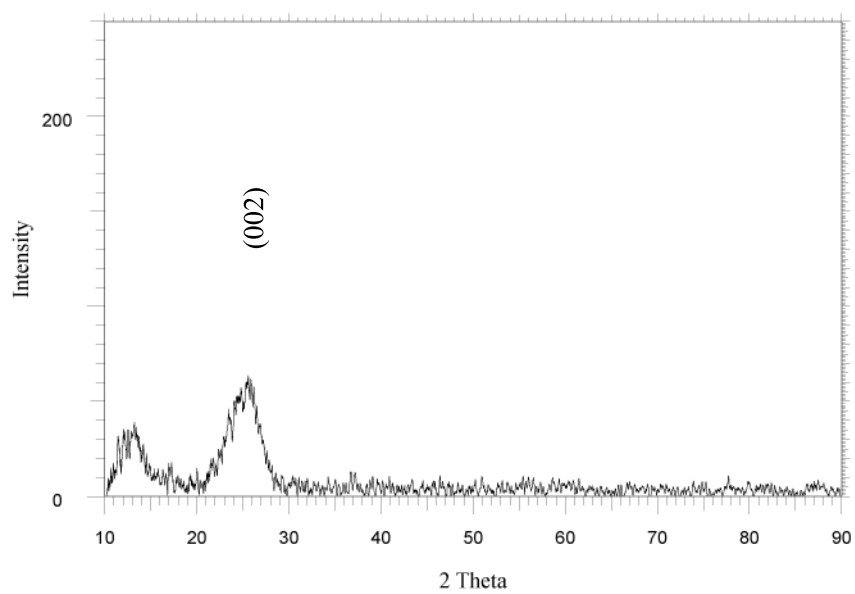
Figure 4.54: XRD pattern of hydrographenes
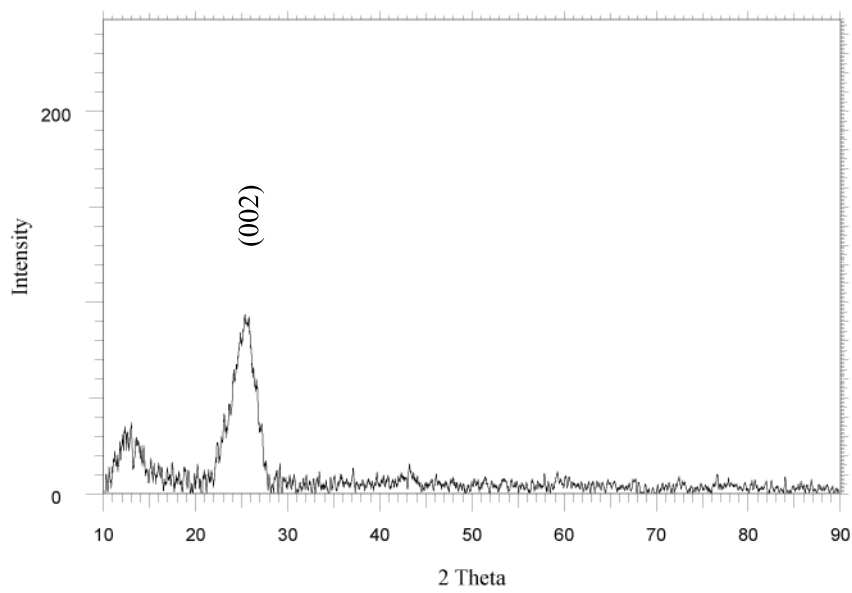
Figure 4.55: XRD pattern of oxidized hydrographenes
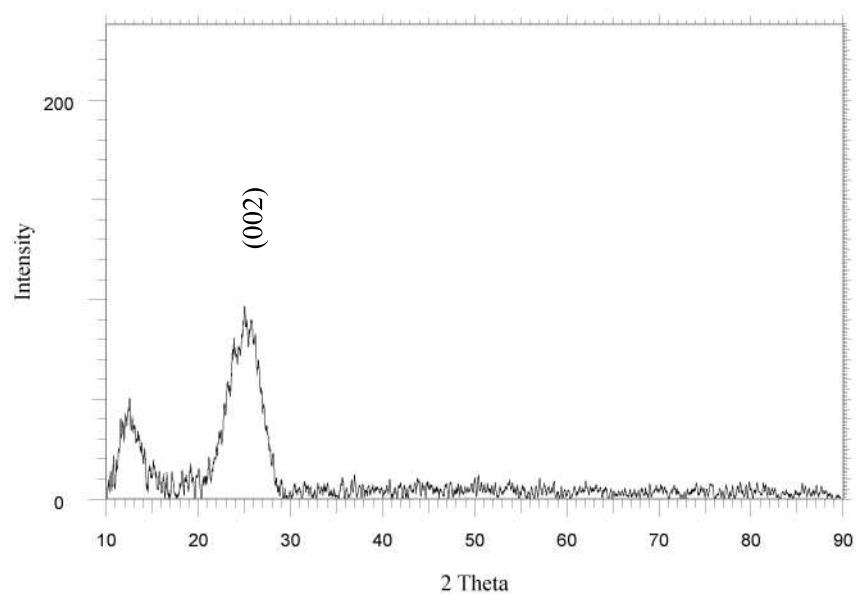
Figure 4.56: XRD pattern of oxidized hydrographenes after expansion at 900°C for 15 min
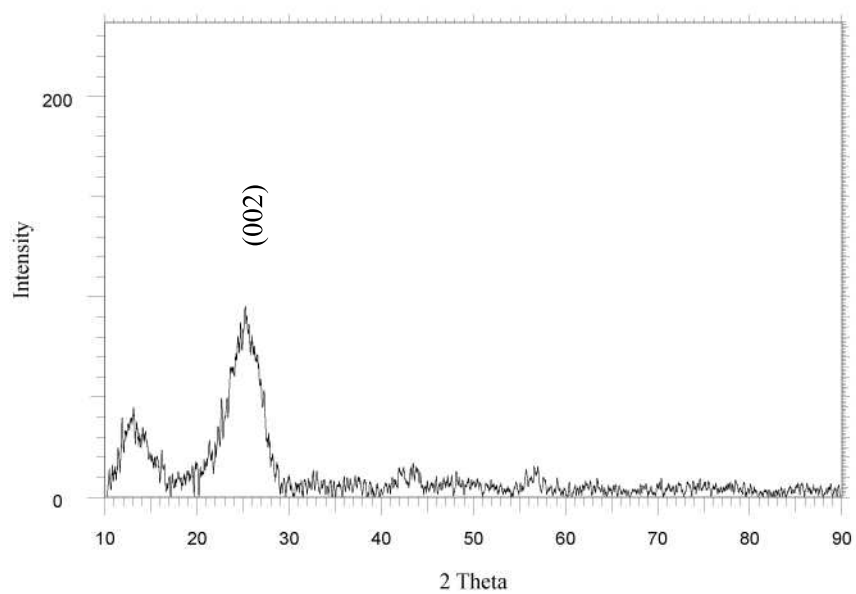
Figure 4.57: XRD pattern after chemical reduction of expanded hydro-graphene oxides

XRD patterns obtained from the each experimental step were analyzed

88

to obtain the structural parameters of FWHM, L_c, and d_{002} in order to make estimations on changing number of graphene layers with respect to varying conditions of oxidation, expansion, and reduction. FWHM and d_{002} values were estimated by utilization of the Bruker axs DiffracPLUS software program. Both values used in Debye-Scherer equations in order to estimate the average number of graphene layers in each experimental step. Average number of layers calculated for hydrographenes, hydrographene oxides, expanded hydrographene oxides, and reduced hydrographenes were 7.7, 7.5, 5.2, and 5.5, respectively as shown in Table . Up to reduction reactions, average number of layers reduced steadily, whereas d_{002} values increased steadily. Increase of interlayer spacing was probably due to the introduction of oxygen groups between the layers in hydrographenes during the oxidation reaction and continuity of the increase in expansion step was because of possible oxygen groups in between layers leading more expansion between the layers. Both changes in average number of layers and interlayer spacing explained how each experimental step affected the crystalline structure of hydrographenes.

Table 4.8: Comparison of graphene layers of hydrographenes, oxidized hydrographenes, oxidized hyrographenes after expansion and reduced hydrographenes regarding to d_{002} in their XRD patterns

	Hydrographenes	Oxidized hydrographenes	Expanded hydrographenes oxide	Reduced hydrographenes
Average number of graphene layers, n	7.7	7.5	5.2	5.5
d_{002} (Å)	3.48	3.50	3.56	3.53

Chapter V

5   Conclusions and Future Works

Our purpose in this research was to investigate the change in the molecular, crystalline and morphological structures of the products of pyrolysis of different petroleum pitches under different conditions. Two petroleum pitches, pitch A and pitch B, were pyrolyzed at a temperature range between 500-1000°C for 30, 60, and 120 minutes under an inert atmosphere. As a result 36 different hydrographenes, which were highly amorphous materials containing rich turbostratic structures, were obtained from the pyrolysis reactions. Because it was not possible to collect all the products inside the quartz tube, there was some sample loss which could not be measured. As a result, there was not a proper correlation of the mass percentages of products with temperature and time variables in order to make a kinetic study of the pyrolysis of pitches. Therefore, non-isothermal kinetic studies of pyrolysis of the pitches were based on the thermogravimetric measurements at different heating rates (β) of 5 K/min, 10 K/min, 20 K/min and 30 K/min. The main zones of the weight loss versus temperature curves of both pitch A and pitch B indicated the devolatilization reactions taking place during pyrolysis process. Pyrolysis of pitch A showed, depending on the heating rate at about 479-515°C, 72-73% of the volatiles were lost. On the other hand, pyrolysis of pitch B showed, depending on the heating rate at about 489-533°C, 75-77%

of the volatiles were lost. So, mass loss of the pitch B was higher than the mass loss of pitch A. The calculated activation energies of pyrolysis of pitch A and pitch B were compared up to conversion of 70% due to the absence of fast reactions in pyrolysis of pitch B. The average activation energy of pitch B, 213.2 kJ/mol, was higher than the average activation energy of A, 185.7 kJ/mol. These results indicated that pitch B was harder to pyrolyze whereas pitch A had probably more degradable compounds in its structure. Also, calculations of reaction order values of pitch A were changing from 1.12 to 1.56 with increasing temperature, while the reaction order for the pyrolysis of pitch B was a lower value, 0.91. Reaction orders closer to zero in the case of pitch B, indicated that the pyrolytic reactions might probably occurred in more heterogeneous media, such as solid-liquid or solid-gas. Variations of activation energies and reaction orders were dependent on the complex and different structures of pitches.

In order to be able to understand the effect of the pyrolysis reactions on the pitches, molecular structures of pitch A, pitch B, and their products were analyzed by both NMR and FTIR. Comparison of both FTIR and ^{1}H-NMR spectra of the pitches demonstrated that pitch A probably had a more aromatic structure due to the ratio of the aliphatic and aromatic peaks. FTIR spectra of hydrographenes clearly indicated changes in the structures of pitch A and pitch B during pyrolysis. FTIR spectra of hydrographenes from both pitch A and pitch B demonstrated that there was decrease in the aliphatic hydrocarbon peaks and conversely an increase in the aromatic peaks with increasing pyrolysis temperature. In addition to these, solid-state ^{13}C-NMR spectra showed that the aromaticity of the hydrographenes increased from 0.69 to 0.81 as temperature increased from 500 to 800°C, respectively. These consistent results of both FTIR and solid-state ^{13}C-NMR spectra proved that aromatic structure formation in hydrographenes was favored with increasing pyrolysis temperature. On the other hand, comparison of FTIR spectra of hydrographenes with respect to pyrolysis time demonstrated that aromatic

structure formation was favored with increasing pyrolysis time due to the continuous decrease of ratio of aliphatic intensities to aromatic intensities and elimination of aliphatic groups attached to aromatic. Also, according to the solid-state ^{13}C-NMR spectra, the aromaticity of the hydrographenes obtained at 500°C increased from 0.59 to 0.69 as time increased from 30 to 120 minutes, respectively. As a result, solid-state ^{13}C-NMR spectra of hydrographenes produced at high and low temperatures with various pyrolysis times supported the FTIR results.

In addition, Raman spectra and XRD patterns of the hydrographenes clearly indicated the change in their crystalline structure at various pyrolysis temperatures and times. The D and G bands in Raman spectra demonstrated the disordered multi-layered structure, and the broadness and low intensity of (002) peak demonstrated the amorphous structure of the hydrographenes. The effect of temperature on the crystalline structures can be explained by the increase in I_D/I_G ratio and decrease in the intensities of D and G bands indicating a decrease in the disorderness of the hydrographenes with increasing pyrolysis temperature. At both high and low temperatures, shorter residence time produced graphitic structures with less disorder due to the higher I_D/I_G ratios. Also, calculations due to the change in the area below the (002) peak showed there was increase in the crystallinity percentage of hydrographenes with increasing temperature and time. So, the results of Raman spectroscopy and XRD mainly supported each other in the case of temperature effect. On the other hand, decrease in the intensity of the G bands with increasing temperature indicated there might be a decrease in the number of graphene layers in hydrographene materials. The calculated average numbers of graphene layers were 5 to 7 layers at temperature higher than 700°C and 7 to 10 at temperatures 500-600°C but there was not a distinct correlation between experimental conditions and the calculated results, n values. The d_{002} and n values obtained from XRD patterns did not show a distinct correlation with pyrolysis parameters. The possible reason

was the small dimensions of crystallites perpendicular to aromatic layers. So the results presented for average number of graphene layers and interlayer spacings in this work might be considered as indications for the presence of turbostratic structures in the hydrographene materials.

The morphological analyses of hydrographenes by SEM also supported the other results of this work. The SEM images demonstrated the amorphousity of hydrographenes containing turbostratic structures. The SEM micrographs at low temperatures like 600°C clearly indicated that there was formation of pores due to the devolatilization reactions taking place in the pyrolysis process as wells formation of layered structures (Figure 4.47). The effect of increasing temperature clearly indicated that there were the formation of turbostratic structures and expansion of carbon layers sequel to formation of layering at lower temperatures in the SEM micrographs of hydrographenes produced at higher pyrolysis temperatures (Figures 4.48 and 4.49)

Beside these, an experimental demo on the oxidation, expansion, and reduction of hydrographene materials concluded that treatment of the pyrolyzed pitches seemed not to be very promising in terms of separating the graphene layers in terms of SEM exhibitions. The XRD results indicated there was a slight decrease in the average number of graphene layers in each step until reduction.

To sum up, highly amorphous hydrocarbon materials containing turbostratic structures were produced by two different types of pitches. Temperature seemed to be the dominating parameter of the pyrolysis reactions. As the pyrolysis temperature was increased aromatic structure formation was favored with an increasing crystallinity and orderness in the hydrographene materials.

The forthcoming studies will be based on recovery of volatile materials during pyrolysis of pitches in tube furnaces; analysis of volatiles; repetition of pitch pyrolysis experiments under higher pyrolysis temperatures in order

to form more graphitic carbon structures; and control of heating rate of the pitch pyrolysis experiments in a bigger furnace.

References

[1] B. Sakintuna, Y. Yürüm, and S. Çetinkaya. Evolution of Carbon Microstructures During the Pyrolysis of Turkish Elbistan Lignite in the Temperature Range 700-1000ºC. *Energy and Fuels*, 18:883–888, 2004.

[2] C. Yue and A.P. Watkinson. Pyrolysis of Pitch. *Fuel*, 77(7):695–711, 1998.

[3] 4.24 Pyrolysis, July 2009. [online] `http://www.frtr.gov/matrix2/section4/4-25.html`.

[4] S. Çetinkaya and Y. Yürüm. Oxidative pyrolysis of Turkish lignites in air up to 500°C. *Fuel Processing Technology*, 67:177–189, 2000.

[5] D. Erçin and Y. Yürüm. Carbonisation of Fir (Abies bornmulleriana) wood in an open pyrolysis system at 50-300°C. *Journal of Analytical and Applied Pyrolysis*, 67:11–22, 2003.

[6] E. Fitzer, K.H. Köchling, and H. Marsh. Recommended Terminology for the Description of Carbon as a Solid. *Pure and Applied Chemistry*, 67(3):473–506, 1995.

[7] D.W. Van Krevelen. *Coal.* Elsevier, May 1993.

[8] R.H. Schosberg. *Chemistry of Coal Conversion.* Plenum Press, 1985.

[9] Pyrolysis, April 2009. [online] `http://en.wikipedia.org/wiki/Pyrolysis`.

[10] M.A. Elliot. *Chemistry of Coal Utilization.* Wiley, 1981.

[11] A.V. Bridgwater. Thermal Conversion Of Biomass And Waste. The Status, Bio-Energy Research Group, Aston University, Birmingham, UK.

[12] J. Kovacs. What is Biomass Pyrolysis? [online] `http://www.handbook.itrf.net`.

[13] A.V. Bridgwater. Biomass Fast Pyrolysis. *Thermal Science*, 8(2):21–49, 2004.

[14] D. S. Scott, J. Piskorz, and D. Radlein. Liq uid Products from the Continuous Flash Pyrolysis of Biomass. *Ind. Eng. Chem. Pro cess Des. Dev.*, 24:581–586, 1985.

[15] A. Robson. 25 tpd Bor der Biofuels/DynaMotive Plant in the UK. *PyNe Newsletter*, 11:1–2, 2001.

[16] B.M. Wagenaar. The Rotating Cone Flash Pyrolyzer, Department of Chemical Engineering, University of Twente, Enschede, The Netherlands.

[17] C. A. Zaror and D. L. Pyle. The pyrolysis of biomass: A general review. *Proc. Indian Acad. Sci. (Engg. Sci.)*, 5:1269–1285, 1982.

[18] A. K. Sharma, M.R. Ravi, and S. Kohli. Modelling Product Composition in Slow Pyrolysis of Wood,Mechanical Engineering Department, Indian Institute of Technology, Delhi110016.

[19] C.G. Jung and A. Fontana. Slow Pyrolysis vs Gasification : mass and Energy balances using a predictive model. *CEB Working Paper*, 7(26), 2007.

[20] M. Yılgın, N.D. Durunay, and Pehlivan D. Odunun Flaş Pirolizi. *Symposium of Renewable Energy Sources*, 2005.

[21] C. Vasile, M. Brebu, Y. Sakata, H. Pakdel, C. Roy, and R. Miranda. Solid Waste Treatment by Pyrolysis Methods. *Journal of Environmental Protection and Ecology*, 3(1):230–235, 2002.

[22] E.M. Suuberg. *Rapid pyrolysis and Hydropyrolysis of Coal.* PhD thesis, MIT, 1977.

[23] E. H. Lars, A. A. Lars, and B. Ingemar. Investigation of Peat Pyrolysis Under Inert Gas Atmosphere . *Fuel*, 70(9):1017–1022, 1991.

[24] R. Kandiyoti, J.I. Lazaridis, B. Dyrvold, and C. Weerasinghe. Pyrolysis of a ZnCI2-Impregnated Coal in an Inert Atmosphere. *Fuel*, 63(11):1583–1587, 1984.

[25] D.B. Anthony, J.B. Howard, H.C. Hottel, and H.P. Meissener. Rapid Devolatilization and Hydrogasification of Bituminous Coal. *Fuel*, 55(2):121–128, 1976.

[26] P.L. Agrawal. Nature of coal. In *Proc. Symp.*, pages 121–128, 1959.

[27] R.E. Franklin. A study of the Fine Structure of Carbonaceous Solids by Measurements of True and Apparent Densities. Part II.-Carbonized Coals. *Trans.Faraday Soc.*, 45:668, 1949.

[28] D.L. Perrya and A. Grint. Application of XPS to Coal Characterization. *Fuel*, 62(9):1024–1033, 1983.

[29] H.A.G. Chermin and D.W. Van Krevelen. . *Fuel*, 36:85–104, 1957.

[30] Wang J. Study on the Structure and Pyrolysis Characteristics of Chinese Western Coals. *Fuel Processing Tech*, 36, 2009.

[31] T.S. Bandara, K.G.S. Kannangara, and M.A. Wilson. The Study of Australian Coal Maturity: Relationship between Solid-State NMR Aromaticities and Organic Free-Radical Count. *Energy and Fuels*, 19:954–959, 2005.

[32] H. Marsh, E.A. Heintz, and F. Rodrıguez-Reinoso. *Introduction to Carbon Technologies*. Universidad de Alicante, Alicante, Spain, 1997.

[33] P. Davini. Desulphurization Properties of Active Carbons Obtained from Petroleum Pitch Pyrolysis. *Carbon*, 37:1363–1371, 1999.

[34] M. Pérez, M. Granda, R. García, R. Santamaría, E. Romero, and R. Menéndez. Pyrolysis Behaviour of Petroleum Pitches Prepared at Different Conditions. *Journal of Analytical and Applied Pyrolysis*, 63:223–239, 2002.

[35] D.D. Edie and R.J. Diefendorf. Carbon-Carbon Materials and Composites. In *NASA Reference Publication 1254*, page 19, 1992.

[36] A. Figueiras, J.J. Fernández, M. Granda, J. Bermejo, E. Casal, and R. Menéndez. Journal of Microscopy 177 (1995) 218, 1995.

[37] M. Z. Özel and K. D. Bartle. Production of Mesophase Pitch from Coal Tar and Petroleum Pitches Using Supercritical Fluid Extraction. *Turk. J. Chem.*, 26:417–424, 2002.

[38] K. Oshidaa and S. Bonnamyb. Primary Carbonization of an Anisotropic Mesophase Pitch Compared to Conventional Iisotropic Pitch. *Carbon*, 40:2699–2711, 2002.

[39] H.G. Franck and J.W. Stadelhofer. *Industrial Aromatic Chemistry: Raw Materials, Processes, Products.* Springer, Berlin-Heidelberg, 1988.

[40] H.G. Franck and G. Collin. *Steinkohlenteer: Chemie, Technologie und Verwendung.* Springer, Berlin-Heidelberg, 1968.

[41] Q. Lin, W. Sua, and Y. Xie. Effect of Rosin to Coal-tar Pitch on Carbonization Behavior and Optical Texture of Resultant Semi-cokes. *Journal of Analytical and Applied Pyrolysis*, 2009.

[42] M. Zander. Die Chemie der Pyrolyse von aromatischen Kohlenwasserstroffen in der Gas- und Flüssigphase. *Erdöl-Erdgas-Kohle*, 105:373, 1989.

[43] M. Cooke, K. Loening, and J. Merritt. *Polynuclear Aromatic Hydrocarbons.* Battelle Press, Columbus, 1991.

[44] B. Grzyb, J. Machnikowski, J.V. Weber, A. Koch, and O. Heintz. Mechanism of Co-pyrolysis of Coal-tar Pitch with Polyacrylonitrile. *Journal of Analytical and Applied Pyrolysis*, 67:77–93, 2003.

[45] M. Zander. On the Composition of Pitches. *Journal of Analytical and Applied Pyrolysis*, 66:1536, 1987.

[46] M. Pérez, M. Granda, R. Santamaría, T. Morgan, and R. Menéndez. A Thermoanalytical Study of the Co-pyrolysis of Coal-tar Pitch and Petroleum Pitch. *Fuel*, 83(9):1257–1265, 2004.

[47] J.W. Evans. *Reduction of the PAH Emissions for Horizontal Stud Söderberg Pot Rooms.* Minerals Metals and Materials Society, 1995.

[48] Council Directive 1999/38/EC of 29 April, 1999 amending for the second time Directive 90/394/ECCon the protection of workers from the risks related to exposure to carcinogens at work and extending it to mutagens.

[49] M. Pérez, M. Granda, R. García, R. Santamaría, E. Romero, and R. Menéndez. Pyrolysis Behaviour of Petroleum Pitches Prepared at Different Conditions. *Journal of Analytical and Applied Pyrolysis*, 63:223–239, 2002.

[50] V. Slovák and P. Susàk. pitch Pyrolysis Kinetics from Single TG Curve. *Journal of Analytical and Applied Pyrolysis*, 72:249–252, 2004.

[51] V.G. et.al. Rocha. Pyrolysis Behaviour of Pitches Modified with Different Additives. *Journal of Analytical and Applied Pyrolysis*, 73:276–283, 2005.

[52] M. Martínez-Escandell, P. Carreira, M.A. Rodríguez-Valero, and F. Rodríguez-Reinoso. Self-sintering of Carbon Mesophase Powders:Effect of Extraction/Washing with Solvents. *Carbon*, 37:1662, 1999.

[53] R.A. Greinke and L.H. O'Connor. Determination of Molecular Weight Distributions of Polymerized Petroleum Pitch by Gel Permeation Chromatography with Quinoline Eluent. *Analytical Chemistry*, 52(12):11877–1881, 1980.

[54] W. Gemmeke, G. Collin, and M. Zander. Recent Developments in Basic Research and Technology in the Electrode Pitch Producing Sector. *TMS paper selection (AIME)*, 355, 1978.

[55] H. Marsh, M. Martínez-Escandell, and F. Rodríguez-Reinoso. Semicokes From Pitch Pyrolysis: Mechanisms and Kinetics. *Carbon*, 37:363–390, 1999.

[56] R.A. Greinke. Quantitative Influence of Dealkylation and Polymerization Reactions on Mesophase Formation. *Carbon*, 28:701, 1990.

[57] R.A. Greinke and L.S. Singer. Constitution of Coexisting Phases in Mesophase Pitch During Heat Treatment: Mechanism of Mesophase Formation. *Carbon*, 26:665–670, 1988.

[58] G. Várhegyi, P. Szabó, E. Jakab, and F. Till. Mathematical Modeling of Char Reactivity in Ar-O_2 and CO_2-O_2 Mixtures. *Energy Fuels*, 10:1208–1214, 1996.

[59] K. Ceylan, H. Karaca, and Y. Önal. Thermogravimetric Analysis of Pretreated Turkish Lignites. *Fuel*, 78:1109–1116, 1999.

[60] J. Adánez, L.F. De Diego, F. García-Labiano, A. Abad, and J.C. Abanades. Determination of Biomass Char Combustion Reactivities for fbc Applications by a Combined Method. *Ind. Eng. Chem.Res*, 40:4317–4323, 2001.

[61] M.E. Sanchez, M. Otero, X. Gomez, and A. Moran. Thermogravimetric Kinetic Analysis of the Combustion of Biowastes. *Renew. Energ.*, 34:1622–1627, 2009.

100

[62] A.G. Dumanli and Y. Yürüm. Co-firing of Biomass with Boals. Thermogravimetric Binetic Bnalysis of Bombustion of Fir (abies bornmulleriana) Wood (in review). *Fuel*, 2009.

[63] S. Vyazovkin. Evaluation of Activation Energy of Thermally Stimulated Solid-state Reactionsunder Arbitrary Variation of Temperature. *J. Comput. Chem.*, 18:393–402, 1997.

[64] A. Khawam and DR. Flanagan. Role of Isoconversional Methods in Varying Activation Energies of Solid-state Kinetics: II. Nonisothermal Kinetic Studies. *Thermochim. Acta5*, 436:101–112, 2009.

[65] T. A Ozawa. A New Method of Analyzing Thermogravimetric Data. *Bull. Chem. Soc.*, 38:1881–1886, 1965.

[66] T. A Ozawa. Kinetic Analysis of Derivative Curves in Thermal Analysis. *Therm. Anal.*, 2:301–304, 1970.

[67] J.H. Flynn and L.A. Wall. Structures and Thermal Analysis of 1,1,6,6-tetraphenylhexa-2,4-diyne-1,6-diol. *Therm. Anal.*, 4:323–328, 1966.

[68] CD Doyle. Estimating Isothermal Life from Thermogravimetric Data. *J. Appl. Polym. Sci.*, 6:639–642, 1962.

[69] M.J. Avrami. Kinetics of Phase Change. I. General Theory. *Chem. Phys.*, 7:1103–1112, 1939.

[70] M.J. Avrami. Kinetics of Phase Change. II. Transformation-Time Relations for Random Distribution of Nuclei. *Chem. Phys.*, 8:212–224, 1940.

[71] M.J. Avrami. Kinetics of Phase Change. III. Granulation, Phase Change, and Microstructure. *Chem. Phys.*, 9:177–184, 1941.

[72] J.H. Flynn and L.A. Wall. A General Treatment of the Thermogravimetry of Polymers. *J. Res. Nat. Bur. Stand.*, 70A:487–523, 1966.

[73] M. Inagaki. *New Carbons: Control of Stucture and Functions*. Elsevier, 2000.

[74] A.V. Tamashausky. The Effect of Graphite Type, Purity, and Concentration on the Performance of a Clay Filled Polyalphaolefin Grease, Based on Four Ball Wear (ASTM D2266) with Coefficient of Friction, and Load Wear Index (ASTM D2596). *NLGI Spokesman*, 65(12):10–25, 2002.

[75] A. Legendre. Le Matériau Carbone: des Céramiques Noires aux Fibres de Carbone. *Eyrolles*, 1995.

[76] P. Delhaes. *Graphite and Precursors*. CRC Press, 2001.

[77] N. Ooi, A. Rairkar, and B. Adams. Density Functional Study of Graphite Bulk and Surface Properties. *Carbon*, 44:231–242, 2006.

[78] Graphite (C) - Classifications, Properties and Applications of Graphite, March 2009. [online] `http://www.azom.com/details.asp?ArticleID=1630`.

[79] Bonnissela, L. M. Luob, and D. Tondeurb. Compacted Exfoliated Natural Graphite as Heat Conduction Medium. *Carbon*, 39:2151–2161, 2001.

[80] T. Yamabea, M. Fujii, S. Mori, H. Kinoshita, and S. Yata. The Structural Analysis of Various Hydro-graphene Species. *Synthetic Metals*, 145:31–36, 2004.

[81] S. Stankovich, D. A. Dikin, G. H. B. Dommett, K. M. Kohlhaas, E. J. Zimney, E. A. Stach, R. D. Piner, S. T. Nyguen, and R. S. Rouff. Graphene-based Composite Materials. *Nature*, 444:282–286, 2006.

[82] İ. A. Aksay. Single Sheet Functionalized Graphene by Oxidation and Thermal Expansion of Graphite. *Chem. Mater.*, 19:4396–4404, 2007.

[83] A.K. Geim and K.S. Novoselov. The Rise of Graphene. *Nature Materials*, 6:183–191, 2007.

[84] H. Marsh, E.A. Heintz, and F. Rodrıguez-Reinoso. *Compendium of Chemical Terminology, 2nd ed. (the "Gold Book"). Compiled by A. D. McNaught and A. Wilkinson.* Blackwell Scientific Publications, Oxford, 1997.

[85] Z.Q. Li, C.J. Lu, Z.P. Xia, Y. Zhou, and Z. Luo. X-ray Diffraction Patterns of Graphite and Turbostratic Carbon. *Carbon*, 45:1686–1695, 2007.

[86] Y. F. Jia and G. P. Demopoulos. Adsorption of Silver onto Activated Carbon from Acidic Media: Nitrate and Sulfate Media. *Ind. Eng. Chem. Res.*, 42:72, 2003.

[87] O. Senneca. Combustion and Gasification of Three Biomass Fuels. *Fuel Processing Technology*, 88:87–97, 2007.

[88] G. Svehla. *Comprehensive Analytical Chemistry, Volume VI: Analytical Infrared Spectroscopy.* Elsevier, 1976.

[89] M. Balcı. *Nükleer Manyetik Rezonans Spektroskopisi.* ODTÜ Yayincilik, 2004.

[90] Y. Yürüm, M. Azık, G. Altıntaş, and E. Şanlıtürk. Characterization of the Structural Features of Oxidized Beypazari Lignite Using Devonvoluated Solid State CNMR Spectra. *Fuel Science and Technology INT'L*, 8(8):917–933, 1990.

[91] X. et al Gong. Variation of Char Structure During Anthracite Pyrolysis Catalyzed by Fe2O3 and Its Influence on Char Combustion Reactivity (in press). *Energy and Fuels*, 2009.

[92] A.C. Ferrari, J.C. Meyer, and et. al. Raman Spectrum of Graphene and Graphene Layers. *Physical Review Letters*, 97, 2006.

[93] A.C. Ferrari. Raman spectroscopy of graphene and graphite: Disorder, electron-phonon coupling, doping and nonadiabatic effects. *Solid State Communications*, 143:47–57, 2007.

[94] D. et.al. Graf. Spatially Resolved Raman Spectroscopy of Single- and Few-layer Graphene. *Nano Letters*, 7:238–242, 2007.

[95] H. et.al. Wang. Disorder Induced Bands in First Order Raman Spectra of Carbon Nanowalls. *IEEE*, 2006.

[96] H. Fujimoto. Theoretical X-ray Scattering Intensity of Carbons with Turbostratic Stacking and AB Stacking Structures. *Carbon*, 41:1585–1592, 2003.

[97] D. Yang and R.P. Frindt. Powder X-ray Diffraction of Turbostratically Stacked Layer Systems. *J. Matter. Res.*, 11:1777–1781, 1996.

[98] J. Li, L. Feng, and Z. Jia. Preparation of Expanded Graphite with 160 μm Mesh of Fine Flake Graphite. *Materials Letters*, 60:746–749, 2006.

[99] B. Saner, F. Okyay, and Y. Yürüm. Utilization of Graphene Layers in Fuel Cells. 1. An Improved Technique for the Exfoliation of Graphene-based Nanosheets from Graphite, (in review). *Fuel*.